PNE-600F
FINAL REPORT

Plowshare / peaceful uses for nuclear explosives

UNITED STATES ATOMIC ENERGY COMMISSION / PLOWSHARE PROGRAM

project DUGOUT

NEVADA TEST SITE — JUNE 24, 1964

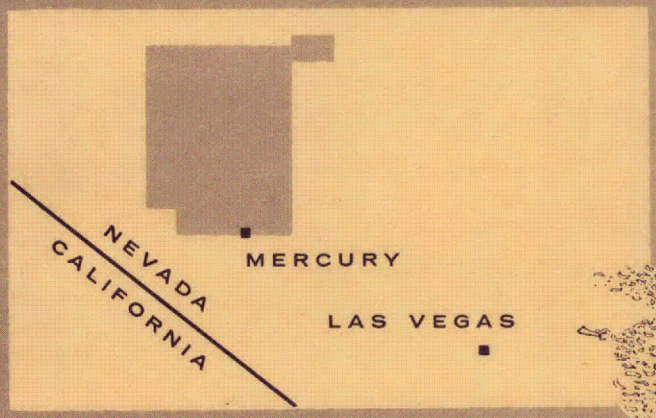

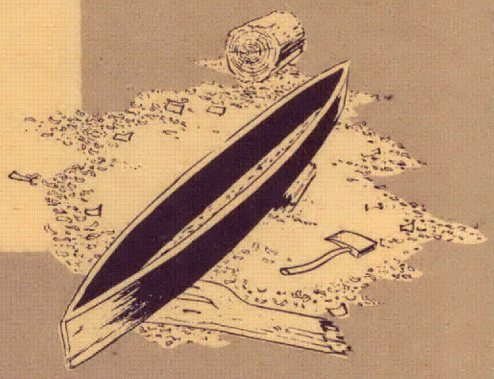

Technical Director's Summary Report

M. D. Nordyke

Lawrence Radiation Laboratory

Issuance Date: May 10, 1965

LEGAL NOTICE

Printed in USA. Price $4.00. Available from the Clearinghouse for Federal Scientific and Technical Information, National Bureau of Standards, U. S. Department of Commerce, Springfield, Va.

USAEC Division of Technical Information Extension, Oak Ridge, Tennessee

PNE-600F
NUCLEAR EXPLOSIONS—PEACEFUL APPLICATIONS
(TID-4500, 40th Ed.)

PROJECT DUGOUT

TECHNICAL DIRECTOR'S SUMMARY REPORT

M. D. Nordyke
Lawrence Radiation Laboratory

R. W. Terhune
Lawrence Radiation Laboratory

R. F. Rohrer
Lawrence Radiation Laboratory

L. J. Cauthen*
U. S. Army Corps of Engineers

J. L. Spruill**
U. S. Army Corps of Engineers

Livermore, California

December 1964

---

*Assigned to the Lawrence Radiation Laboratory as a research associate.

**Assigned to the Nuclear Cratering Group.

CONTENTS

FIGURES

ABSTRACT

Project Dugout was a chemical explosive row charge cratering experiment in hard rock conducted at the AEC Nevada Test Site as part of the Plowshare Program for development of nuclear excavation technology. The purpose of Dugout was to extend knowledge of row-cratering phenomenology to a hard rock medium. The Dugout design consisted of five nominal 20-ton spherical charges of nitromethane emplaced at a depth of 18 m (59 ft) in basalt with a spacing between charges of 13.7 m (45.0 ft). All five charges were detonated simultaneously at about 0806 PDT on 24 June 1964.

The crater produced had an average apparent crater width over the center 60% of the crater of 41.5 m (136 ft). The average apparent crater depth was 10.7 m (35.2 ft) and the length from one end to the other was 87.5 m (287 ft). The lip height along the sides of the crater averaged about 7.3 m (24 ft), whereas off the ends its height was about 4 m (13 ft). The total apparent crater volume was about 16,080 m^3 (21,030 yd^3). The crater volume in the center 60% corresponded to 3640 m^3 (4,765 yd^3) per 20-ton charge. The resulting crater was 36.5% wider and 41% deeper than predicted. This is believed to be due to the use of too small a spacing resulting from reliance too heavily on earlier cratering results in basalt using TNT charges. Comparison of Dugout results with nitromethane cratering data only indicates that the Dugout width was only 13% too large and the depth was 6% less. Based on these considerations it is concluded that the row charge concepts developed earlier in alluvium may be extended, at least approximately, to hard rock media.

Comparison of early surface-motion data from high-speed photography of surface-motion targets, and from accelerometers

in the ground zero area, indicates very good agreement with a peak surface velocity of about 48 m/sec (145 ft/sec). Data from strong motion measurements at ranges of 170 to 1580 m on lines south and west of the east-west array indicates anisotropic propagation only at the two closest stations. Beyond 200 km the motions were isotropic and consistent with a single 100 ton source.

Air blast signals measured close to the detonation indicated anisotropic propagation with signals in a direction perpendicular to the array being about a factor of 1.5 to 2.0 above those in a direction parallel to the array. The close-in air blast measurements from Dugout compared favorably with results from single cratering detonations in basalt if it is assumed that (1) signals propagated in a direction parallel to the array result from superposition of the air blast waves at the source, and (2) signals in the perpendicular direction result from superposition at the gauge. The long range air blast signals demonstrated somewhat similar anisotropy whereby the signals in the parallel direction were about a factor of 2 greater than the signals in the perpendicular direction. Assumption of source superposition leads to an average transmissivity factor for long range air blast of 0.11, in excellent agreement with previous experience.

The maximum cross wind base surge radius was about 320 m. The maximum base surge height was about 350 m and the maximum main cloud height was about 1220 m.

The above results and conclusions are based on preliminary data and are subject to revision. Final results will be given in referenced reports.

CHAPTER 1

INTRODUCTION

Project Dugout was a chemical explosive row-charge cratering experiment in hard rock conducted as part of the Plowshare Program for development of nuclear excavation technology. In general terms, the purpose of Dugout was to extend our knowledge of row-cratering phenomenology, presently limited to alluvium and playa, to a hard rock medium. This report outlines experiments conducted on Dugout and summarizes the preliminary results. More detail on the experimental plans and the final results will be found in the final project report for each experimental program listed at the end of the document.

1.1 PURPOSE OF DUGOUT

As a result of a considerable amount of experimental work on row craters with high explosives in alluvial material (Refs. 1-5) some general conclusions had been reached prior to Dugout concerning effects of spacing and depth of burial in such explosions, as follows:

1. Spacing the charges a distance apart approximately equal to a single-charge-crater radius results in smooth ditches with average dimensions from 10 to 20% larger than single-charge crater dimensions for the same depth of burst. A 25% greater spacing gives a less regular ditch with average dimensions approximately equal to the corresponding single-charge crater dimensions.

2. Row charges result in craters with no appreciable lip or upthrust material off the ends of the row and with lips along the sides which are 50 to 100% higher than result in single-charge craters of the same depth.

3. Ground-shock and air blast signals recorded close to the detonation are consistent with superposition of the signals from the individual charges.

There had been no comparable experiments with multiple charges in hard rock, although there had been a number of single-charge cratering programs in basalt (Refs. 6 and 7). The effect of a rock medium on the foregoing conclusions is important because almost all practical applications of large-scale nuclear excavations are in rock. Thus, Dugout was designed to extend the above row-charge concepts from alluvial material to hard rock. Experimental programs included on Dugout to study these phenomena are as follows:

1. Crater studies including pre- and postshot geological reconnaissance;
2. Surface motion studies using high speed photographic coverage and surface accelerometers;
3. Ground shock studies including strong motion instruments, subsurface particle velocity measurements and drill hole shock damage and survival investigations;
4. Air blast studies of both the close-in and long-range air blast signals; and
5. Base surge studies to determine base surge dynamics as a function of time.

The Lawrence Radiation Laboratory had the over-all technical responsibility for conducting the Dugout event. Other participating agencies were the U. S. Army Engineers Nuclear Cratering Group, Sandia Corporation, Edgerton, Germeshausen, and Grier, Inc., U. S. Coast and Geodetic Survey, Waterway Experiment Station, and the U. S. Weather Bureau.

1.2 DESCRIPTION OF CHARGE EMPLACEMENT

The Dugout design consisted of five 20-ton chemical explosive charges placed at a depth of 59 ft (18 m) in basalt. All five

charges were to be detonated simultaneously. Because of its superior handling characteristics, the liquid explosive nitromethane (CH_3NO_2) was used for the Dugout charges. To contain the explosive, a spherical cavity was constructed at the proper depth by first drilling a 36-in.-diam hole and mining out a roughly spherical room (Fig. 1.1). This room was then lined with chicken-wire netting and a grout was applied to produce a sphere of the desired dimensions. To seal the walls and prevent absorption or leaking of the nitromethane, a coating of Adiprene L-100 was applied to the grout surface. A booster charge, consisting of 2.3 kg of C-4, and a pair of SE-1 detonators were placed in the center of the sphere, a plug was placed in the 36-in. access hole, and the hole was stemmed to the surface with a concrete grout which was designed to match the physical properties of the existing basalt. To insure against failure of the plug stemming, two keys with reinforcing steel were placed in the walls of the hole.

Figure 1.2 shows an east-west section through the Dugout array. Table 1.1 gives the actual dimensions of the cavities and the array as they were constructed. The cavity diameters shown are the average of four diameters and the volumes shown were calculated from the mean diameters.

Filling of the cavities was accomplished by means of a 1-1/2-inch diameter pipe. When the cavities were initially filled, holes G and K developed severe leaks which would have resulted in almost complete emptying of these two cavities by the date originally planned for the detonation. Operations were suspended and additional nitromethane was procurred within one week. To be assured of a maximum quantity of nitromethane in these two cavities at shot time, the cavities were subsequently filled a few hours before shot time and the levels recorded as long as possible to obtain the rate of loss.

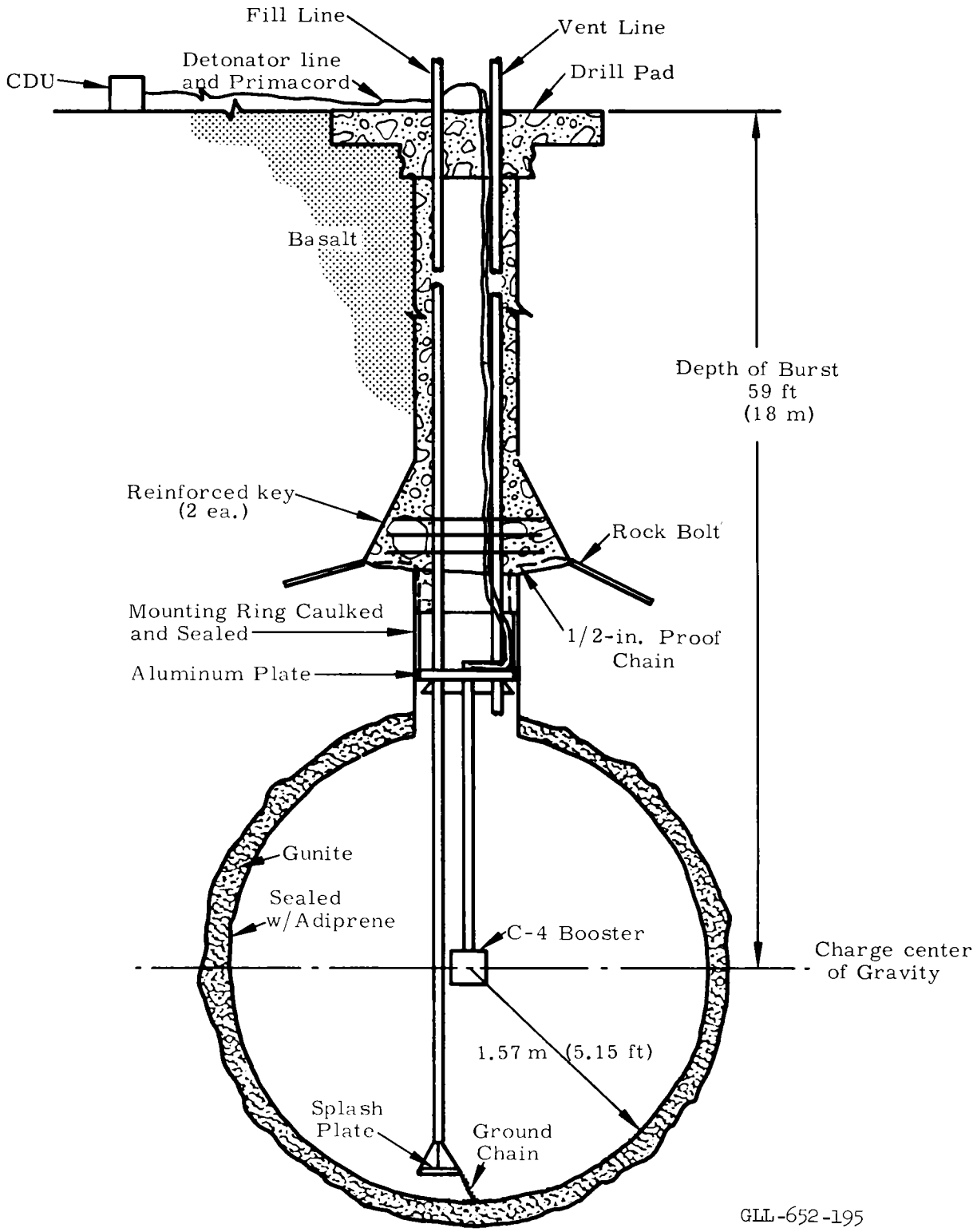

Fig. 1.1 Centerline section of typical charge emplacement.

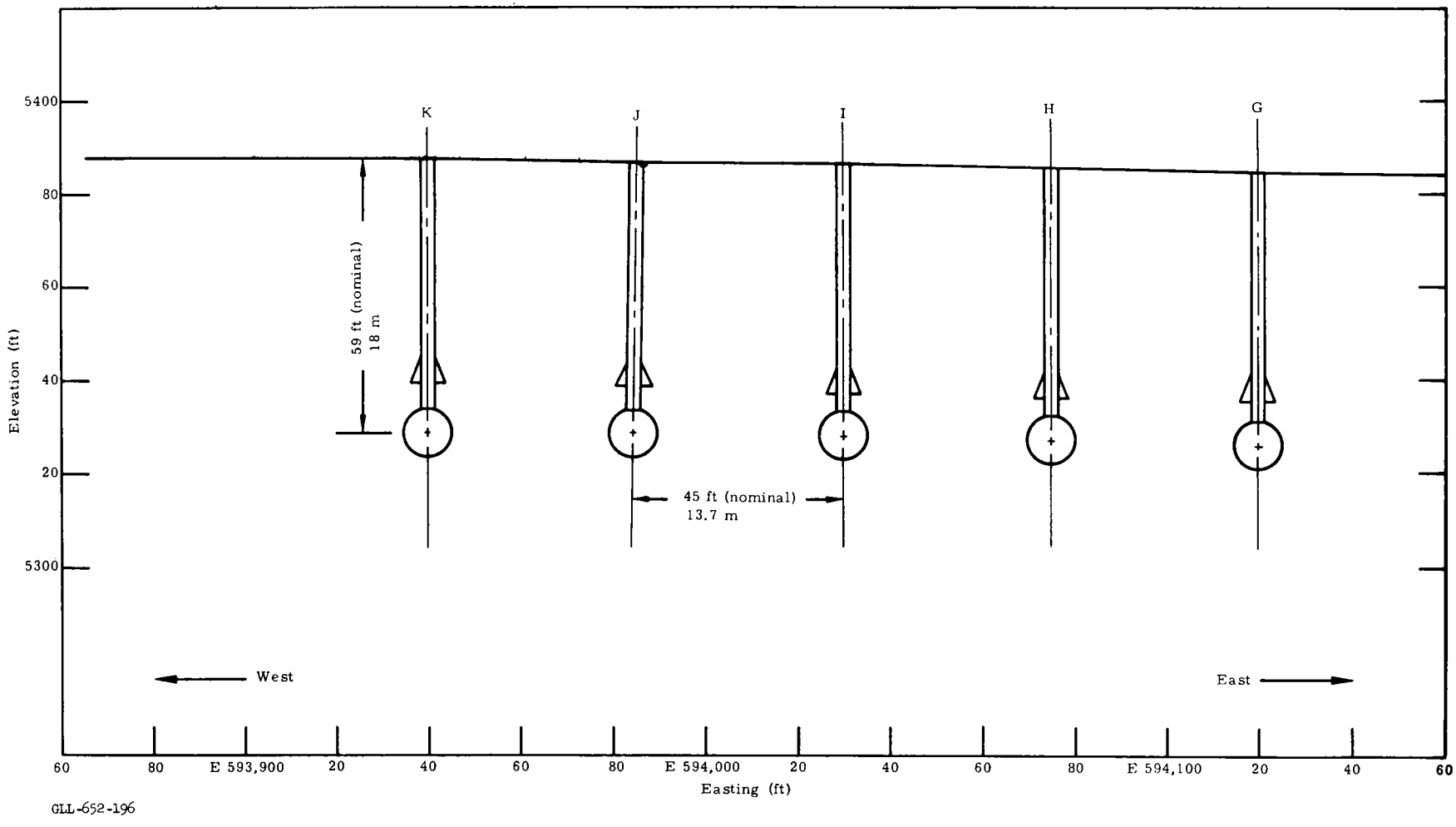

Fig. 1.2 East-west cross section of Dugout array.

TABLE 1.1 DUGOUT CAVITY DIMENSIONS

Hole	Collar coordinates	Collar elevation (ft)	Cavity center coordinates	Cavity center elevation (ft)	Mean cavity diameter[a]	Depth of burst	Spacing	Cavity volume
U 18g	N853,289.90 E594,120.20	5384.56	N853,290.10 E594,119.80	5325.79	10.33 ft (3.15 m)	58.77 ft (17.91 m)		575.8 ft^3 (16.31 m^3)
							44.90 ft (17.91 m)	
U 18h	N853,290.00 E594,075.00	5385.45	N853,289.20 E594,074.90	5326.75	10.05 ft (3.06 m)	58.70 ft (17.89 m)		530.4 ft^3 (15.02 m^3)
							44.68 ft (13.63 m)	
U 18i	N853,289.94 E594,030.06	5386.51	N853,290.28 E594,030.22	5327.68	10.44 ft (3.18 m)	58.83 ft (17.92 m)		594.6 ft^3 (16.84 m^3)
							45.54 ft (13.89 m)	
U 18j	N853,290.00 E593,985.12	5386.90	N853,289.96 E593,984.68	5328.30	10.36 ft (3.16 m)	58.60 ft (17.86 m)		580.9 ft^3 (16.45 m^3)
							44.87 ft (13.69 m)	
U 18k	N853,290.10 E593,940.00	5387.50	N853,290.10 E593,939.81	5328.74	10.47 (3.19 m)	58.76 ft (17.90 m)		599.8 ft^3 (16.99 m^3)
				Averages	10.33 ± 0.11 ft (3.15 ± 0.03 m)	58.73 ± 0.06 ft (17.91 ± 0.02 m)	45.00 ± 0.27 ft (13.73 ± 0.08 m)	

[a]Average of four diameters.

In view of the highly fractured nature of the basalt media and the known presence of highly porous cinder zones in the basalt, it is felt that the nitromethane that leaked from the cavities was drained away from the area of the cavities and ultimately found its way to the alluvial material at the base of the basalt. Laboratory experiments have shown that nitromethane will not propagate in a geometry where the cross section is less than about 2 cm. Therefore, no detonation beyond the surface of the cavities is believed to have occurred.

Shown in Table 1.2 are the weights of nitromethane estimated to be in the cavities at shot time and the heights of the empty spherical segments remaining above the nitromethane. Also given in Table 1.2 are the "equivalent" charge weights, in tons, assuming an energy release for nitromethane of 1220 cal/g and a definition of 10^9 calories/equivalent ton. The scaled depth of burst calculated in Table 1.2 shows an average of about 54.9 $m/kt^{1/3.4}$ (180 $ft/kt^{1/3.4}$). The scaled spacing using the average charge weight of 22.4 tons was 42.0 $m/kt^{1/3.4}$ (138 $ft/kt^{1/3.4}$). This corresponds to an equivalent line charge (w) of 0.00167 kt/m, a linear scaled depth of burst of 256 $m/(kt/m)^{1/2.4}$, and a linear scaled spacing of 196 $m/(kt/m)^{1/2.4}$.

1.3 THE DETONATION

Dugout was detonated on 24 June 1964 at approximately 0806 Pacific Daylight Time (1506 GMT). All charges appeared to detonate as planned. The firing circuits used assured simultaneity between charges of better than one millisecond. No evidence of partial or nonsimultaneous detonation was observed. Inspection of the crater a short time after the detonation showed occasional minor rock falls and subsurface rumblings which persisted intermittently (about every 5 to 10 minutes) for almost an hour.

TABLE 1.2 DUGOUT CHARGE LOADINGS

Hole	Estimated weight of nitromethane at shot time (kg)	Fraction of cavity volume filled (%)	Height of spherical segment[a] (m)	Equivalent charge weight[b] (tons)	Scaled depth of burst ($ft/kt^{1/3.4}$)	Scaled depth of burst ($m/kt^{1/3.4}$)
U 18 g	18,100 + 110 - 340	98.4	0.25	22.1 + 0.1 - 0.4	180.0	55.0
U 18 h	16,970 ± 110	100.1	Full sphere[c]	20.7 ± 0.1	183.5	55.9
U 18 i	18,110 ± 110	99.6	0.025	23.1 ± 0.1	178.0	54.4
U 18 j	18,280 + 110 - 230	98.5	0.21	22.3 + 0.1 - 0.3	178.5	54.5
U 18 k	18,010 + 230 - 450	94.0	0.47	22.0 + 0.3 - 0.6	180.0	54.9
			Average	22.4 + 0.4	180 ± 1.4	54.9 ± 0.4
			Total equivalent charge weight	110.2 + 0.7 - 1.5		

[a]Height of spherical segment above the partially filled sphere. An additional 30 cm of 36-in.-diam cylindrical void space existed between the top of the full spherical cavities and the cover plate at the bottom of the stemming in the access hole.

[b]Based on one equivalent ton equals an energy releast of 10^9 calories and an energy release for nitromethane of 1220 calories/gram.

[c]Measurements indicate hole U 18h was over-filled slightly so that the nitromethane stood about 2.5 cm high in the cylindrical access hole.

REFERENCES

1. R. H. Carlson, "High Explosive Ditching from Linear Charges," Final Report, Sandia Corporation, SC-4483(RR), July 1961.

2. L. J. Vortman and L. N. Schofield, "The Effect of Row Charge Spacing and Depth on Crater Dimensions," Sandia Corporation, SC-4730(RR), November 1963.

3. B. Myers, "Project Rowboat," Final Report, Lawrence Radiation Laboratory, UCRL-12118, 1964.

4. E. Graves, W. Wray, and R. Pierce, "Scope of Chemical Explosive Cratering Experiment," Preliminary Report, Nuclear Cratering Group, PNE-300, May 1963.

5. J. Spruill, "Project Pre-Buggy II – Crater Measurements," Nuclear Cratering Group, PNE-315, 1964.

6. L. J. Vortman et al., "Project Buckboard," Final Report, Sandia Corporation, SC-4675(RR), August 1962.

7. J. Spruill, "Project Pre-Schooner – Crater Measurements," Nuclear Cratering Group, PNE-502, 1964.

CHAPTER 2

CRATER STUDIES

2.1 INTRODUCTION

This chapter contains a summary of the objectives, procedures, predictions, and results of the crater studies on Project Dugout. More detailed and final results will be found in Reference 12 to this chapter.

2.1.1 Objectives. The technical objectives of the crater studies on Dugout were:

(1) To accurately determine the dimensions and shape of the apparent crater and lip and to estimate from postshot drilling and limited excavation the dimensions and shape of the true crater and true lip.

(2) To determine the effects of a row of explosive charges simultaneously detonated in dry rock on the engineering properties of the rock by means of a study of the engineering and geologic conditions at the site before and after the detonations.

(3) To study the stability of the slopes of a small row crater in a hard, dry rock medium.

2.1.2 Site Description. The site selected for Project Dugout was Buckboard Mesa in Area 18 of the Nevada Test Site. This basalt-capped Mesa had been the site of two chemical explosive cratering experiments, Projects Buckboard and Pre-Schooner, and of the Danny Boy nuclear cratering experiment (Refs. 1, 2, 3). The geology of Buckboard Mesa has been extensively investigated and reported (Refs. 4, 5). It is briefly described in the following paragraph:

Buckboard Mesa was formed by the differential erosion of a moderately fractured thick basalt, capping older tuffs and alluvium deposits. This basalt cap has a biconvex shape in cross section, being thickest along its northwest-southeast trending

axis and thinning rapidly toward the edges of the mesa. A maximum thickness of 248 ft of basalt has been drilled near the center of the mesa. Typically the basalt consists of a succession of several alternating layers of vesicular and dense basalt, with minor lenses of cinders being frequently encountered. A residual soil has been developed over the mesa, and although it averages less than 3 m, it locally may approach 7 m in thickness.

The physical properties of the Buckboard Mesa basalt are discussed in References 1 and 5.

2.1.3 Background. A number of small-scale high-explosive row charge cratering experiments in alluvial materials have been conducted in recent years as a part of the Plowshare program. The most important of these experiments, from the standpoint of contribution to Project Dugout, are listed in Table 2.1. Their results have led to several conclusions concerning cratering with row charges in dry alluvial materials:

(1) The spacing between charges can be related to the radius of the crater resulting from the detonation of a single charge of the same weight at the same depth of burst. At a depth of burst 15% deeper than optimum, spacing the charges approximately one single-charge crater radius apart results in a smooth, linear crater about 10% wider and 25% deeper than the single-charge crater at the same depth of burst. A spacing of 1.25 radii produces a ditch almost as smooth but which has dimensions that are only slightly larger than the single-charge crater. Curves for the enhancement of the crater dimensions developed from the Pre-Buggy results are shown in Figs. 2.1 and 2.2.

(2) The lip on the side of the row crater is much larger than the single-charge crater lip. The increase over the single-charge crater lip varies with both depth of burst and spacing. At one-radius spacing and a depth of burst 15% deeper than optimum, the row crater lip is about 2.3 times as high as the single-charge

TABLE 2.1 APPLICABLE ROW-CHARGE CRATERING EXPERIENCE

Project	Agency	Date	Location	Medium	No. of rows	Charge weight (lb)	No. of Charges in row	Remarks
	Sandia	1959 thru 1962	Near Albuquerque, New Mexico	Fan delta alluvium	34 4 2	8 8 256	7 9 8	Under direction of L. J. Vortman
Toboggan	Sandia	1959-1960	Yucca Flat, NTS	Playa	5 1	8 256	6 6	Part of an extensive series of line-charge detonations
Rowboat	LRL	1961	Area 10, NTS	Desert alluvium	1 7	278 278	3 4	
Pre-Buggy I	NCG	1962-1963	Area 5, NTS	Desert alluvium	4	1000	5	
Pre-Buggy II	LRL	1963	Area 5, NTS	Desert alluvium	5 1	1000 1000	5 13	

Notes: All charges except Pre-Buggy were cast TNT spheres. The 1000-lb Pre-Buggy charges were the liquid explosive nitromethane contained in spun aluminum spheres.

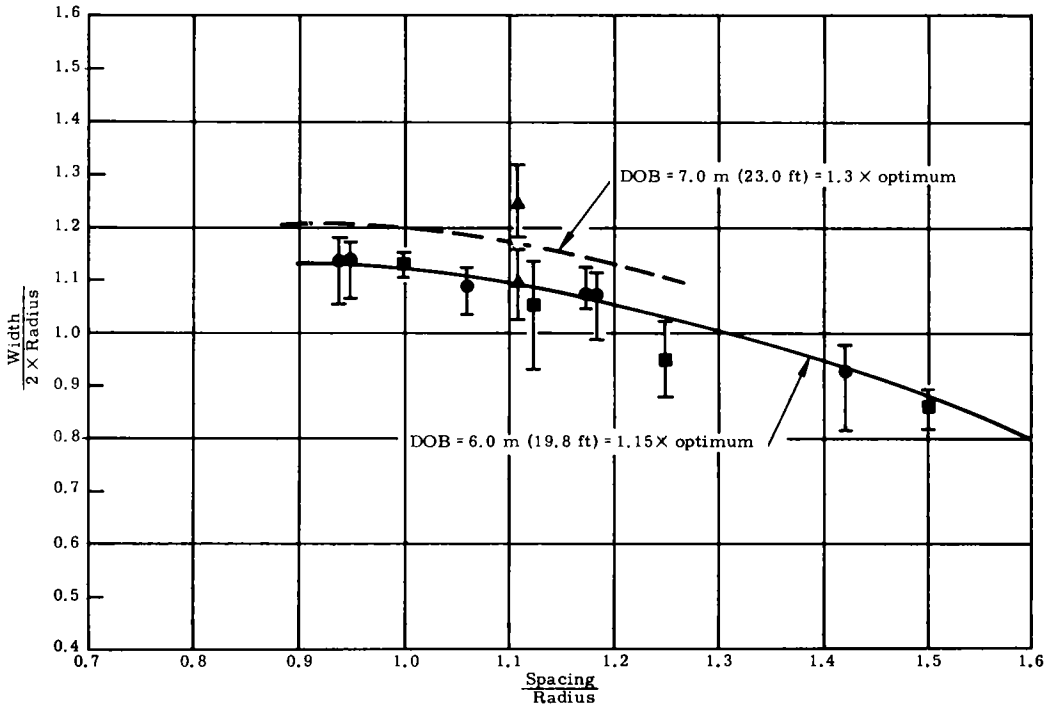

Fig. 2.1 Comparison of row-charge and single-charge crater width in alluvium.

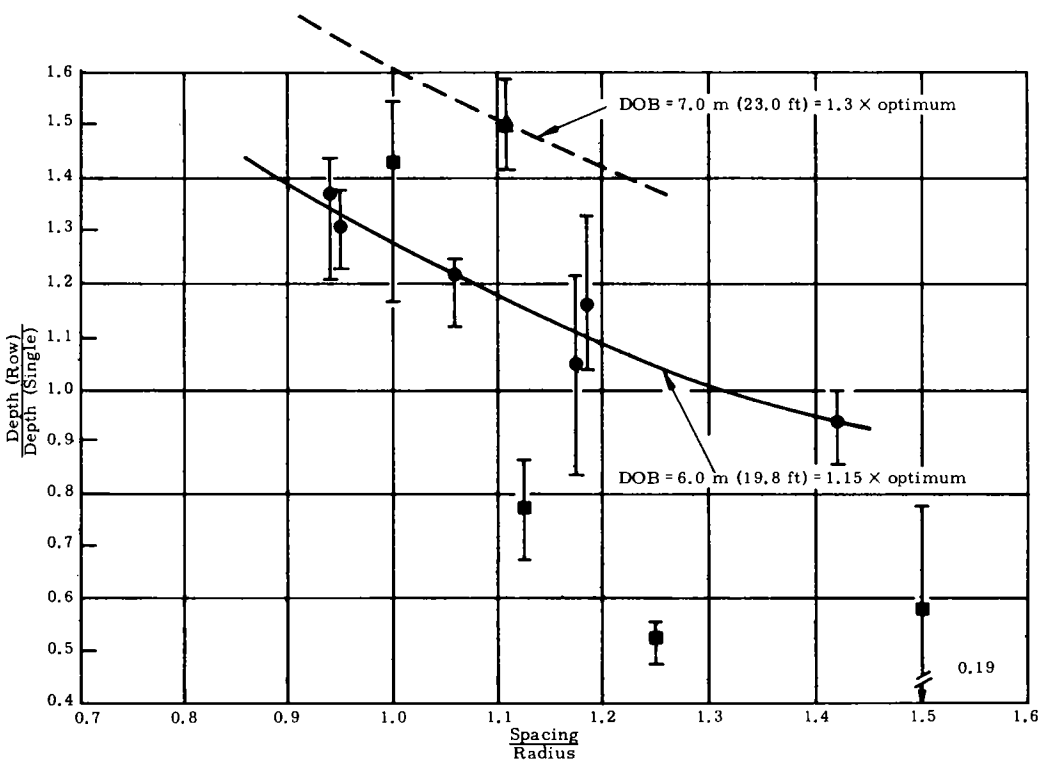

Fig. 2.2 Comparison of row-charge and single-charge crater depth in alluvium.

crater lip. The width of the row crater lip is about 1.5 times the crater width, or about twice the width to be expected for the lip of a single-charge crater. The height and horizontal extent of the lip at the end of the row crater are somewhat less than for the single-crater lip.

(3) The cross section of the row charge crater can be approximated quite well by a hyperbola in which the slope of the asymptotes is the same as the tangent of the angle of internal friction of the material. The shape of the single-charge crater appears to be best approximated by a paraboloid.

One of the important objectives of Project Dugout was to learn whether or not the same relationships hold true for craters in rock.

2.1.4 Comparison of Craters in Alluvium and Basalt. It was apparent that prediction of the dimensions of the Dugout crater had to be based upon the relationships between row-charge and single-charge craters developed for alluvium and upon the dimensions of single-charge craters in basalt. Such a prediction had to take into account the differences between craters in alluvium and in basalt. The high explosive cratering curves for single charges in alluvium and basalt are shown in Fig. 2.3 (Refs. 2 and 6). As would be expected, the basalt craters are smaller than craters in alluvium made by the detonation of the same weight charge at the same depth. The basalt craters are deeper relative to their radius than are the alluvium craters, and are therefore more nearly conical in shape, while the alluvium craters tend to be more paraboloid in shape. This difference in shape is believed to be due to the fact that slopes will stand on a steeper angle in rock than in alluvium.

Figure 2.3 also shows that at depths of burst deeper than optimum, the basalt curves drop to zero more more rapidly than do those for alluvium. This results from the "bulking," or

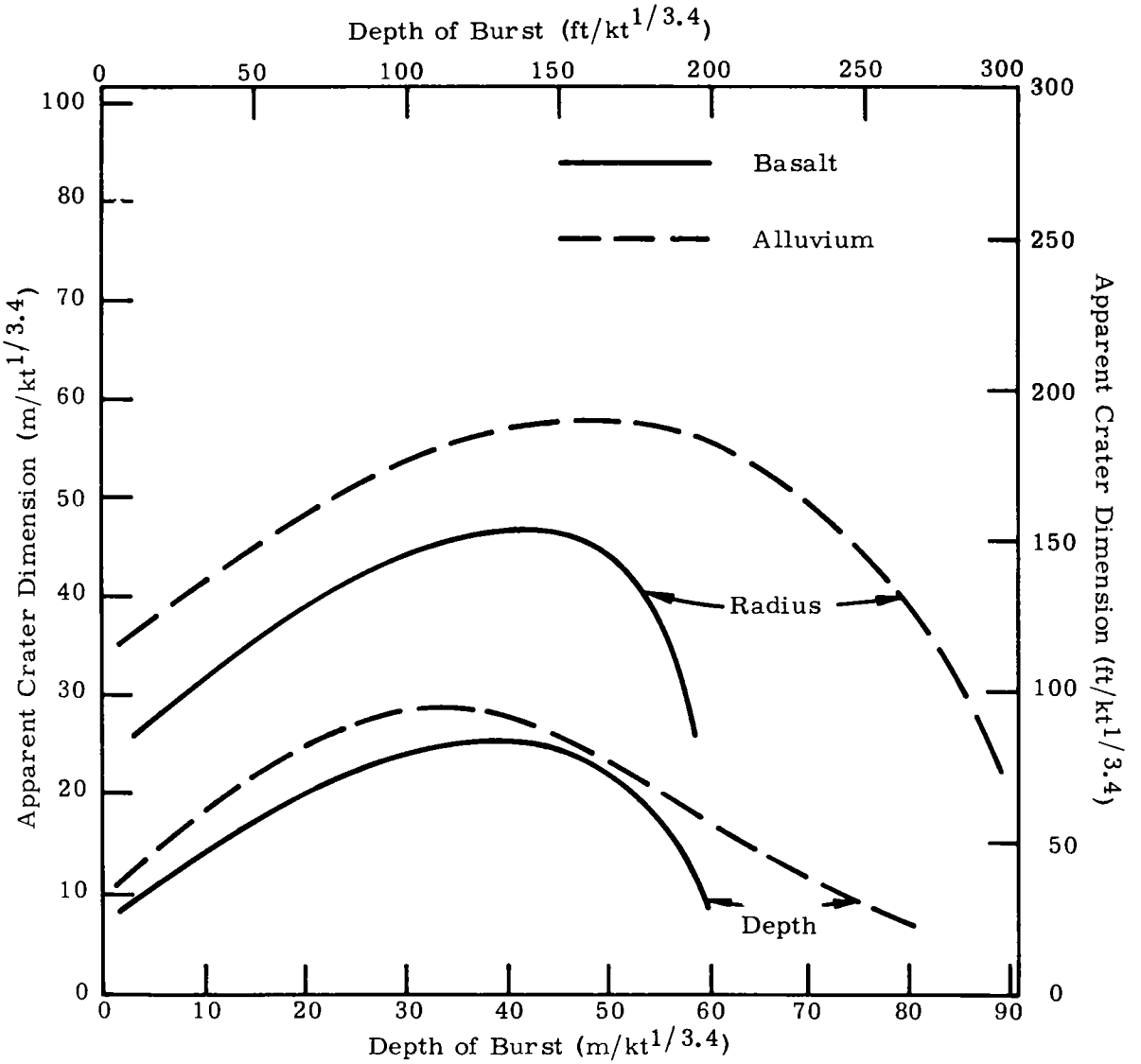

Fig. 2.3 Alluvium and basalt single-charge cratering curves.

increase in volume of the loose rock over its original volume in place. At deeper depths of burst, where proportionately less material is ejected, this increased volume fills the true crater much more rapidly than does the alluvial material. For the basalt of Buckboard Mesa, the increase in volume is variously estimated to be from 25 to 65% (Refs. 7 and 8), and appears to decrease with increasing yield. Nevada Test Site desert alluvium demonstrates almost no bulking when cratered.

Another major difference between the craters in alluvium and in basalt is the lip height. The apparent lip height can be correlated quite well with the crater radius. For craters of all sizes in alluvium it averages about 0.1 radius (Ref. 9); for those recorded in basalt it is about 0.2 the radius. This increase in the lip height in basalt is due both to an increase in the upthrust and to bulking.

2.1.5 Cratering Experience on Buckboard Mesa. Two chemical-explosive cratering experiments had been previously carried out in the basalt of Buckboard Mesa. Project Buckboard (Ref. 1), executed by the Sandia Corporation in 1960, included ten 454-kg shots at five depths of burst, and three 20-ton shots at scaled burst depths of 24, 41, and 56 $m/kt^{1/3.4}$ (80, 135, and 185 $ft/kt^{1/3.4}$). The 20-ton charges were made up of cast TNT blocks stacked to approximate a sphere. Project Pre-Schooner was the detonation of four 20-ton nitromethane charges at scaled depths of 24, 49, 56, and 64 $m/kt^{1/3.4}$ (135, 160, 185, and 210 $ft/kt^{1/3.4}$). The charges were identical with those to be used for Dugout, and the Alfa shot had the same depth of burst as that planned for Dugout, 56 $m/kt^{1/3.4}$ (185 $ft/kt^{1/3.4}$).

The dimensions of the Pre-Schooner Alfa crater were:

Radius:	15.3 m	(50.3 ft)
Depth:	7.0 m	(22.9 ft)
Volume:	215.0 m^3	(2810 yd^3)
Lip height:	3.5 m	(11.5 ft)

A number of factors cast doubt upon the validity of this crater as a meaningful data point. The growth of the dome over the charge and venting observed by high-speed photography indicated the presence of a large vertical fracture, and the crater was somewhat egg-shaped with a high lip and little throwout on one side. The Buckboard 13 crater at the same depth of burst had a much smaller radius and depth, 11.2 m (36.8 ft) and 4.9 m (16.2 ft), respectively. The Pre-Schooner Charlie shot, buried only 2.4 m (8 ft) deeper, produced no crater at all.

2.2 EXPERIMENTAL PROCEDURES

Preshot investigations consisted of exploratory drilling to locate the most suitable site, drilling at the selected site to determine the structure and properties of the basalt, and aerial topographic mapping to establish the configuration of the preshot ground surface.

Site selection investigations for Project Dugout were performed by WES and consisted of the drilling of 14 NX core holes in three general areas described as follows (see Fig. 2.4):

(1) Area #1, 500-ft radius circle with the center at N 852,900; E 594,000.

(2) Area #2, 500-ft radius circle with the center at N854,500; E 591,500.

(3) Area #3, 500-ft radius circle with the center at N 854,900; E 590,300.

The site selection investigation method consisted of drilling 3 NX holes on a line with a length of 107 m. The holes were drilled to a depth of 37 m, or about twice the planned depth of burst for each charge. The criteria which controlled site selection were:

(1) Suitable topography.

(2) Depth of overburden less than 3 m.

(3) No thick layers of highly vesicular basalt, ZP to be in dense basalt.

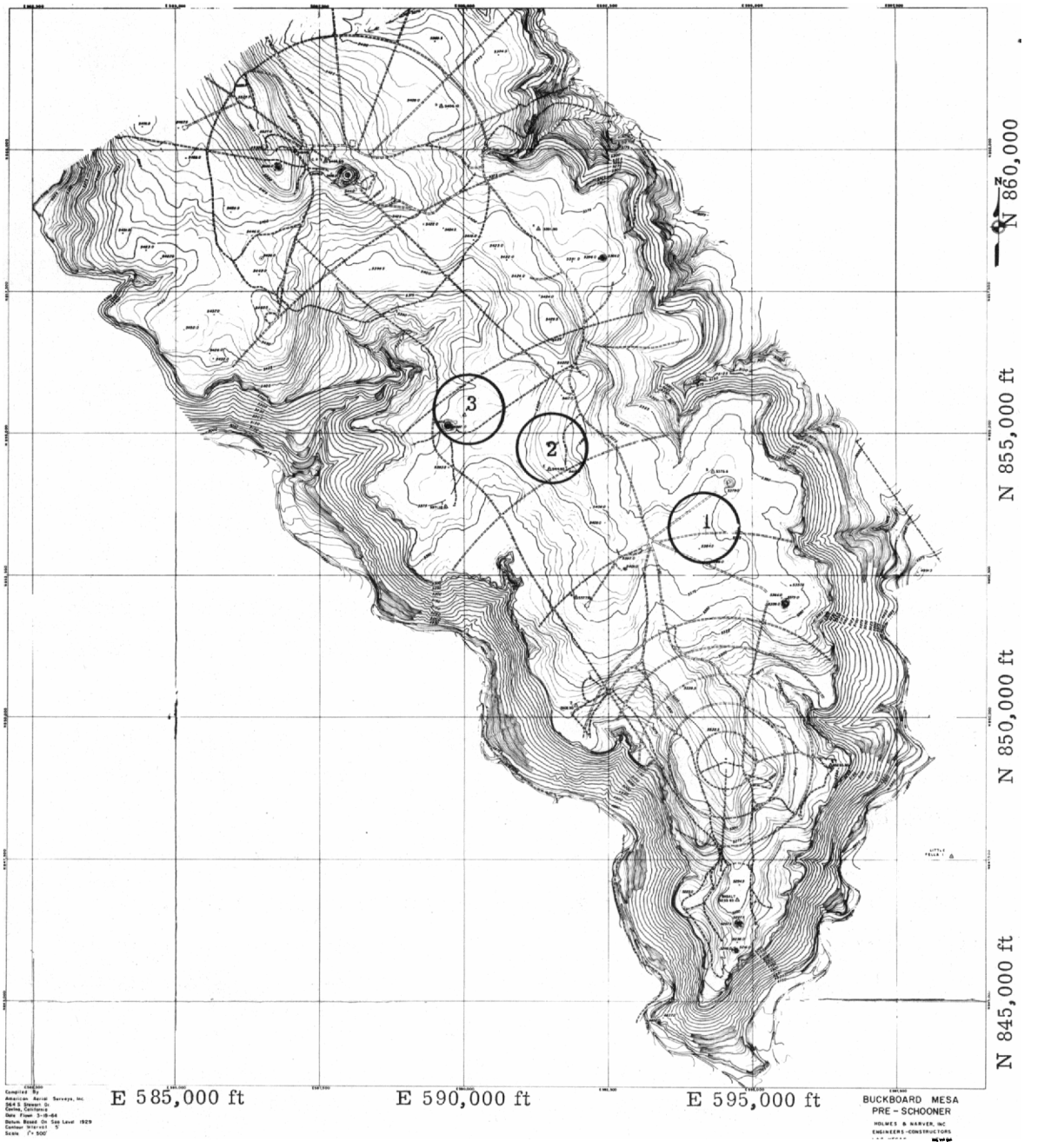

Fig. 2.4 Buckboard Mesa map.

(4) Cinder zones to be minimal in occurrence and not more than 30 cm thick.

(5) Fracturing should be slight to moderate.

Area #3 was eliminated due to excessive overburden. Acceptable lines were located in Areas #1 and #2. The line in Area #1 was chosen for the experiment.

An extensive drilling program was conducted as part of the on-site preshot investigations, Project Dugout. Twelve vertical and two inclined NX-size borings were drilled (see Fig. 2.5), logged lithologically, and photographed with a borehole camera. The five emplacement and five auxiliary 36-in. calyx holes were also lithologically logged and were photographed.

The geologic conditions of the Dugout site were relatively simple and were in close accord with the regional geologic picture of Buckboard Mesa. Of the 24 borings drilled at the site, only one (NCG-36) penetrated the basalt cap of the mesa at a depth of 57 m. The basalt consisted of an alternating succession of vesicular and dense basalt layers (Figs. 2.6 and 2.7) that were variable in thickness; however, the over-all thickness of the basalt cap remained fairly constant over the test site. As shown by sections A'-A' and B'-B', the basalt cap, consisting of three vesicular basalt layers and two intervening dense basalt layers, was masked by residual soil that varies from 1 to 4 m in thickness. The upper vesicular zone was separated from the underlying dense basalt by a transition zone that contains less than 20% vesicules and varies from 1 to 5 m in thickness. The middle and lower vesicular basalt layers were topped by a thin cinder zone. Tuff was found to be present beneath the lower vesicular basalt zone between 57 and 61 m in depth.

The results and analysis of the various lithologic and photographic logs, along with a more thorough description of the procedures employed in instrumenting the five auxiliary calyx holes, will be included in PNE 601F.

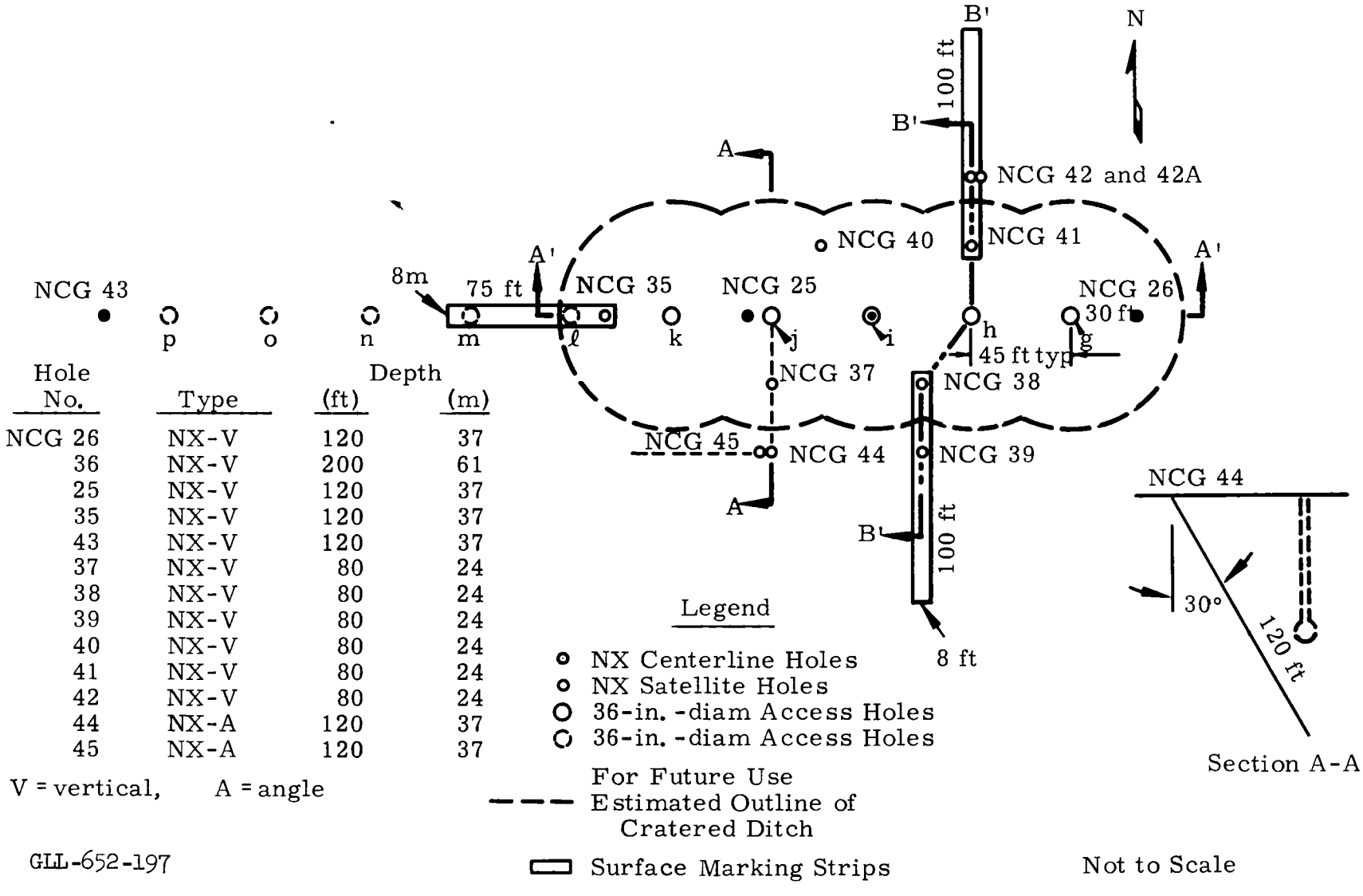

Hole No.	Type	Depth (ft)	Depth (m)
NCG 26	NX-V	120	37
36	NX-V	200	61
25	NX-V	120	37
35	NX-V	120	37
43	NX-V	120	37
37	NX-V	80	24
38	NX-V	80	24
39	NX-V	80	24
40	NX-V	80	24
41	NX-V	80	24
42	NX-V	80	24
44	NX-A	120	37
45	NX-A	120	37

V = vertical, A = angle

GLL-652-197

Fig. 2.5 Plan location of preshot investigation.

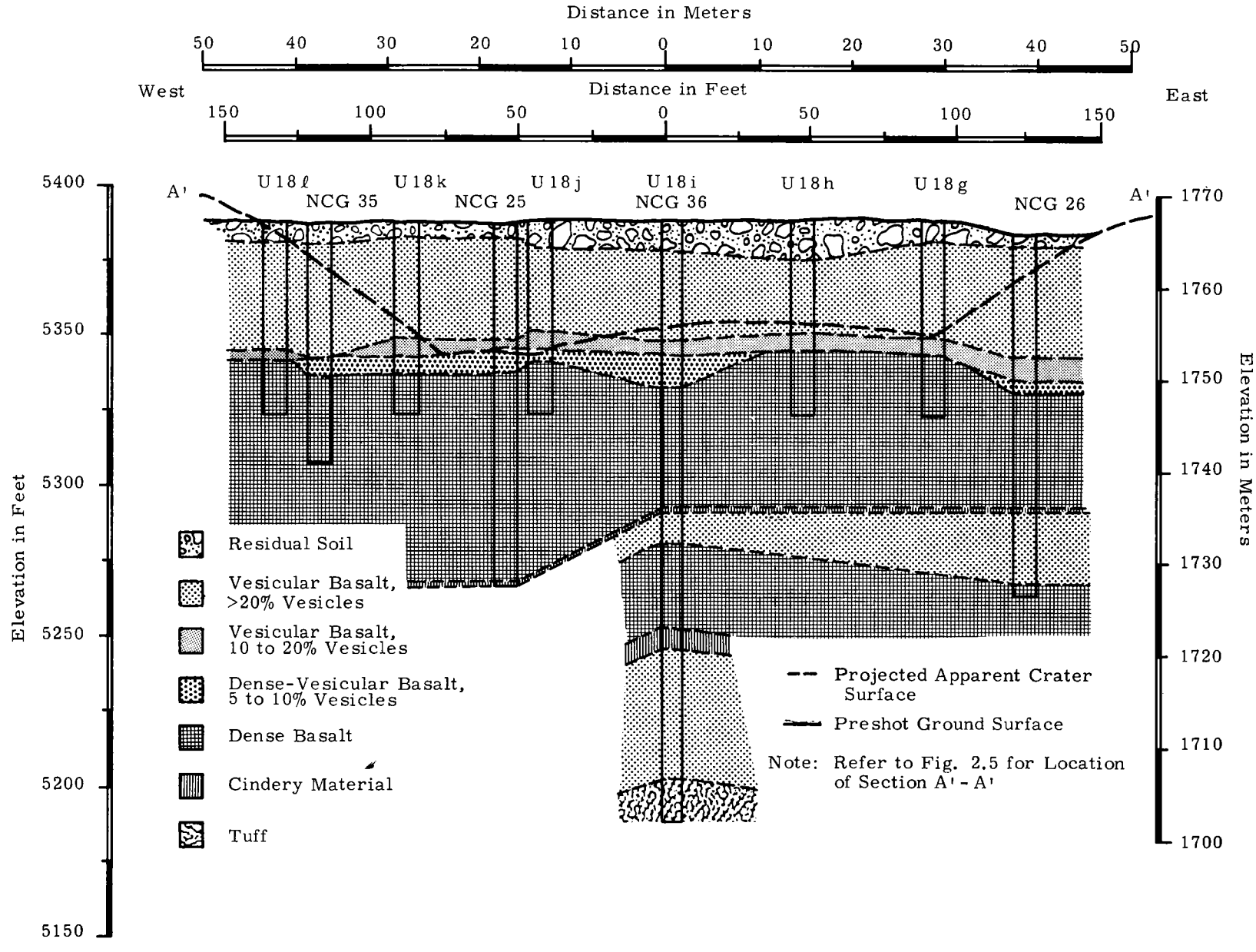

Fig. 2.6 Geologic section of the Dugout site – section A'-A'.

GLL-652-198

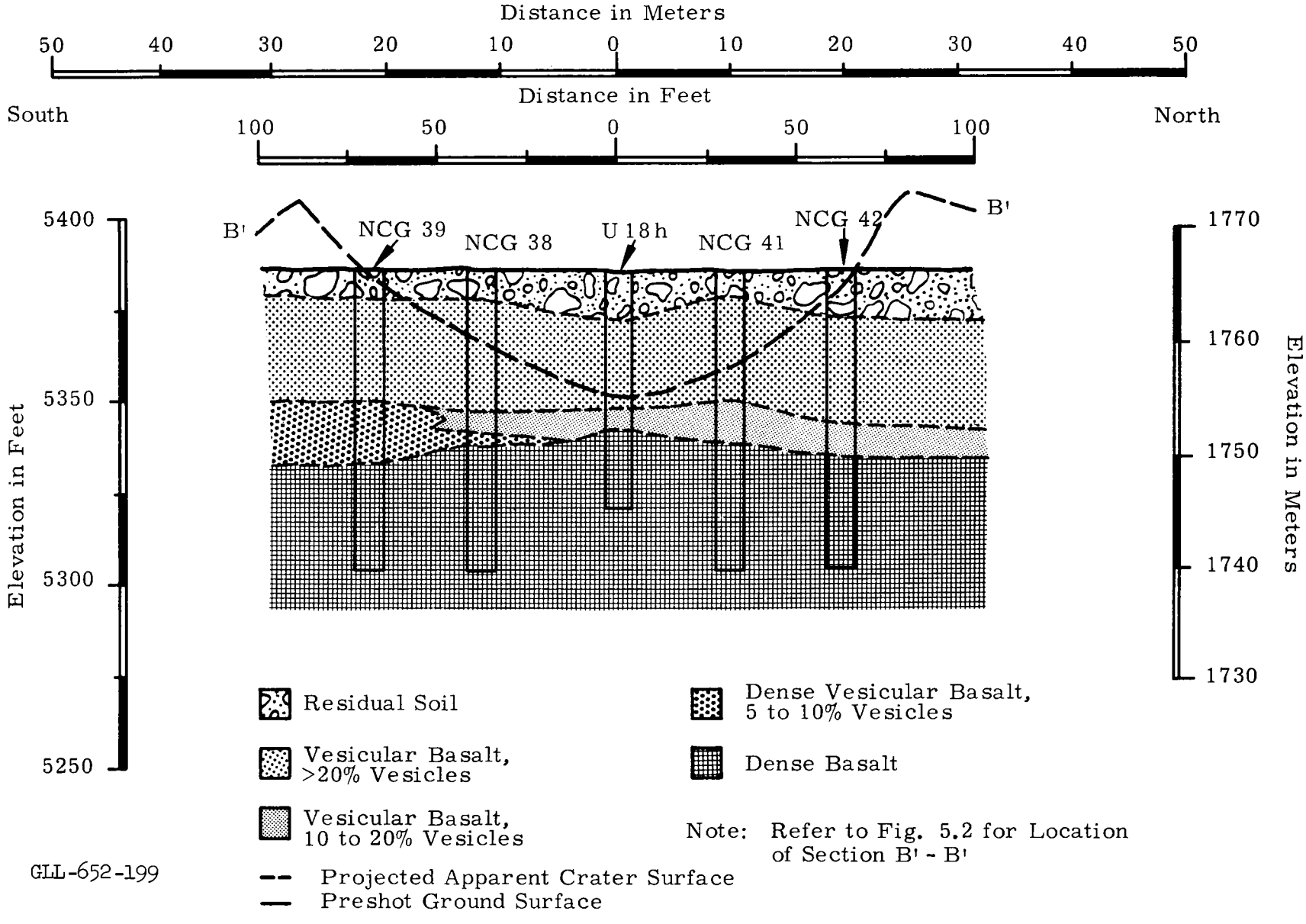

Fig. 2.7 Geologic section of the Dugout site — section B' - B'.

2.3 PREDICTED RESULTS

The depth of burst selected for Dugout was 18 m (59 ft). This is a scaled depth of burst of 56 m/kt$^{1/3.4}$ (185 ft/kt$^{1/3.4}$), about 32% deeper than optimum burial for radius. There had been two 20-ton shots at this depth in Buckboard Mesa to provide single-crater dimensions and the data from Pre-Buggy to indicate the differences between single-charge craters and row-charge craters.

(1) Based on the dimensions of the Pre-Schooner Alfa crater,

Radius = 15.3 m (50.3 ft), Depth = 7.0 m (22.9 ft).

Hence the spacing of 13.7 m (45 ft) that was used, in terms of single charge crater radii, was

$$S = 13.7/15.3 = 0.895.$$

From Figs. 2.1 and 2.2, the expected enhancement over single-crater dimensions was approximately

$$E_w = 1.2, \qquad E_d = 1.7,$$

where E_w is a factor for the enhancement of the row-crater width over single-charge crater width, and E_d a similar factor for depth. Therefore

Width, $W = 2\,(15.3)(1.2) = 37$ m (121 ft); Depth, $d = 7.0\,(1.7) = 11.9$ m (38.9 ft).

(2) Based on the dimensions of the Buckboard 13 crater,

Radius = 11.2 m (36.8 ft), Depth = 4.9 m (16.2 ft),

and $S = 13.7/11.2 = 1.22.$

From Figs. 2.1 and 2.2, $E_w = 1.12$ and $E_d = 1.4$. Thus

$w = 2(11.2)(1.12) = 25$ m (82.4 ft); $d = 4.9\,(0.14) = 6.9$ m (22.7 ft).

(3) Based on the basalt curve,

Radius = 13.3 m (43.6 ft) Depth = 6.2 m (20.2 ft)

$$S = 13.7/13.3 = 1.03.$$

From Figs. 2.1 and 2.2, $E_w = 1.18$ $E_d = 1.57$

$w = 2\ (13.3)(1.18)$ $d = 6.2\ (1.57)$

$= 31.4$ m (103 ft); $= 9.7$ m (31.7 ft).

It is believed that the cavities about each charge grow and eventually coalesce prior to venting, and that this accounts for much of the enhancement in dimensions of row craters over those of the equivalent single craters. Examination of colored sand columns in the Pre-Buggy I craters indicates that the maximum cavity radius was about 2 m, approximately four times the original radius of the charge (Ref. 10). Based upon a study of the cratering properties of nitromethane, the maximum lower cavity radius for Dugout was predicted to be 2 m (Ref. 11), compared with an initial charge radius of 1.57 m (5.15 ft). This indicated that coalescing of the cavities prior to venting was unlikely, and that the average dimensions could have been considerably smaller than those predicted above. This would have produced a scalloped crater with the appearance of a row of partially joined single craters. Such an effect would have reduced the average depth more than the average width.

The height of the lip on the sides of the crater, based upon Pre-Buggy II, was expected to be 2.6 to 2.7 times the height of the single crater lip. The height of the lip of Pre-Schooner Alfa and Buckboard 13 were almost 3.5 to 3.6 m high, leading to a prediction for lip height for the Dugout crater of 9 to 10 m (30 to 32 ft). The lips of the Pre-Buggy craters showed evidence of progressive failure until the natural angle of repose was reached. These failures deposited more material in the bottom of the craters, decreasing the depth. Although steeper angles of repose may be expected in basalt, it was logical to expect some reduction in the depth of the crater.

Based upon the considerations given above and the figures developed in previous paragraphs, a width of 30 m (100 ft) and a

depth of 7.5 m (25 ft) were predicted. The spread in the hard rock cratering data indicated that uncertainties of about 20% should be attached to these predictions. In summary, the predictions were:

Width	30 ± 6 m	100 ± 20 ft
Depth	7.5 ± 1.5 m	25 ± 5 ft
Lip height	9.5 ± 1.9 m	31 ± 5 ft

2.4 RESULTS

Figures 2.8 and 2.9 are general views of the crater. Figure 2.10 shows the interior of the crater looking southwest from the eastern end. The large size of many of the blocks is quite obvious, as is the relative flatness of the side slopes. Figure 2.11 is the topographic map of the crater. The cross section of the crater at its center, U 18i, is shown in Fig. 2.12, and Fig. 2.13 is its longitudinal profile.

2.4.1 Crater Measurements. The dimensions and shape of the Dugout crater were determined from topographic maps prepared by stereophotogrammetry from aerial photographs. Preshot photography was flown on D - 1 (23 June); postshot photography was made on D + 1 (25 June). The maps were made at a scale of 1 in. = 100 ft with a contour interval of 1 ft. Individual rocks whose average dimensions were greater than 3 ft were contoured separately, all smaller ones were averaged in contouring the crater.

The width, depth, and lip heights at each shot point, and halfway between each shot point are given in Table 2.2. Average dimensions were determined by planimetry as indicated in Fig. 2.14. The center three-fifths of the crater was used for the determination of the average dimensions because that portion of the crater is approximately linear. The average dimensions so obtained are given at the bottom of Table 2.2.

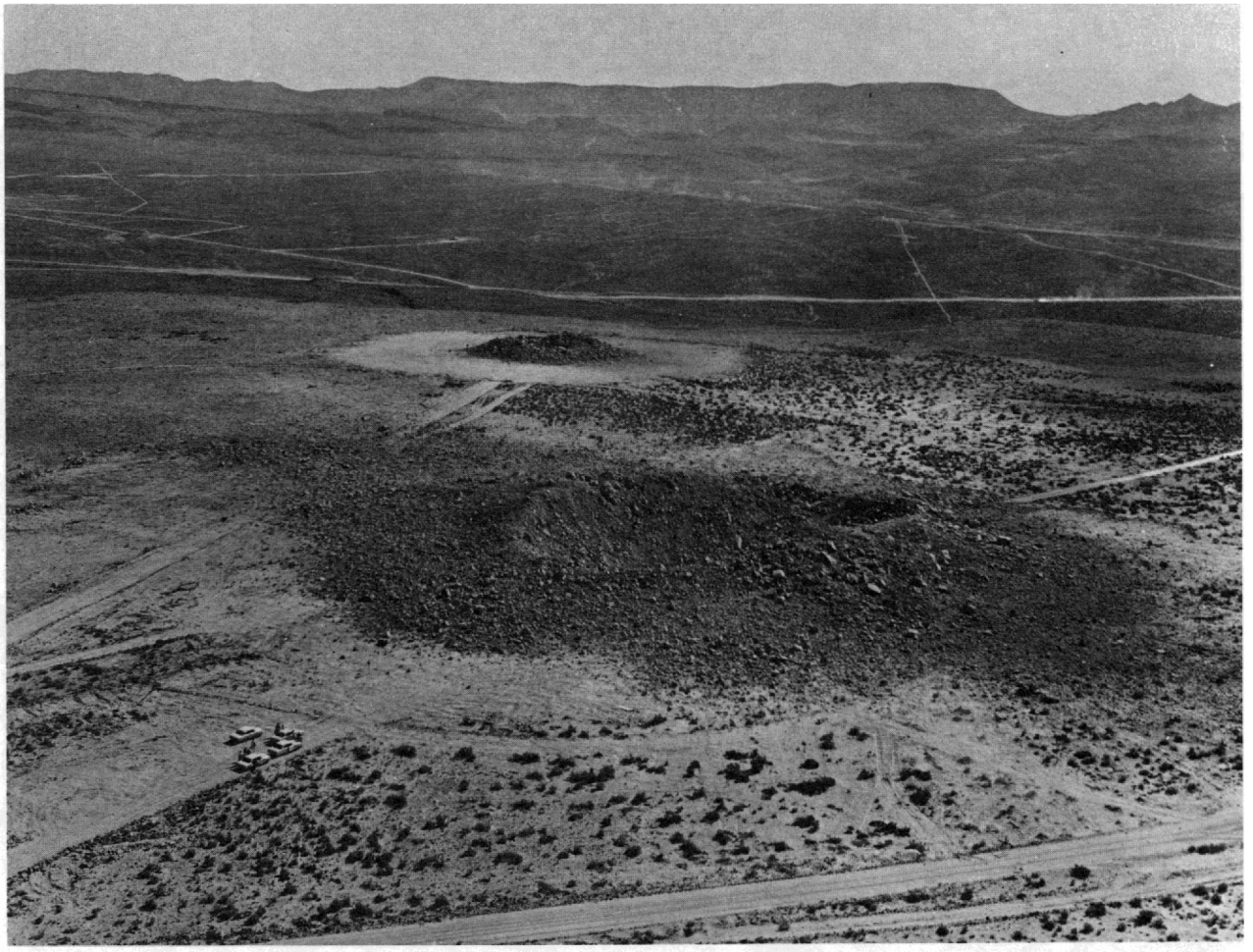

Fig. 2.8 Aerial view of the Dugout crater from the southwest.

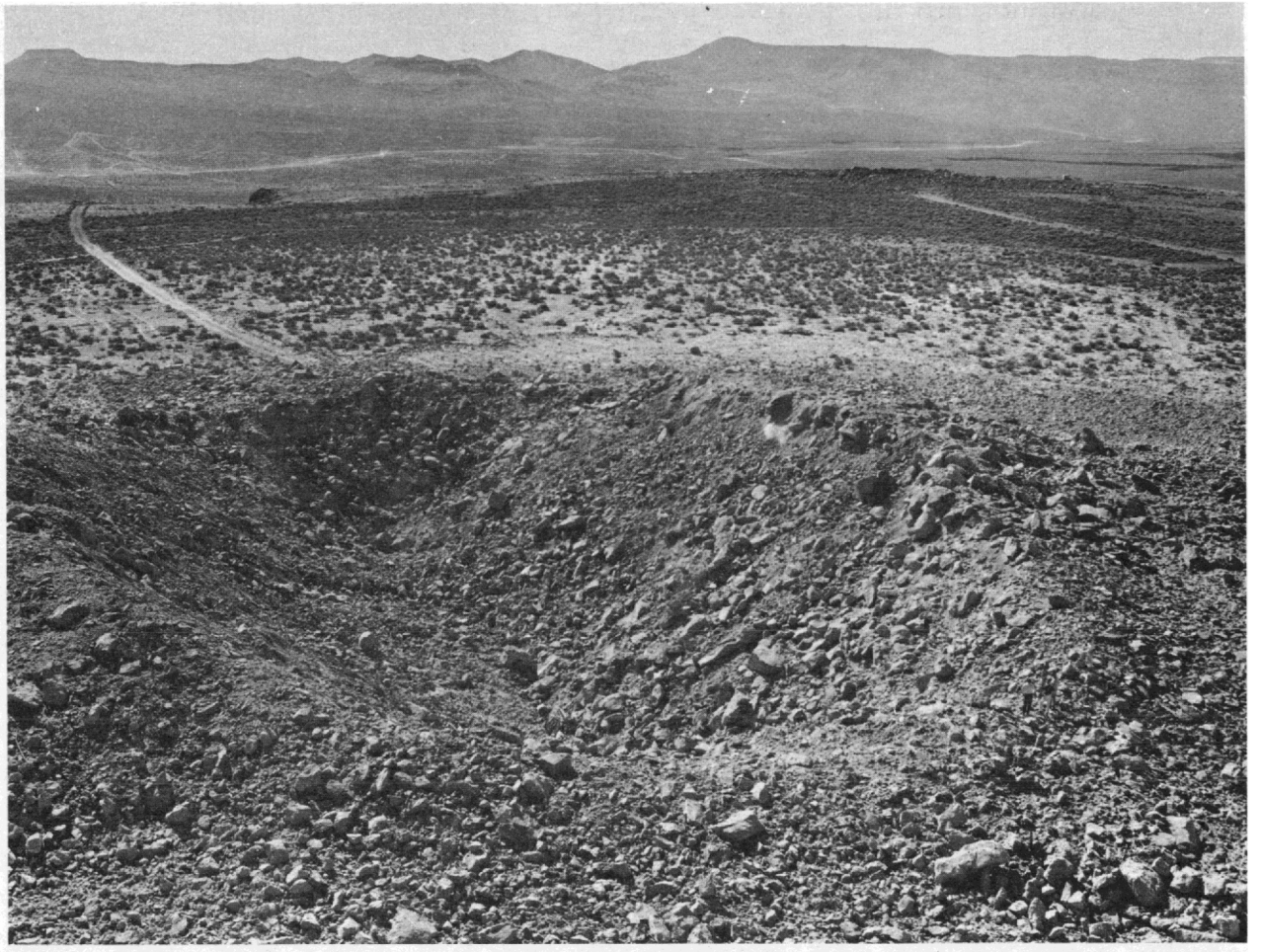

Fig. 2.9 Dugout crater from the west.

Fig. 2.10 Interior of the Dugout crater looking southwest.

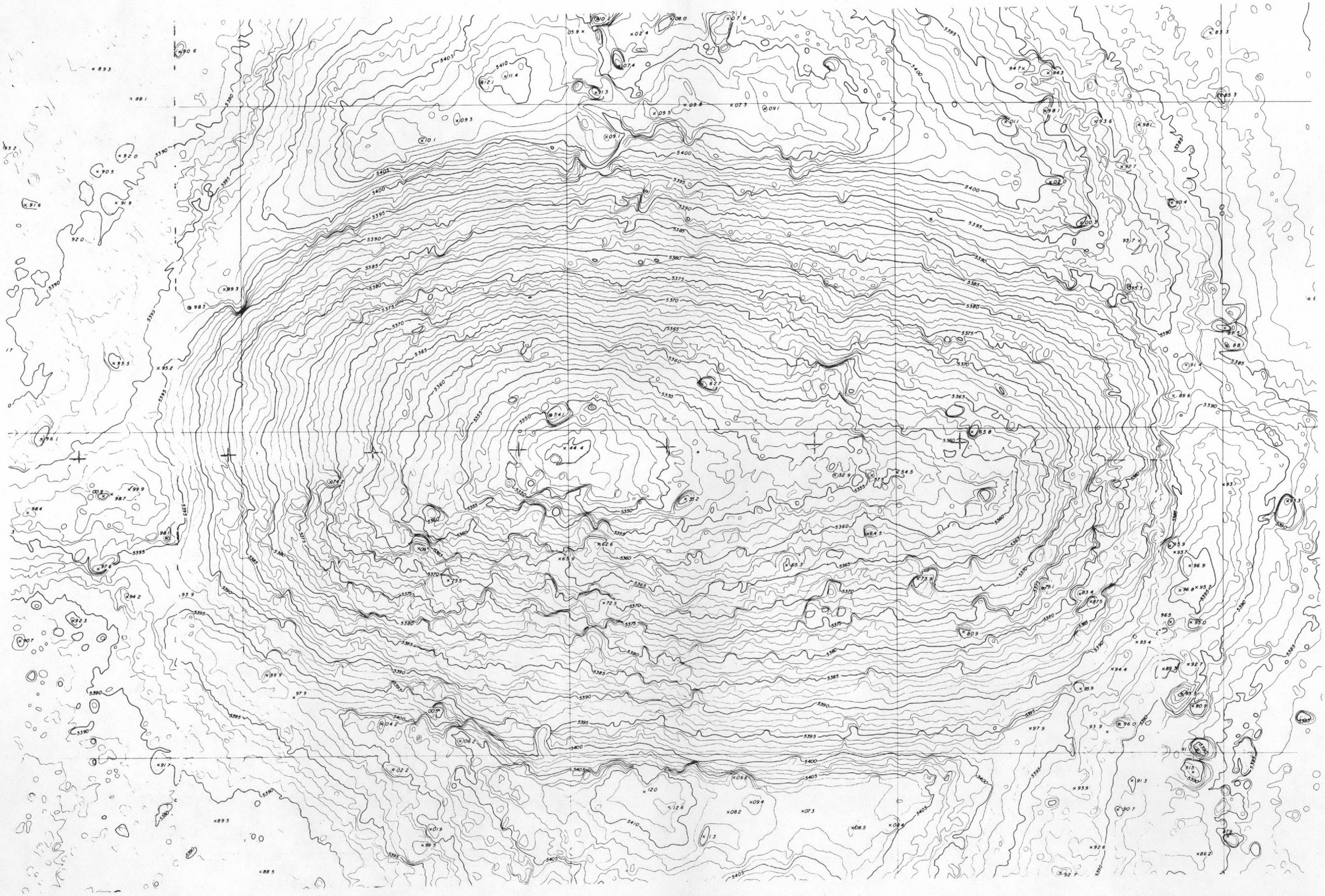

Fig. 2.11 Topographic map of crater.

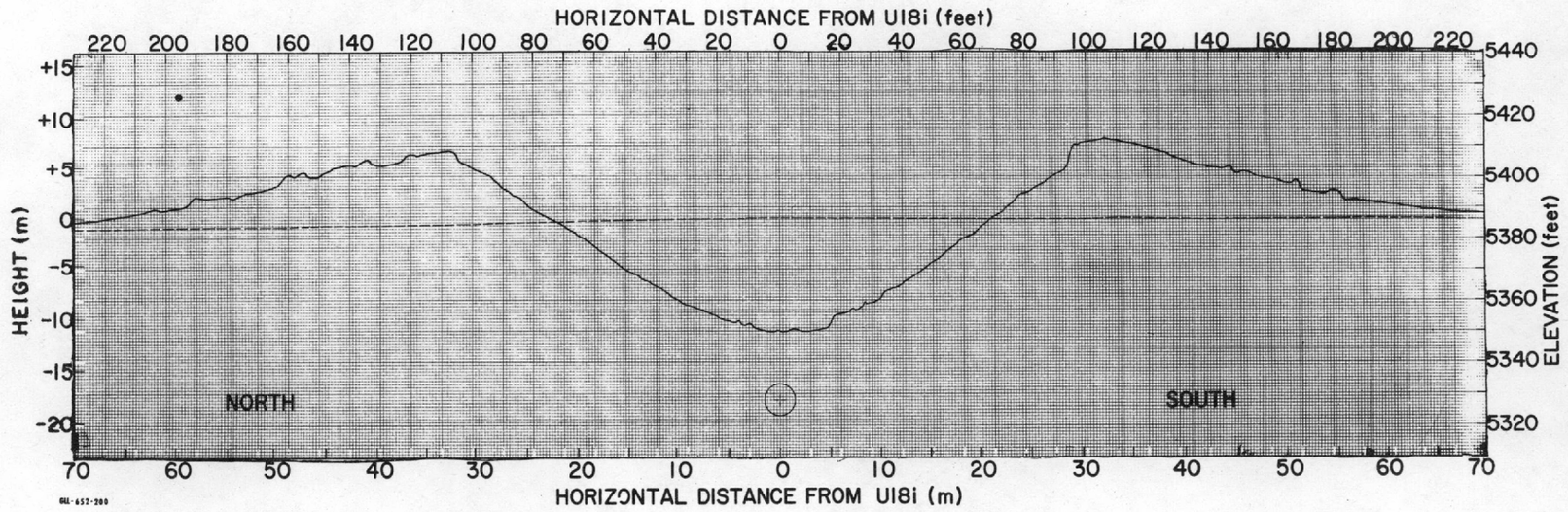

Fig. 2.12 Lateral section of the Dugout crater through U 18i.

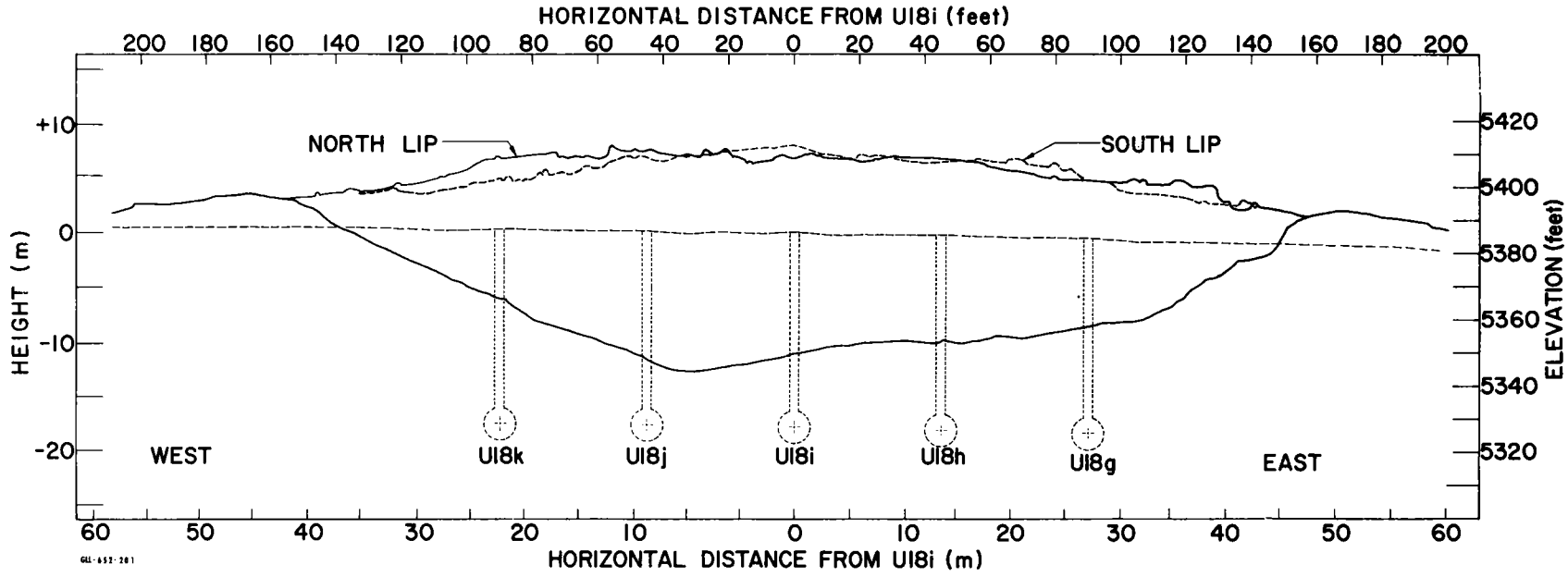

Fig. 2.13 Longitudinal section of crater.

TABLE 2.2 CRATER DIMENSIONS

Station		Width (m)	Width (ft)	Depth (m)	Depth (ft)	N. lip height (m)	N. lip height (ft)	S. lip height (m)	S. lip height (ft)
U18k	90.0 ft (27.4 m) west	36.0	118	6.32	20.9	7.13	23.4	4.69	15.4
	67.5 ft (20.6 m) west	39.6	130	9.27	30.4	7.28	23.9	5.24	17.2
U18j	45.0 ft (13 7 m) west	42.4	139	11.8	38.7	8.02	26.3	6.86	22.5
	22.5 ft (6.9 m) west	43.0	141	12.5	40.9	7.99	26.2	7.48	24.4
U18i	0	43.0	141	11.2	36.6	7.38	24.2	7.96	26.1
	22.5 ft (6.9 m) east	42.1	138	9.88	32.4	7.10	23.3	7.01	23.0
U18h	45.0 ft (13.7 m) east	40.2	132	9.69	31.8	7.56	24.8	6.68	21.9
	67.5 ft (20.6 m) east	37.8	124	9.17	30.1	6.46	21.2	7.10	23.3
U18g	90.0 ft (27.4 m) east	35.4	116	8.02	26.3	5.76	18.9	5.21	17.1
Maximum	6.7 ft (2.0 m) west	43.9	144						
Maximum	31.4 ft (9.6 m) west			12.7	41.7				
Average dimensions:									
(Center 3/5 of crater)		41.6	136	10.7	35.2	7.50	24.6	6.95	22.8

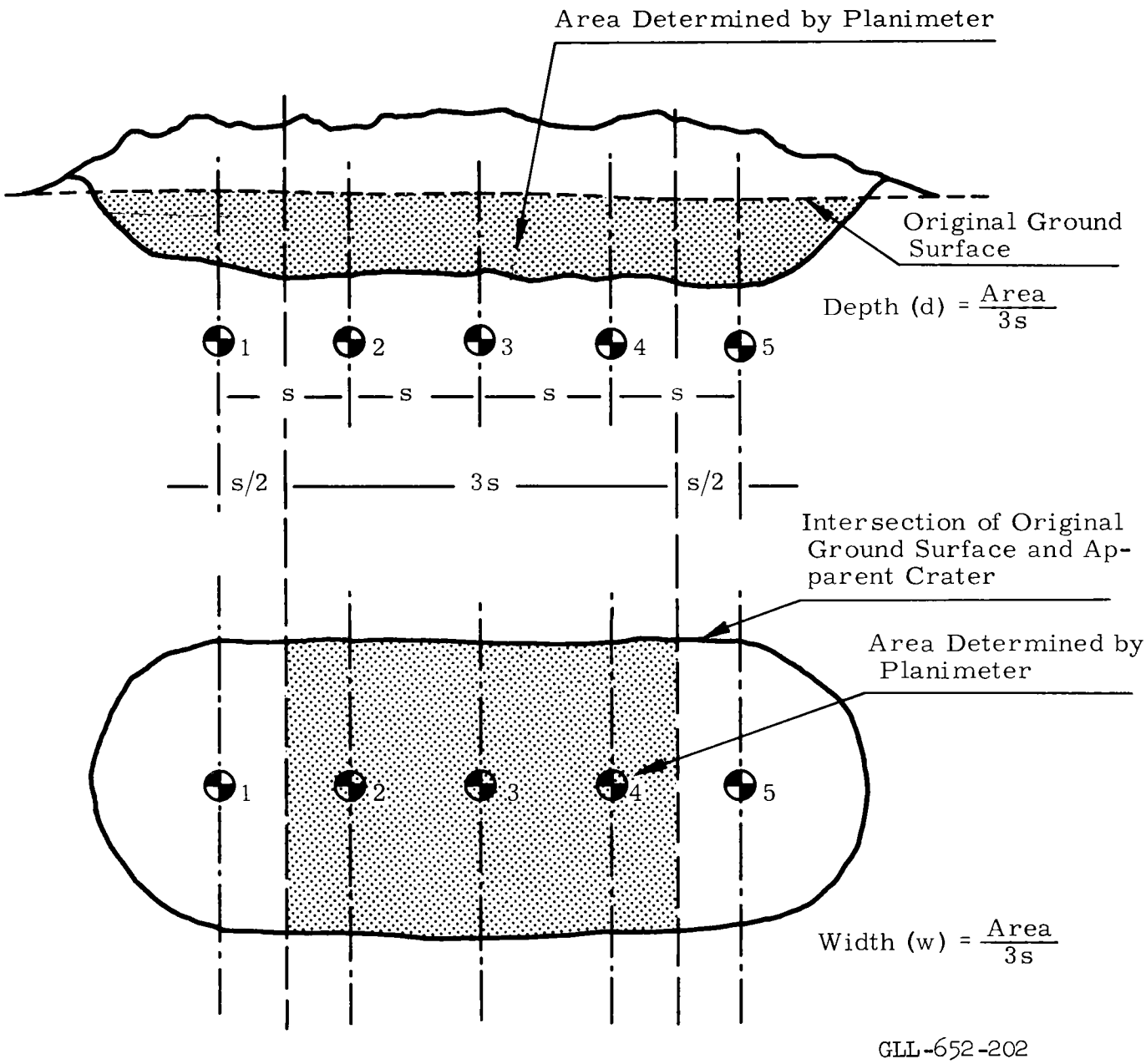

Fig. 2.14 Method of determining average apparent radius and depth.

a. Width. The average width of the center three-fifths of the crater is 41.5 m (136 ft). The greatest width is 44 m (144 ft) at a point 2 m (6.7 ft) west of the center charge, U 18i. Examination of the widths given in Table 2.2 shows that the crater is not completely linear, but is widest near the center and narrows toward the end charges.

b. Depth. The average depth of the center portion of the crater is 10.7 m (35.2 ft). The greatest depth is 12.7 m (41.7 ft) at a point 9.6 m (31.4 ft) west of U 18i. There is great variation in the depth — the depths at the end charges are 6.4 and 8.0 m (20.9 and 26.3 ft), much less than the greatest depth (see Fig. 2.12).

c. Length. The length of the crater along the centerline of the charges is 87.5 m (287 ft). The distance from the west end charge, U 18k, to the edge of the crater is 14.8 m (48.5 ft) from the east end charge, U 18h, to the east end of the crater the distance is 17.7 m (58 ft).

d. Lips. In the center three-fifths of the crater, the average lip heights are 7.5 m (24.6 ft) on the north side and 7.0 m (22.8 ft) on the south side. The maximum lip heights are 8.4 m (27.5 ft) on the north side and 8.0 m (26.1 ft) on the south side. The lips on the ends are much smaller than those on the sides, and are irregular in height. Figure 2.15 is a view of the crater from the west showing the high lips on the sides and the relatively small lip on the end. The greatest lip height on the west end is 3.7 m (12 ft); on the east end it is 4.3 m (14 ft). These heights and irregular section at the ends are somewhat less than would be expected for a single-charge crater at the same scaled depth of burst. Figure 2.16 is a view of the crater from north showing the north lip in profile.

e. Volume. The volume of the apparent crater is 16,080 m^3 (21,030 yd^3). The volume of the linear portion of the crater

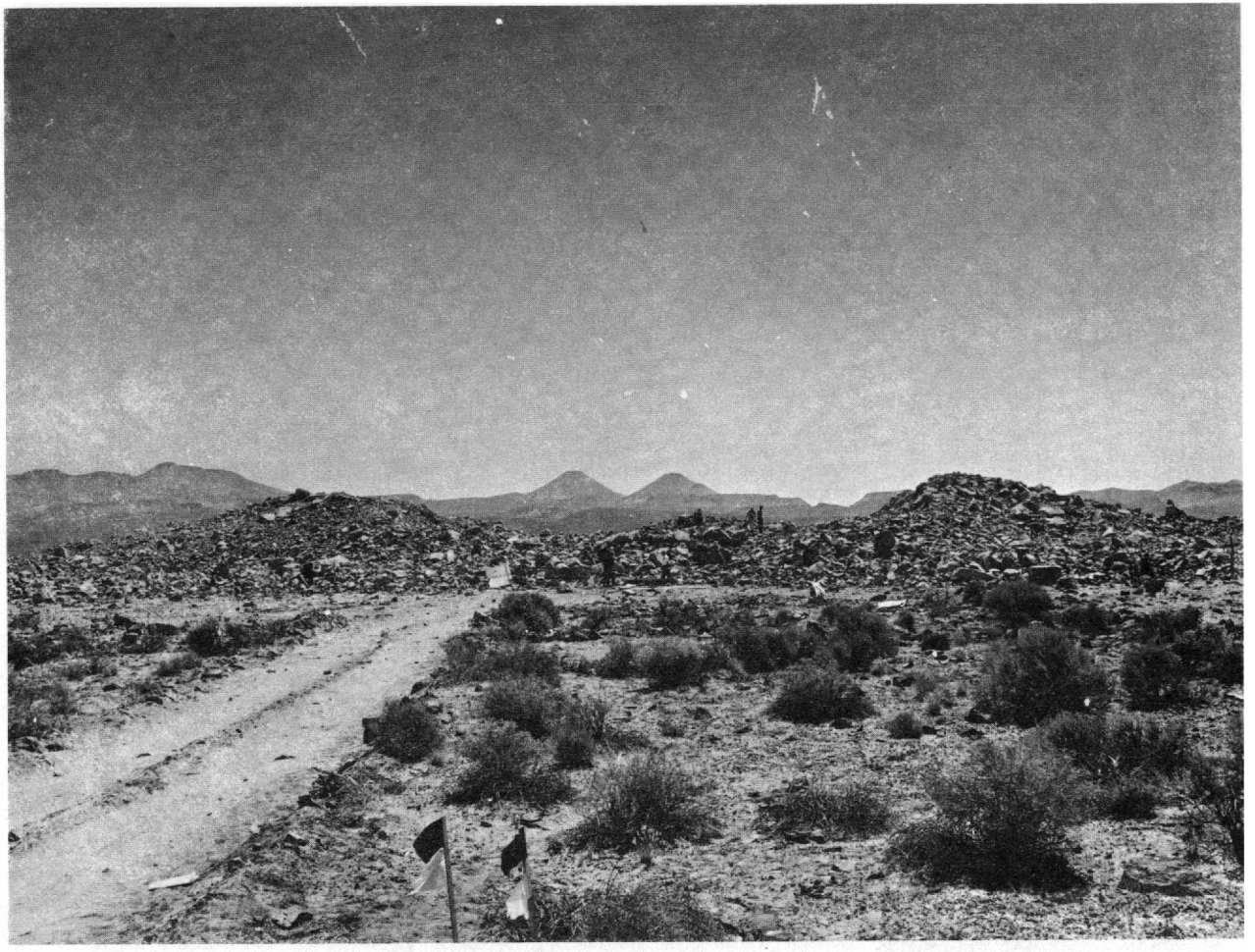

Fig. 2.15 Dugout crater lips from the west.

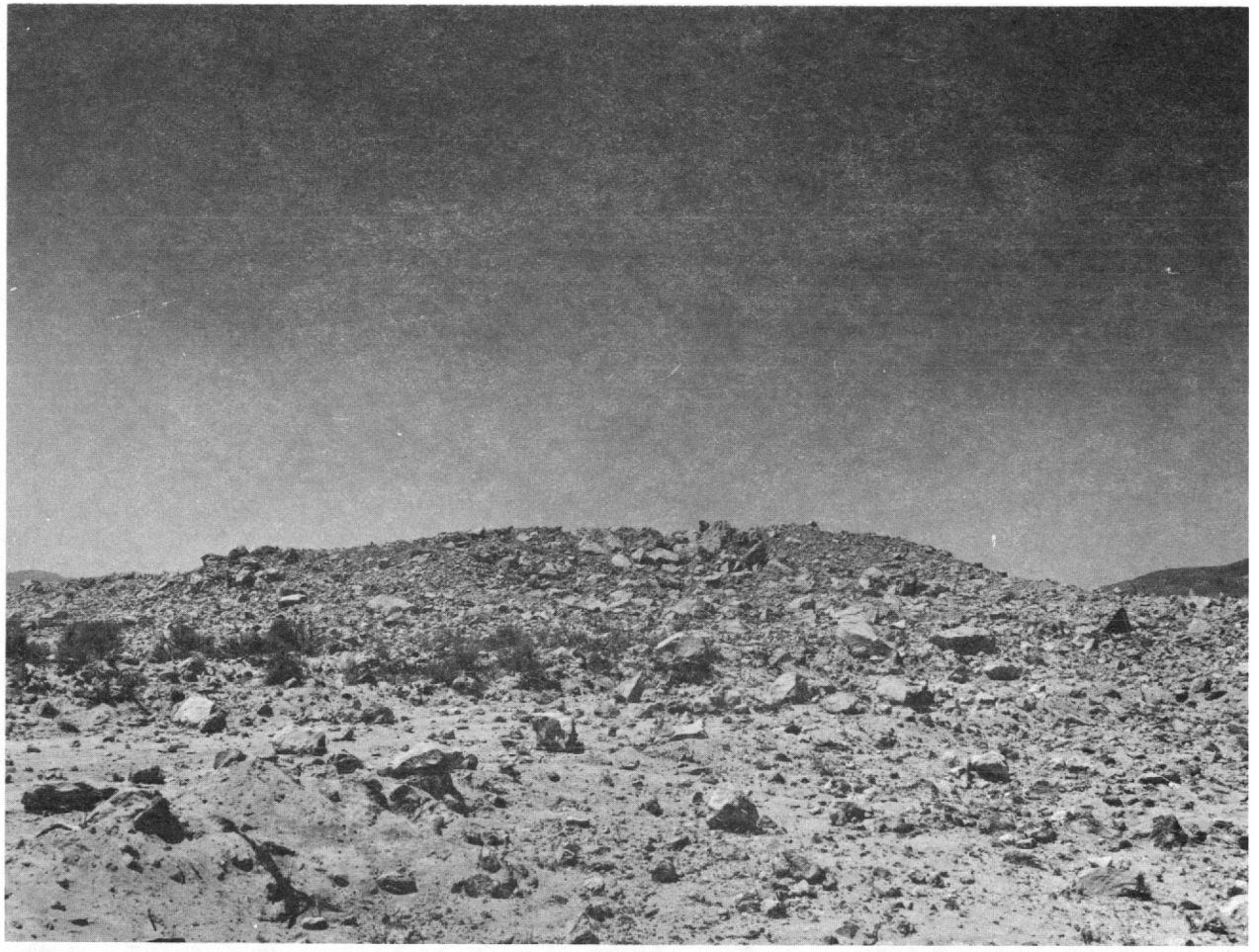

Fig. 2.16 Dugout crater lip from the north.

is 10,938 m^3 (14,295 yd^3), or 3640 m^3 (4765 yd^3) for each of the center three charges. This compares with a volume of 2150 m^3 (2810 yd^3) for Pre-Schooner Alfa.

2.5 PRELIMINARY CONCLUSIONS

The crater is 36.5% wider and 41% deeper than predicted. Two possible explanations present themselves:

a. Partial detonation or burning of the additional nitromethane added to the end charges to replace that which had leaked out. The crater shape, shallow on both ends, does not support this hypothesis, and the size of the natural fractures in the basalt as determined from drilling logs is too small to permit detonation of the NM. For these reasons this explanation does not appear credible.

b. The dimensions of the Pre-Schooner Alfa crater are more nearly correct than those of Buckboard 13. If such be the case, then the 13.7 m spacing (0.895 R) was too close to produce a linear crater. The ellipsoidal crater shape, markedly different from the shape of the Pre-Buggy craters at wider spacings, strongly supports this conclusion. The shape is quite apparent in Fig. 2.11. The Dugout width is 13% greater than would have been predicted using only the Pre-Schooner Alfa crater, and the depth 6% less. The bulking of the fallback, not present in alluvium, easily explains the smaller depth.

The second explanation proposed suggests that consideration be given to altering the basalt single-charge cratering curves. It may also indicate that the enhancement factors developed from Pre-Buggy in alluvium are independent of material.

Investigation of the engineering properties and the true crater will be discussed in the final report by the Waterways Experiment Station, PNE-601.

REFERENCES

1. L. J. Vortman et al., "20-Ton and 1/2-Ton High Explosive Cratering Experiments in Basalt Rock, Project Buckboard, Final Report," SC-4675(RR) Sandia Corporation, 1962.

2. J. L. Spruill, "Project Pre-Schooner, Crater Measurements," PNE-502, U. S. Army Engineer Nuclear Cratering Group, November 1964.

3. M. D. Nordyke and W. Wray, "Cratering and Radioactivity Results from a Nuclear Cratering Detonation in Basalt," UCRL-6999 Rev. II, Lawrence Radiation Laboratory, 1963.

4. D. C. Banks and R. T. Saucier, "Geology of Buckboard Mesa," PNE-5001, U. S. Army Engineer Waterways Experiment Station, July 1964.

5. U. S. Army Engineer Waterways Experiment Station, CE; "Project Danny Boy, Petrographic examination and Physical Tests of Selected Cores," Misc. Paper No. 6-570, January 1963.

6. M. D. Nordyke, "On Cratering, A Brief History, Analysis, and Theory of Cratering," UCRL-6578, Lawrence Radiation Laboratory, August 1961.

7. J. F. Leisek, "Postshot Geologic Investigations of the Danny Boy Nuclear Cratering Experiment in Basalt," UCRL-7803, Lawrence Radiation Laboratory, March 1964.

8. A. D. Frandsen, Unpublished Memorandum, Subject: "Pre-Schooner Postshot Exploration," U. S. Army Engineer Nuclear Cratering Group, 12 October 1964.

9. R. H. Carlson and W. A. Roberts, "Project Sedan: Mass Distribution and Throwout Studies," PNE-217F, The Boeing Company, August 1963.

10. A. D. Rooke and L. K. Davis, "Project Pre-Buggy, Emplacement and Firing of High Explosive Charges and Crater Measurements," PNE-302, U. S. Army Engineer Waterways Experiment Station, to be published.

11. Personal communication from J. Toman, Nuclear Cratering Group.

12. J. L. Spruill, "Project Dugout, Apparent Crater Studies," PNE-601, U. S. Army Engineer Nuclear Cratering Group, to be published.

CHAPTER 3

SURFACE MOTION STUDIES

3.1 INTRODUCTION

Detailed description of the surface motion is desired in order to develop general diagnostic information concerning cratering physics for row-charge events. Surface motion measurements for the Scooter event (Ref. 1) led to the development of a simple, two-dimensional model of cratering for single charge H. E. events in alluvium (Refs. 2, 3). Project Dugout provided a key experiment which may contribute to an extension of this model work to a hard-rock medium and to row-charge events. Final and complete results from Dugout will be found in Reference 9.

Examples of problems under study are: (1) the relative contributions to cratering of hard rock by spall and the gas acceleration phase, (2) the extent of the coalescence of the cavities prior to vent, and (3) end effects on row-charge cratering.

Evaluation of surface motion data of past events has been such a tedious and lengthy process that the published data have been restricted to a few targets measured at relatively large-time intervals. Accuracy and completeness of data has been further restricted by poor fiducial markers and loss of targets from the initial shock. From experimentation on Pre-Buggy I, II (Ref. 4), and the Pre-Schooner series (Ref 5), a program of targeting and data analysis has been developed to eliminate the majority of these problems (Ref. 6).

3.2 EXPERIMENTAL PROCEDURE

Three separate experiments were developed to obtain surface-motion information on Dugout. These were: (1) accelerometers, (2) falling-mass experiment, and (3) surface-motion targets.

The accelerometers and falling-mass experiments were designed to determine accurately the surface motion at very early times ($t < 50$ msec). The surface-motion target experiments were designed to give surface motion information over the entire mound, up to the time of vent.

3.2.1 Accelerometer Program. The layout of the accelerometers over the cratering area is shown in Fig. 3. 1. The accelerometers were triaxial, piezoelectric, Endevco type 2223C. Each accelerometer was mounted on a wood block, which was in turn mounted on a concrete slab poured into the base of the respective target. This mounting scheme minimized ringing of the accelerometer. Each accelerometer was connected by a short length of coaxial cable to a cathode follower.

The cathode followers used are of special design, incorporating negative feedback to provide stable, linear, near-unity gain, and a very low output impedance, so that they may maintain gain when driving standard low-impedance coaxial cable. The cathode followers and associated battery pack were shock mounted and isolated from initial earth movement by suspending them from a cable stretched between two telephone poles.

The cathode follower outputs were fed, via coaxial cable, to an Ampex FR 1300 instrumentation tape recorder where shock information was recorded on magnetic tape. A zero-time fiducial pulse was summed with a precision, 4-kc time reference, and recorded. A voice channel containing the countdown was also recorded for convenience in data reduction.

3.2.2 Falling-Mass Experiment. A 3.6×1 m graduated-plywood target was mounted on a 7.6-m telephone pole, emplaced in concrete at a depth of 1.2 m, 1.5 m east of hole U 18i. A 7.3-kg ball, 0.3 m in diameter, was suspended 0.4 m in front of the graduated target by means of a supporting cable attached to the top of the telephone pole. The plywood target was

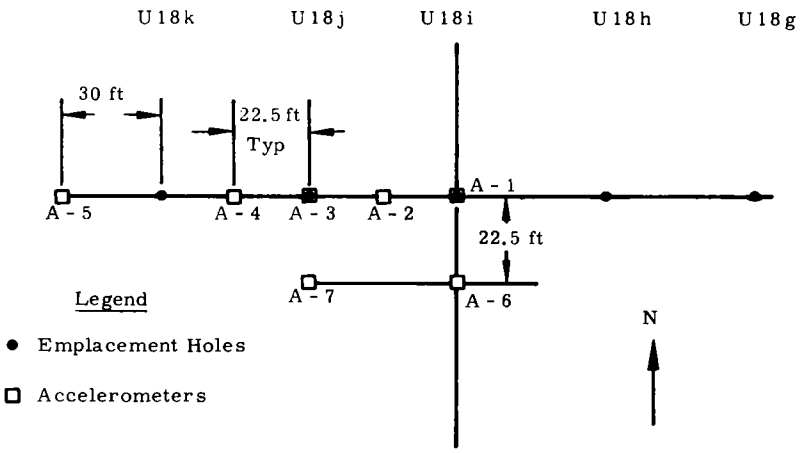

Fig. 3.1 Accelerometer layout.

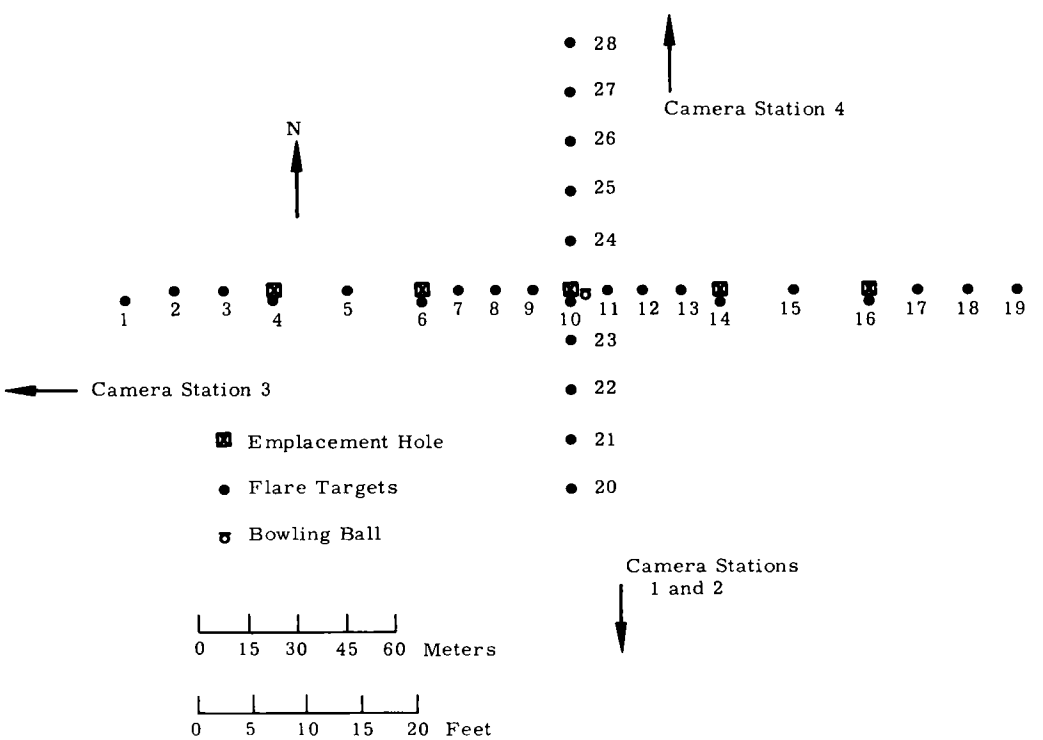

Fig. 3.2 Target array.

graduated by alternating black and white lines, 0.1524 m apart. The ball was released at the time the charges were detonated by means of a detonator inserted in the supporting cable. The relative displacement between the ball and the graduated target, which moved with the surface spall velocity, was obtained by photography from a close-in camera station.

3.2.3 Surface Motion Photography. a. Target Arrays. The target layout for Dugout is shown in Fig. 3.2. All targets over the cratering area are MK III targets with 250,000-candle power flares attached. Two independent fiducial systems were used as shown in Fig. 3.2 for each array. The target array along the charge line was photographed by Camera Station 2. The target array perpendicular to the charge line was photographed from Camera Station 3.

In order to obtain the detailed description of the surface motion over the entire mound, required to develop general diagnostic information concerning cratering physics, a large number of targets were required.

This would require a tremendous data reduction job if done by standard procedure. Flares were used to facilitate the reading and analysis of the film by computers. The film for the general surface motion will be read by PDPI computer equipped with a visual CRT. The PDPI computes the center of each flare image and stores the target position-coordinate data (for each flare image) for each frame on tape. The tape is then used as input for a 7094 code which does a coordinate transformation, independently smooths the position data, and then computes velocity and acceleration components of each target as a function of time.

The accuracy of this method is known to give a repeatable reading of position coordinates within ±0.1 ft out of a field width of 300 ft (e. g. , the error is one part in 3000) (Ref. 6).

b. Camera Complement. Table 3.1 shows the camera stations and contents for scientific photography on Dugout.

Cameras 1, 3, 9, 13, and 15. Mainly documentary films.

Cameras 10, 14, and 16. Base surge and cloud development studies; will be discussed in the base surge report.

Cameras 4 and 5. The falling-mass experiment.

Cameras 2, 7, and 8. Film from these cameras are to be used to obtain surface motion data along the row charge, and to study mound development and venting.

Cameras 11 and 12. The purpose of these films is the same as for 2, 7, and 8, but for the north-south row of targets.

3.3 PRESHOT PREDICTIONS

Empirical equations for peak spall velocities and accelerations from single detonations in basalt have been developed (Ref. 7) based primarily on Danny Boy and the Buckboard shots. These are:

$$aW^{1/3} = 3.2 \times 10^{9} \Lambda^{-3.9} \text{ g's}$$

$$v = 1.6 \times 10^{5} \Lambda^{-2.1} \text{ m/sec}$$

where

$$\Lambda = R/W^{1/3},$$

R is the radial distance from the shot point to the free surface in meters, and W is the equivalent charge weight in kilotons.

Assuming superposition of velocity and acceleration components from each charge, estimates were made as to maximum surface motion over the crater area. Numbering the charges from the center charge out, i.e., 1, 2, and 3,

TABLE 3.1 DUGOUT CAMERA STATIONS

No. – Camera	Frames per second (FPS)	Lens (mm)	Type of film
Station #1 500 ft S of GZ			
1 Hulcher	20	80	Neg color
2 Fastax	1000	25	TRI-X Rev.
3 Anricon	24	13	Color – K-II
4 Fastax	5000	255	Black and white
5 Photo Sonics	1000	300	MS color
Station #2 1000 ft S of GZ			
6 Photo Sonics	1000	50	IR
7 Photo Sonics	1000	50	TRI-X
8 Photo Sonics	200	100	Color
9 Hulcher	20	80	Neg Color
10 Bell and Howell	24	13	K-II
Station #3 1650 ft W of GZ			
11 Photo Sonics	1000	50	IR
12 Photo Sonics	1000	50	TRI-X
13 Photo Sonics	100	25	K-II
14 Bell and Howell	24	13	K-II
Station #4 3000 ft N of GZ			
15 Photo Sonics	100	50	K-II
16 Bell and Howell	24	13	K-II

	Velocity	Acc
1	53.9 m/sec	445 g
2	51.8 m/sec	430 g
3	40.5 m/sec	350 g

Time of vent was estimated to be at 1.0 sec.

Height of dome at vent was estimated to be at 14.9 m.

3.4 RESULTS

3.4.1 Photography. Table 3.2 gives pertinate remarks on observations made from a study of the film from Dugout. The description of the venting of Dugout is fairly complete. The height of the dome at the time of primary vent was 20.4 m and width of dome as measured from east to west was 104.8 m.

A major fault in the dome developed early about 7.6 m south of the charge row, extending over almost the entire dome, and continued to grow rapidly.

3.4.2 Accelerometer Experiment. The magnetic tape from the Ampex FR 1300 tape recorder was read by a Pace 231 R analog computer. The data tape was stretched 2^8 times before processing, then was calibrated and plotted on an x-y plotter. Figures 3.3, 3.4, and 3.5 show samples of the accelerometer data for accelerometers over two separate shot holes, between two shot holes, and 6.9 m south of the line of charges, respectively.

Table 3.3 gives the time of arrival of the compression wave at each accelerometer, peak acceleration values, and mean compressional wave velocities. The compressional wave velocities were calculated by the time of arrival of the shock and the distance to the nearest shot point. All velocities seem to be in good agreement with each other.

3.4.3 Falling-Mass Experiment. The photographic film of the falling mass and the graduated target were read by means of the Oscar film reader. The zero-time reference frame was established as the frame on which detonation of the supporting

TABLE 3.2 CHRONICAL OF SIGNIFICANT EVENTS

Time (msec)	Comments
0	Supporting cable on falling ball experiment detonated.
11.1 - 24.2	Targets illuminated by light from an unknown source.
40.0	Small venting of nitromethane gas from hole H. Magnitude of venting did not increase with time.
72.5 - 73.5	Zero-time flashbulbs ignited as they fell.
483.4	Primary vent occurred: approximately 5 m north of target over hole U 18 j.
523.6	Secondary venting along fault line in southeast quadrant. Also, simultaneous venting on north side at 45° from hole U 18 i.
543.8	Spotty venting along fault in southwest quadrant.
624.3	Vent along fault complete and main cloud beginning to form.

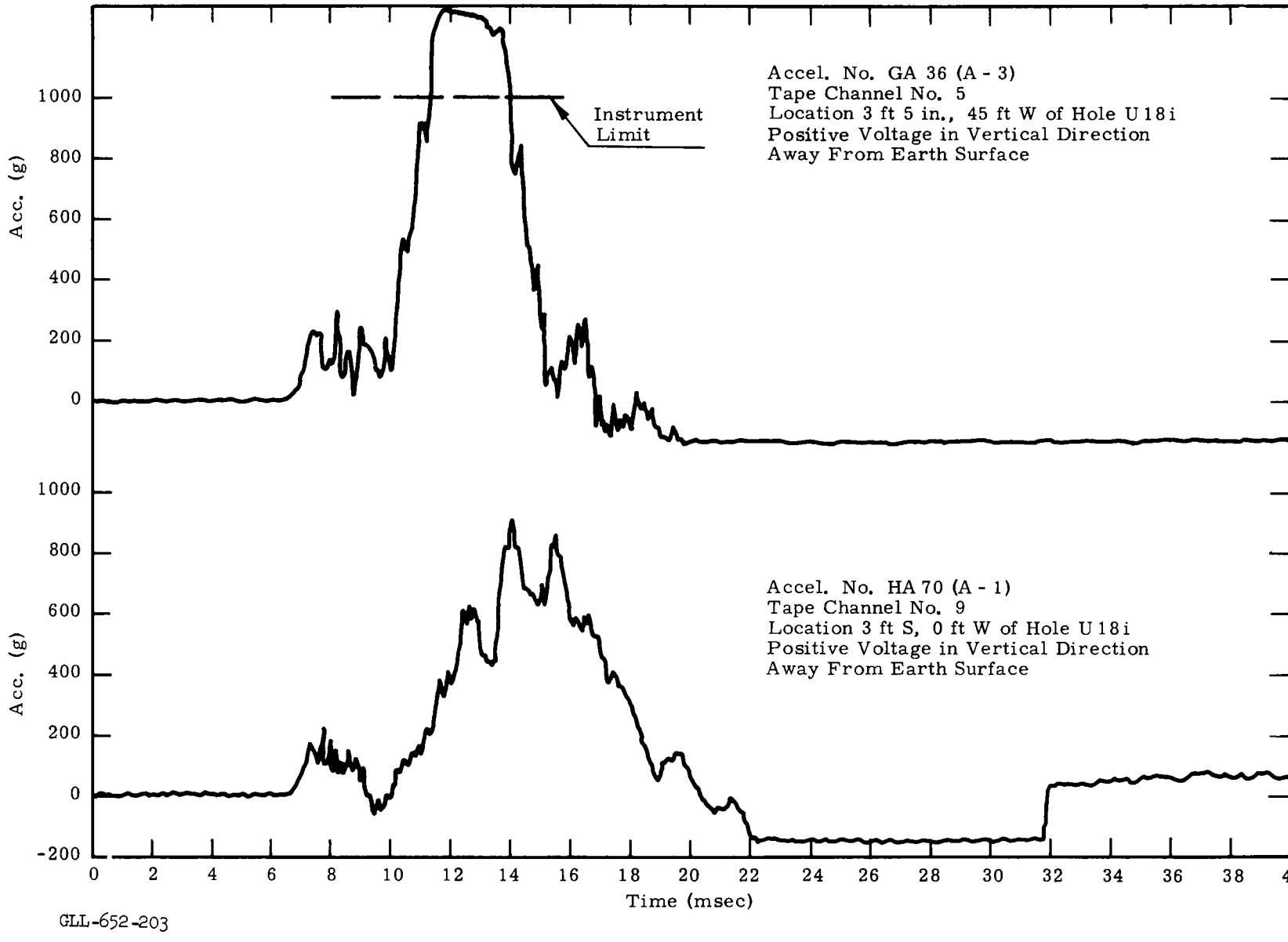

Fig. 3.3 Selected accelerometer records.

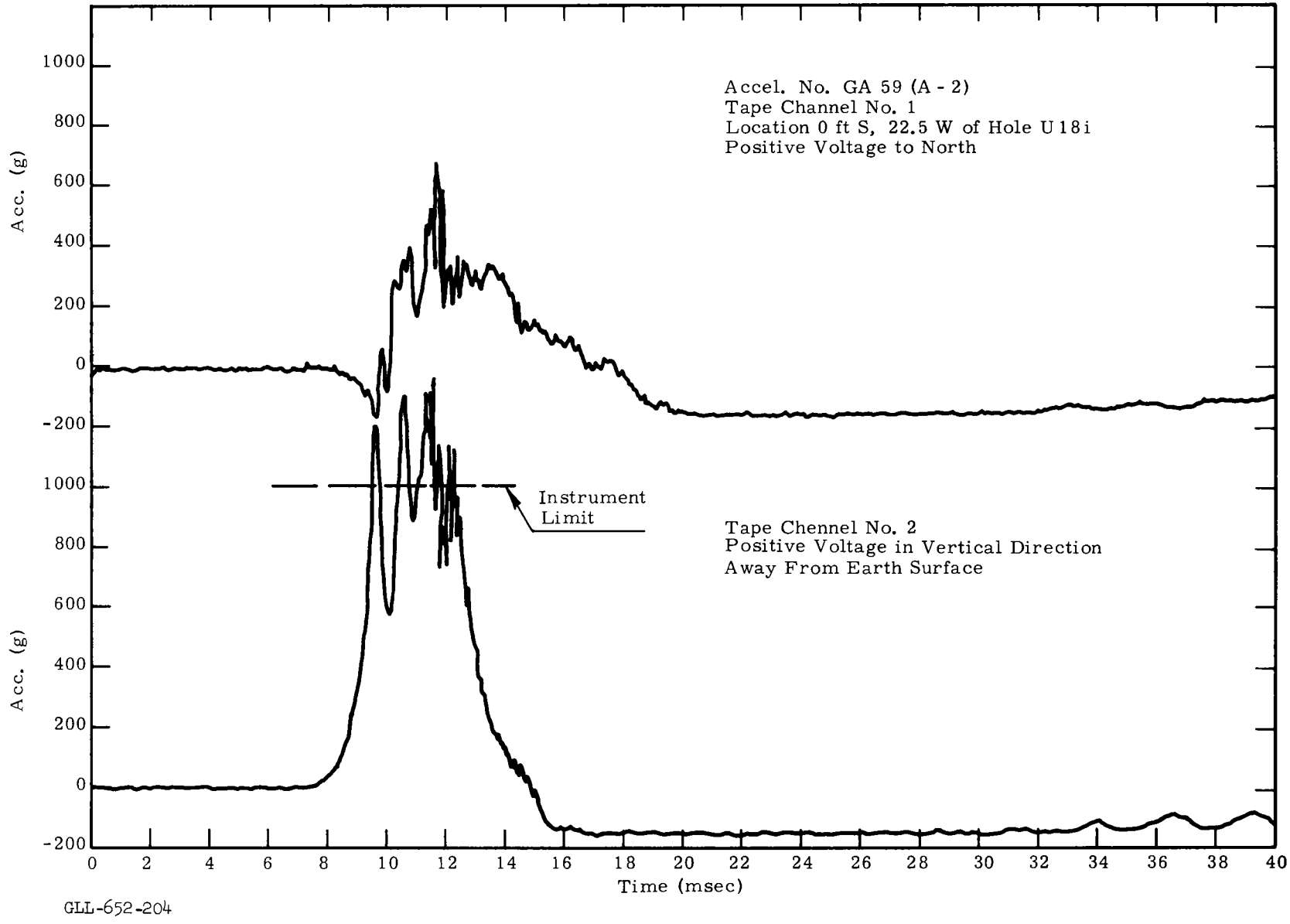

Fig. 3.4 Selected accelerometer records.

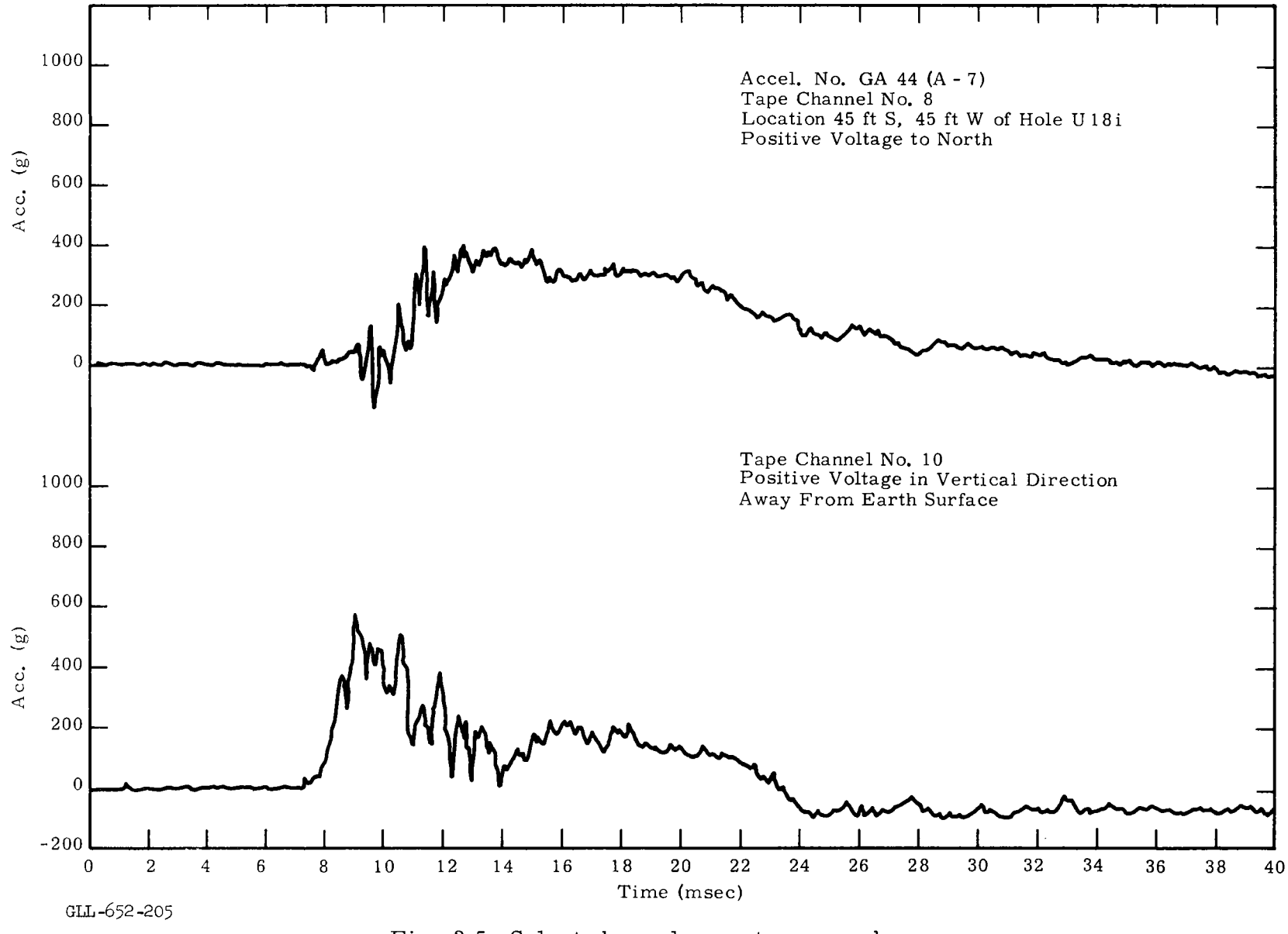

Fig. 3.5 Selected accelerometer records.

TABLE 3.3 SURFACE ACCELEROMETER DATA

Tape channel	Accel. No.	Time of arrival (msec)	Time of peak g (msec)	Peak g[a]	Compressional velocity[b] (m/sec)
1	A-2N[c]	8.0	11.8	660	
2	A-2V	7.4		>1000	2525
3	A-6N	9.0	12.0	80	
4	A-6V	8.0		>1000	2006
5	A-3V	6.4		>1000	2313
6	A-4E	8.2		>1000	
7	A-4V	7.2		>1000	2525
8	A-7N	7.6	12.6	400	
9	A-1V	6.6	14.1	900	2243
10	A-7V	7.2	9.0	580	2204
11	A-5E	10.0	15.0	460	
12	A-5V	9.0		>1000	1846

[a]All accelerations >1000 g exceeded the limits of the measuring instruments.

[b]Based on arrival times.

[c]N, V, E are direction of positive voltage where N = north, V = vertical up, and E = east.

cable was observed. Readings were taken at the top of the ball and at two points on the graduated target, on every other frame. The reference coordinate system used from frame to frame was determined by a line parallel to the film edge and passing through the center of the ball. Analysis of the timing marks on the film determined the framing speed as 5225 ± 10 fps resulting in a time interval between data points of 0.385 msec. Repeated readings of the film gave an average reading error of ±0.015 m.

Figures 3.6, 3.7, and 3.8 show the smoothed displacement, velocity, and acceleration in the vertical direction. The solid curve is from measurements made from a point on the east edge of the target, and the dashed curve refers to a point on the west edge of the target. The quantity $0.5\ gt^2$ was subtracted from the vertical coordinates to account for the displacement of the ball due to gravity. The difference between the curves for the two points is due to rotation of the target. The effect of rotation on the vertical coordinate is relatively small but must be removed from the horizontal coordinates before a meaningful data analysis can be performed.

The normal smoothing operation (Ref. 8) with a smoothing period of 10 msec was applied 10 times to each displacement, velocity, and acceleration curve. The derivative of the displacement and velocity was determined by a linear least-squares fit between three data points, evaluated at the center point.

From Fig. 3.7, the peak spall velocity of the two curves averages 65 m/sec. This is high when compared to the predicted velocity of 53.9 m/sec.

The oscillations observed in both velocity curves have peaks and lows at corresponding times, suggesting that they are real and correspond to the actual motion of the mound.

3.4.4 General Surface Motion. The reading and analysis of the infrared film has not been completed because of difficulty

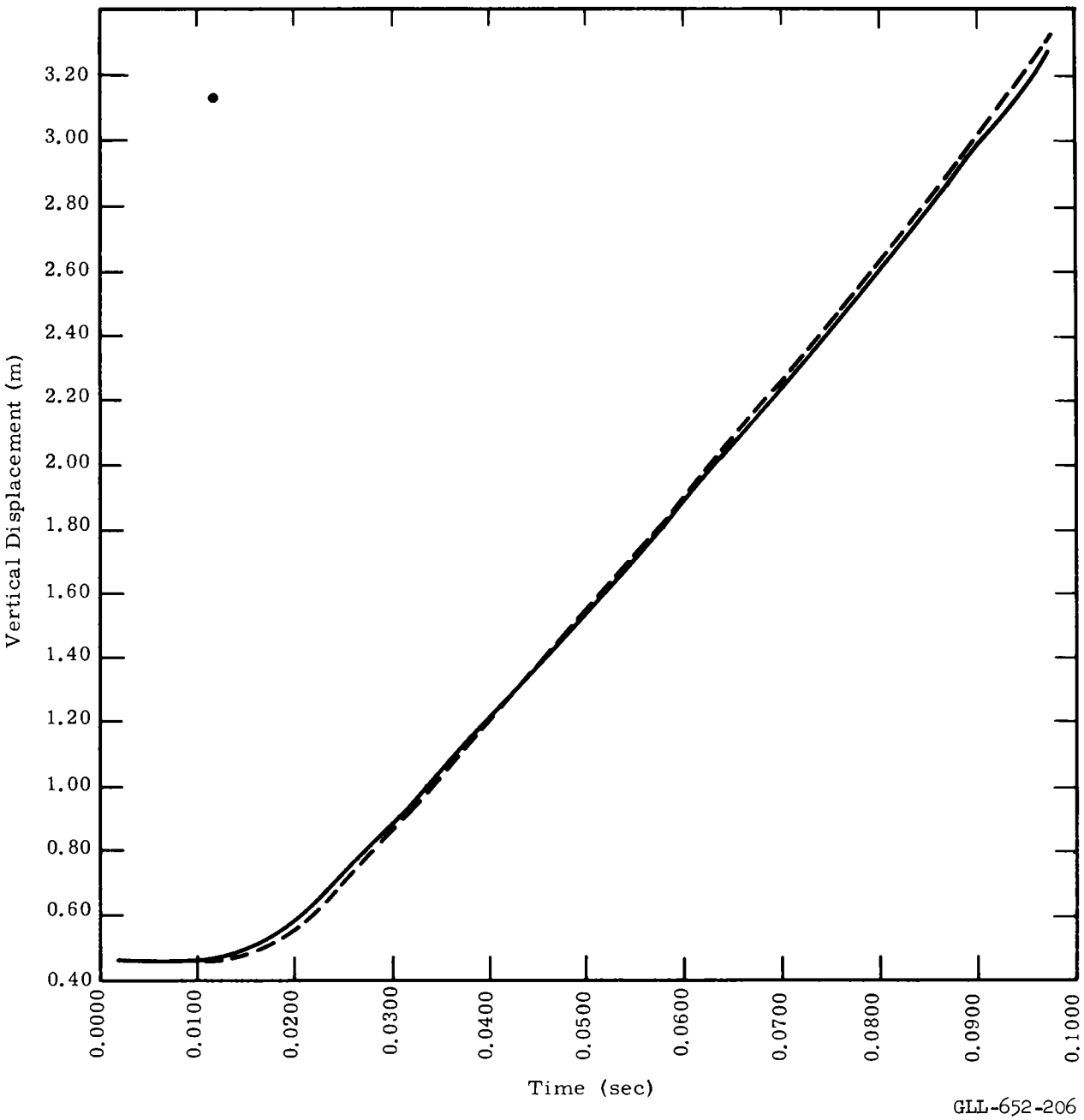

Fig. 3.6 Vertical target displacement (smoothed 10 times).

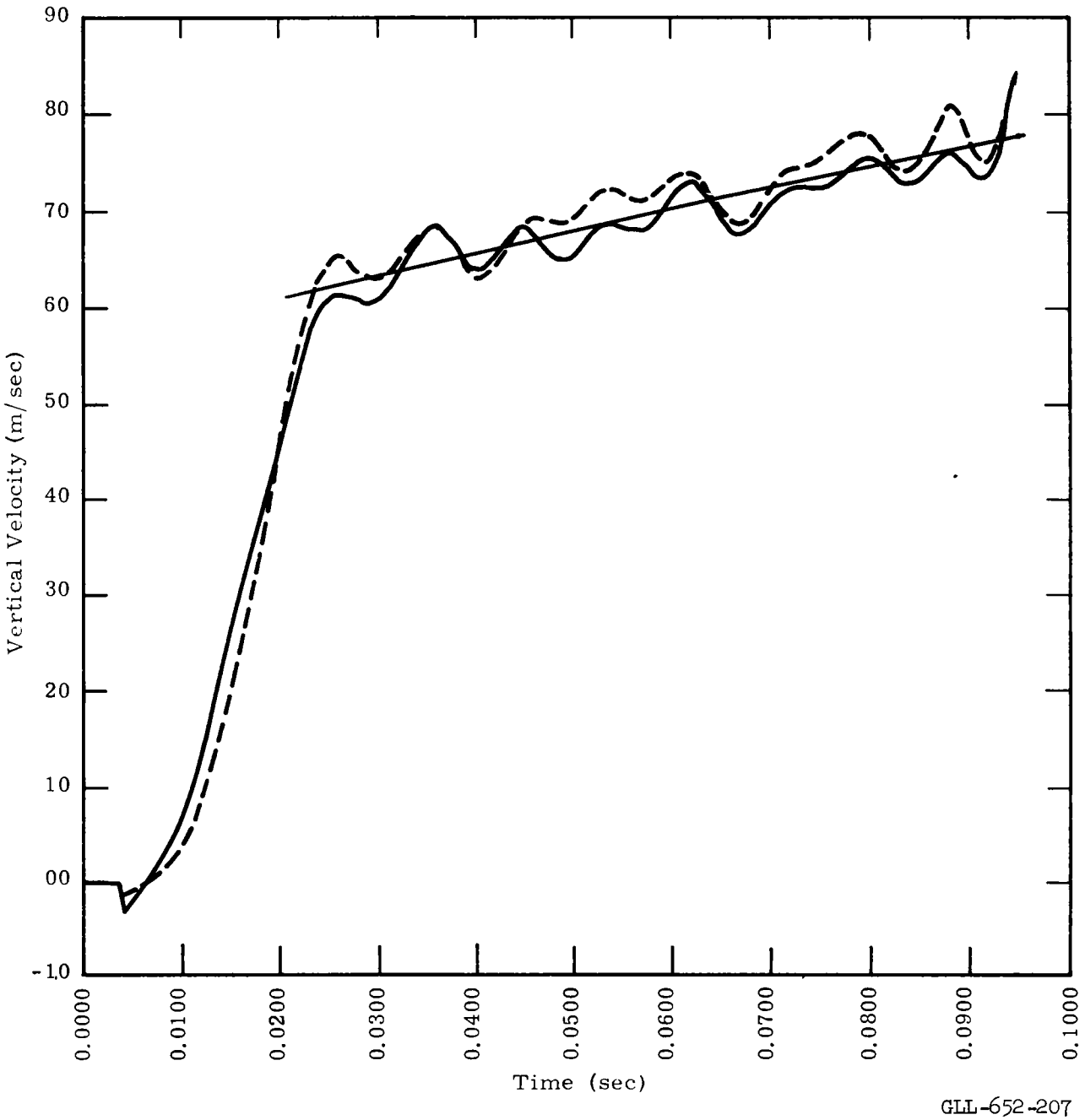

Fig. 3.7 Vertical target velocity (smoothed 10 times).

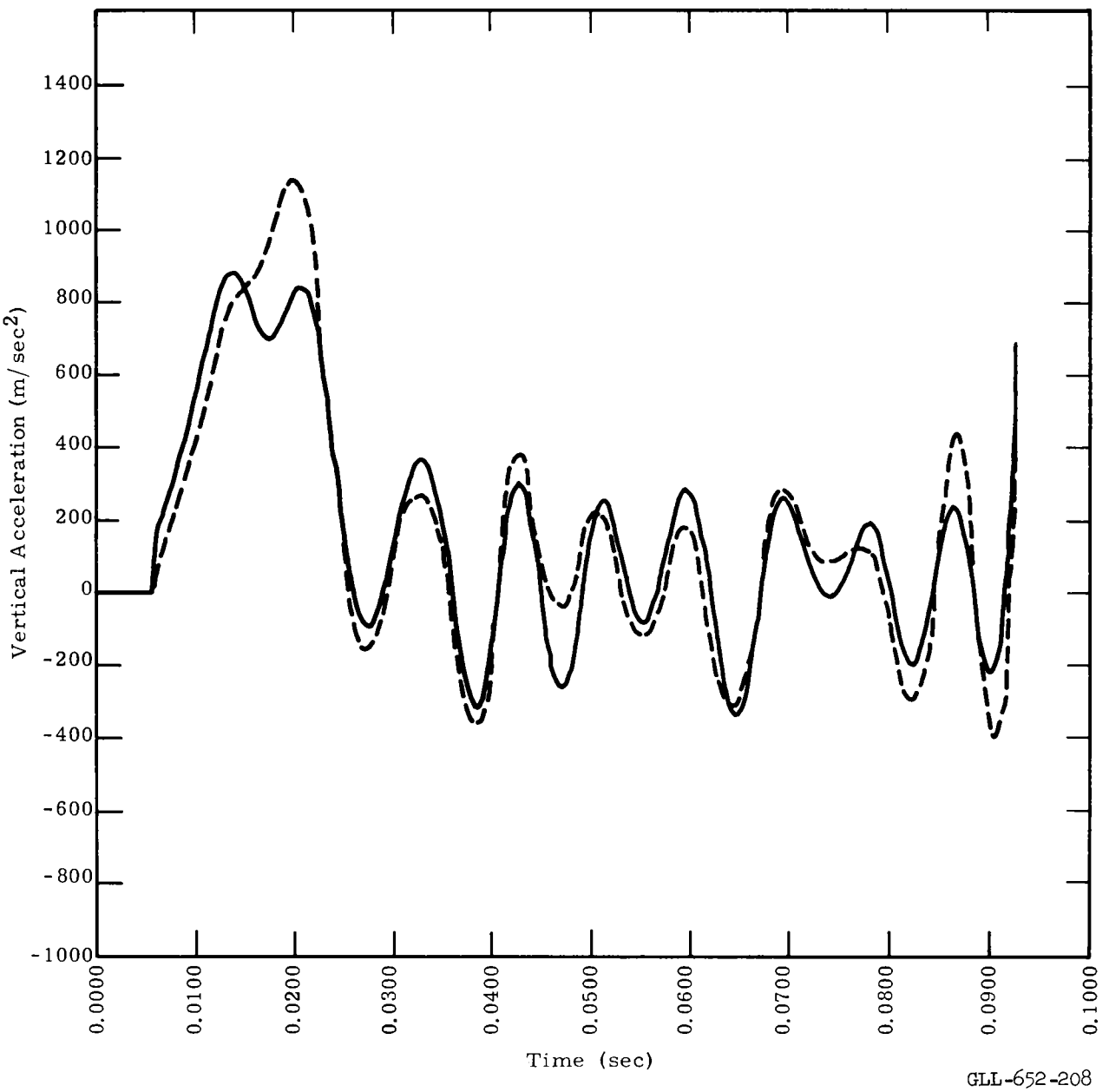

Fig. 3.8 Vertical target acceleration (smoothed 10 times).

in processing the film. Figure 3.2 shows the target distribution over the cratering area. Of the 19 flare targets running from east to west over the cratering area, all but 9 broke and dropped off. The two targets at the extreme east end fell on their sides. The seven that now remain for analysis are targets 1, 2, 7, 8, 11, 12, and 17. (The flare targets, #20-28, running from north to south, Fig. 3.2, were obscured by sun and smoke and will not be processed.)

3.5 DISCUSSION AND CONCLUSIONS

Figure 3.9 shows a comparison of the acceleration curves for the two points on the graduated target of the falling-mass experiment and accelerometer #HA70(A-1), (Fig. 3.3, lower). The time of arrival, time of first peak acceleration, and magnitude are in excellent agreement, considering the inherent errors in determining accelerations from displacement measurements. The accelerometers can only be considered reliable up to the time of peak acceleration because of voltage errors introduced by various R-C time constants in the whole circuit. A numerical integration of the accelerometer curve results in a peak velocity of 48 m/sec at 20.5 msec, which compares favorably with the velocity (47 m/s) of the falling-mass target at that time.

The SOC model (Ref. 3) was used to simulate the shock phenomena for a single 20-ton charge in basalt at the appropriate DOB for Dugout. The time t_s in Fig. 3.9 denotes the calculated time of arrival of the shock at the free surface, and t_r denotes the estimated time the rarefaction returns to the top of the expanding cavity. Experience with the SOC code has demonstrated that it calculates subsurface velocity and surface arrival time quite well but is consistently incorrect in calculating surface phenomena such as velocity.

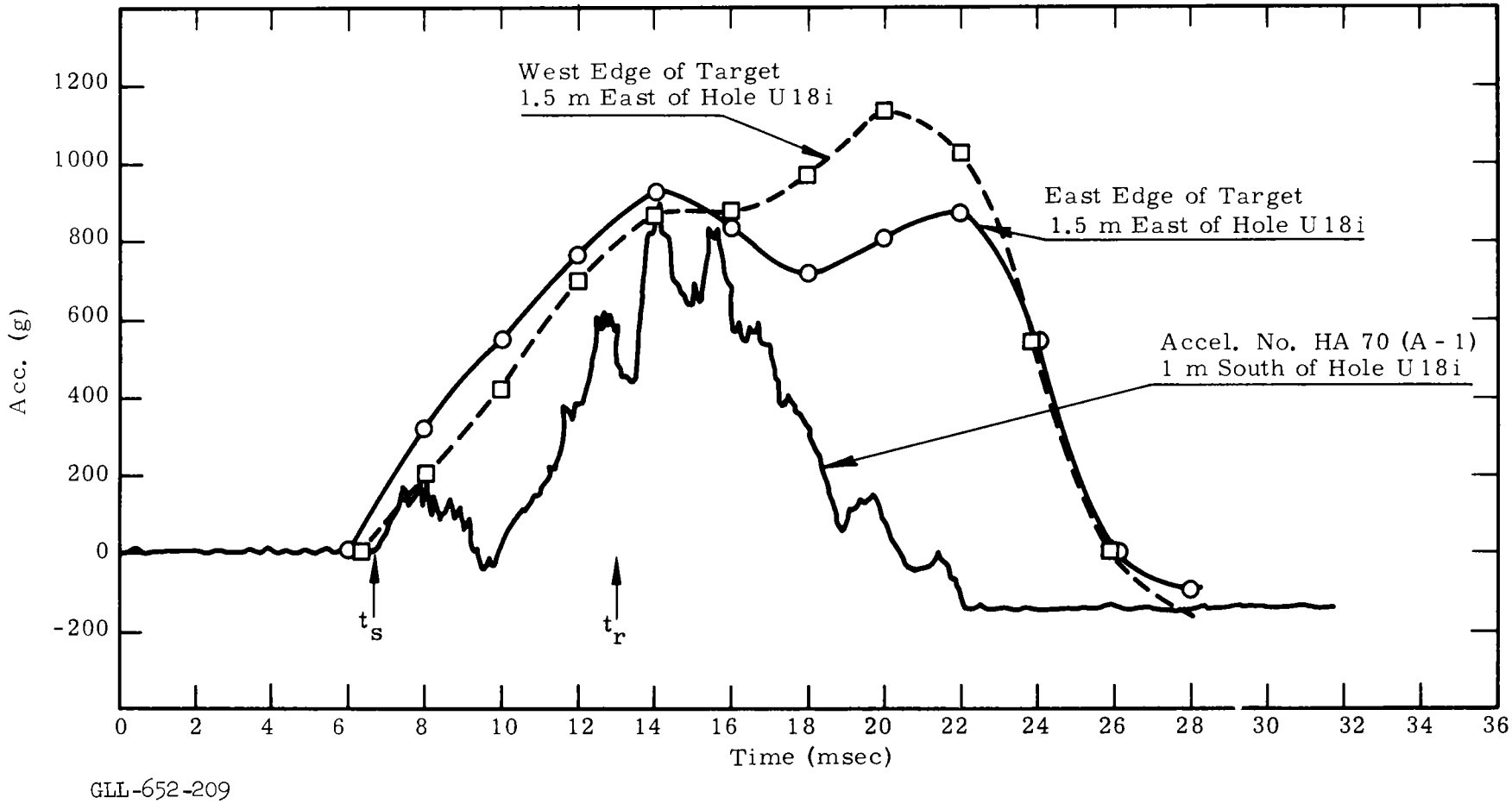

Fig. 3.9 Comparison of acceleration traces and surface-motion target data.

Interpretation of the results of the accelerometers and falling-mass experiments will be deferred until analysis of the surface-motion flare targets is completed.

The falling-mass experiment has proved to be an excellent method of obtaining early surface-motion history and should be added to future surface motion measurement programs.

REFERENCES

1. S. A. Feegenbaum and P. L. Wegkamp, Final Report "Photographic Earth Motion Study Scooter Event," Edgerton, Germeshausen, and Grier, Inc., Rept. No. L-510, 1961.

2. J. B. Knox and R. W. Terhune, "Cratering Physics Concepts Derived from an Analysis of Ground Surface Motion," Lawrence Radiation Laboratory, Livermore, UCID-4669, 1963.

3. J. B. Knox and R. W. Terhune, "Calculation of Explosion Produced Craters – H.E. Sources," Lawrence Radiation Laboratory, Livermore, UCRL-7738 Rev. I, 1964.

4. E. Graves, W. R. Wray, and R. B. Pierce, "Project Pre-Buggy, Scope of Chemical Explosive Cratering Experiment," USA Engineering Nuclear Cratering Group, Lawrence Radiation Laboratory, Livermore, PNE-300, 1963.

5. J. Spruill, private communication.

6. R. W. Terhune, R. L. Fulton, and J. B. Knox, "Surface Motion Photography Data Reduction by Digital Computers," Lawrence Radiation Laboratory, Livermore, to be published.

7. L. Vortman, "Project Buckboard," Sandia Corporation, Albuquerque, N. Mex., 1960.

8. J. L. Holloway, "Smoothing and Filtering of Time Series and Space Fields," Advances in Geophysics, Vol. 4, pp. 351-388, 1958.

9. R. W. Terhune, "Project Dugout, Surface Motion Studies," PNE-603, Lawrence Radiation Laboratory, Livermore, to be published.

CHAPTER 4

DUGOUT GROUND SHOCK STUDIES

4.1 INTRODUCTION

4.1.1 The Studies. Two ground shock studies were included in the Dugout Technical Program. The first, conducted by the Waterways Experiment Station (WES), was a two-phase evaluation of the close-in shock effects of a row-charge cratering detonation. WES prepared preshot geologic logs of five 36-in.-diam emplacement holes drilled at 45-ft (13.7-m) spacings along the extension of the Dugout row. Accurate caliper measurements of diameters were made in these holes. The second phase of the WES study involved recording Dugout radial acceleration or velocity at shot horizon in these five holes. Details of this program will be found in Reference 6.

The second ground shock study program, conducted by the U. S. Coast and Geodetic Survey (USC and GS), recorded surface acceleration and displacement time histories at four stations west of GZ and four south of GZ at ranges between 170 and 1580 m from U 18k. This program is reported in Reference 5.

4.1.2 Objectives. The primary objectives of the WES project were to study the transmission of shock from a row-charge cratering detonation and to evaluate its effects on nearby emplacement holes. Interpretation of shock transmission data should yield a better understanding of the coalescence of the waves from individual charges in a multiple-charge detonation. From velocity or integrated acceleration records, strain as a function of range can be studied for correlation with observed damage to the five drilled holes. Such data will lead toward the development of criteria for predicting minimum safe spacing between existing emplacement holes and detonations, which must be determined before meaningful drilling schedules can be developed for large-scale excavation projects.

The USC and GS strong motion seismic measurements were made to satisfy the following objectives:

(1) To determine the degree of asymmetry of seismic energy propagation from a row-charge cratering experiment.

(2) To determine the rates of attenuation of maximum transitory earth particle displacements and accelerations.

(3) To compare the Dugout seismic phenomena with the results obtained from previous underground detonations, both contained and cratering.

4.1.3 Background. The great amount of data available pertaining to ground motion from contained underground nuclear explosions permits reasonably good predictions of free field motion and stress time histories from similar shots to be made. Data from cratering detonations is quite limited and is almost entirely from small-scale chemical explosive experiments.

No data from row-charge experiments, either nuclear or chemical explosive, have been reported. For this reason there is no experimental basis for predicting effects from such detonations.

The effects of detonations on nearby emplacement holes have not been well documented in the past, but a conservative safe-range criterion for emplacement holes in alluvium has been empirically developed (Ref. 1). Some theoretical work has been carried out on the effect of elastic waves on cylindrical cavities, and tunnel damage from explosions has been surveyed. However, it is not clear that any of these cases are applicable to emplacement holes at scaled ranges on the order of 46 $m/kt^{0.3}$ (150 $ft/kt^{0.3}$), the approximate spacing of emplacement holes for channel excavations.

The USC and GS has studied the seismic effects of both high explosive and nuclear cratering shots at the Nevada Test Site, including Projects Scooter, Danny Boy, and Sedan. Scooter, a

0.5-kt chemical explosive shot, and Sedan, a 100-kt thermonuclear event, were both detonated in deep alluvium. Danny Boy was a 0.42-kt nuclear cratering experiment in basalt in Area 18.

It was determined that yield exponents of 0.27 for acceleration and 0.38 for displacement satisfied scaling of the results from the low-yield experiments to the Sedan data. The Scooter high-explosive shot produced about four times the seismic energy of the nuclear project Danny Boy, although the two events were of similar yield.

Maximum transitory surface earth particle motions from contained underground nuclear detonations in alluvium generally satisfy the following expressions (Ref. 2):

$$a = 0.0041\, \underline{W}^{0.54}\, \underline{R}^{-1.4} \qquad 0.4 \text{ to } 21.3 \text{ km}$$

$$d = 0.0027\, \underline{W}^{0.8}\, \underline{R}^{-1.2} \qquad 0.4 \text{ to } 21.3 \text{ km}$$

where

a = peak maximum surface acceleration in g's;
d = peak maximum surface displacement in cm;
$\underline{W}$ = equivalent high explosive yield in tons;
$\underline{R}$ = distance from source-to-detector in km.

Explosions in tuff result in ground motions about 2.5 times greater than for alluvium.

4.2 EXPERIMENTAL PROGRAMS

4.2.1 WES Hole Survival Program. Figure 4.1 shows a plan view of the hole array. The desired data consisted of static hole diameter measurements and dynamic earth motion measurements. The diameter measurements were obtained by a large spring-actuated inside caliper. The earth motion measurements were obtained by using particle-velocity gauges and accelerometers, buried at the bottom of the calyx holes. Holes "L" and "M" were instrumented with velocity gauges while holes "N," "O," and "P" contained accelerometers.

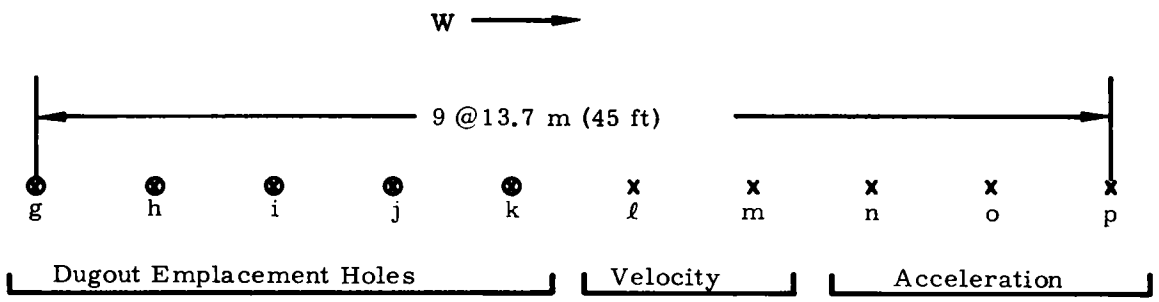

Fig. 4.1 WES instrument and Dugout emplacement array.

4.2.2 Strong Motion Seismic Program. The seismic signal from Project Dugout was recorded at eight seismograph stations, four in line with the row charges and extending to the west from the westernmost shotpoint, and four on a line perpendicular to the line of charges and extending south from the central shot location.

Figure 4.2 is a diagram of the shot and station arrangement for Project Dugout. Table 4.1 lists for each seismograph station the Nevada State Coordinates and shot to station distance.

4.3 PREDICTED EFFECTS

4.3.1 WES Studies. Peak accelerations and particle velocities were predicted using the experience from the underground explosion test series in rock (Ref. 3). The predictions involved many uncertainties.

(1) Acceleration. The least-squares equation obtained for several shots fired in sandstone was used to predict subsurface peak accelerations. This was taken from Figs. 3.5 of Reference 3.

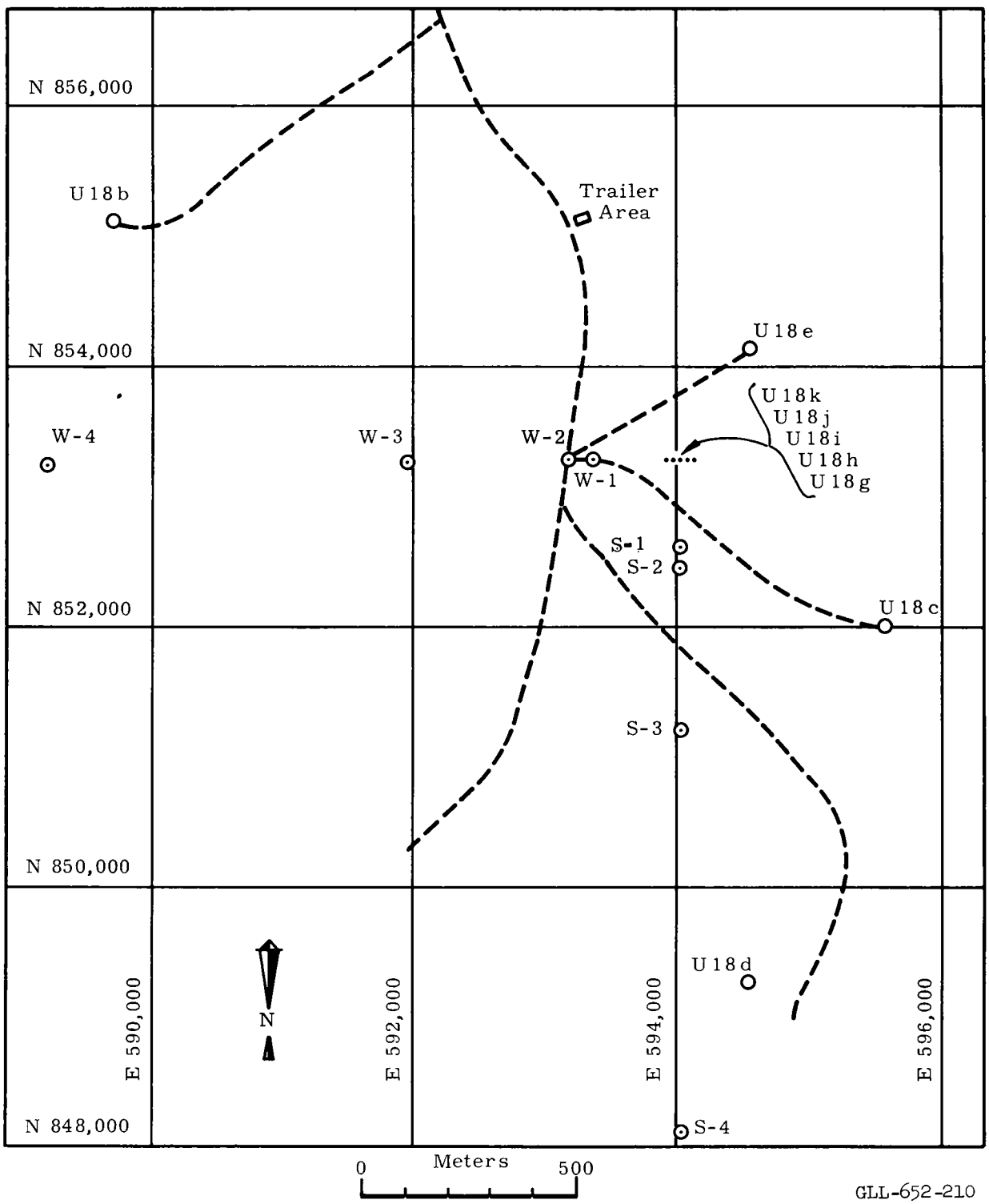

Fig. 4.2 Instrument station locations for Dugout.

TABLE 4.1 SEISMOGRAPH STATION LOCATIONS

Station	Nevada central zone grid coordinates N	E	Horizontal distance to event (km)	Parameters measured a = acceleration d = displacement
1 West	853 290	593 374	0.173	a
1 South	852 634	594 030	0.200	a
2 West	853 290	593 210	0.222	a
2 South	852 470	594 030	0.247	a
3 West	853 290	591 964	0.602	d, a
3 South	851 224	594 030	0.632	d, a
4 West	853 290	589 232	1.440	d, a
4 South	848 108	594 030	1.580	d, a

The equation is:

$$a\, W^{1/3} = 1.2 \times 10^{15}\, (\Lambda)^{-4.1},$$

where

a = peak horizontal radial acceleration in g's;

$W^{1/3}$ = the charge weight, kilotons;

Λ = scaled range = $R/W^{1/3}$, and

R = distance from the nearest charge in meters.

The assumption was made that the motion contribution from other than the nearest charge would arrive at the measurement point too late to reinforce the first arrival.

Using W = 0.02 kt, the tabulation shown in Table 4.2 was computed.

(2) Velocity. Predictions for particle velocity values were computed in a similar manner from the same source using the granite data. The predicted values, calculated by assuming no reinforcement are given in Table 4. 3.

TABLE 4.2 PREDICTED PEAK ACCELERATION, CLOSE-IN

Hole	Range (ft)	Range (m)	Scaled range ($m/kt^{1/3}$)	($ft/kt^{1/3}$)	a (g)
L	45	13.7	51	166	27,600
M	90	27.5	101	332	1,620
N	135	41.2	152	498	300
O	180	54.9	202	664	95
P	225	68.6	253	830	37

TABLE 4.3 PREDICTED PEAK VELOCITIES, CLOSE-IN

Hole	(ft)	(m)	Scaled range ($m/kt^{1/3}$)	($ft/kt^{1/3}$)	Peak velocity (ft/sec)	(m/sec)
L	45	13.7	51	166	118	36
M	90	27.5	101	332	29.4	9.0
N	135	41.2	152	498	13.1	4.0
O	180	54.9	202	664	7.4	2.3
P	225	68.6	253	830	4.7	1.4

(3) Hole Damage. Because this work represented the initial effort at accessing damage to drilled holes caused by cratering detonations, no applicable experimental data were available for predicting (or defining) hole damage. The uncertainties involved and the purpose of the project indicated that theoretical calculations were unwarranted.

4.3.2 USC and GS Projects. As no row-charge detonation had previously been instrumented with seismic gauges in the strong motion range, predictions were limited to those required for preshot safety estimates and instrument setting. The results of the Danny Boy strong motion seismic program were used for these, with the assumption that the five 20-ton sources would

produce the same seismic effects as a single 100-ton explosion at the center of the array. The Danny Boy results, scaled to 100 tons, using $W^{0.38}$ scaling for displacement and $W^{0.29}$ for acceleration, are shown in Fig. 4.7. The station array in line with the row charges would be expected to record earth motion slightly less than the normal array.

4.4 RESULTS AND DISCUSSION

4.4.1 WES Project. (a) Instrument Performance. All command signals were received at the instrument trailer, and the WES sequence timer performed properly. The zero time signal was received; however, a voltage surge appeared on three "close-in" channels approximately three milliseconds before the time zero relay closure. This surge is believed to have been caused by induction of the electromagnetic pulse into the transducer cables and therefore would be the true zero time. If so, the time zero relay apparently was delayed about three milliseconds. Use of the transient pulse at time zero is justified in that the average seismic velocity calculated from arrival time to the nearest gauge is 10,700 ft/sec (3200 m/sec) compared to 32,100 ft/sec (9800 m/sec) when using the relay zero time. The first value is in better agreement with the expected value of 17,000 ft/sec (5200 m/sec) which has been obtained with competent basalt cores in the laboratory.

All gauges gave an output and were all recorded. The preliminary recorded values are tabulated in Table 4.4. Two distinct pulses are visible on the velocity meters records, especially on the gauge nearest the charge. The accelerometers performed satisfactorily, although the output was lower than had been predicted.

TABLE 4.4 TABULATED RESULTS – OPERATION DUGOUT

Gauge No.	Range (ft)	Range (m)	Scaled range ($ft/kt^{1/3}$)	Arrival time (msec)	Average seismic velocity (ft/sec)	Average seismic velocity (m/sec)	Peak acceleration (g's)	Peak particle velocity (ft/sec)	Peak particle velocity (m/sec)
1-VH	45	13.7	166	4.2	10,700	3260	22,200	214	65.1
2-VH	90	27.5	332	9.8	9,180	2800	546	38.5	11.7
1-AH	135	41.2	498	16.3	8,250	2520	60	7.1	2.2
2-AH	180	54.9	664	25.5	7,060	2150	33	4.5	1.4
3-AH	225	68.6	830	36.7	6,140	1870	9	1.7	0.52

(b) Acceleration. All the accelerometers gave good records. The two velocity records were manually differentiated to obtain maximum accelerations from Holes L and M. The acceleration data are plotted in Fig. 4.3 together with the predictions from Table 4.2.

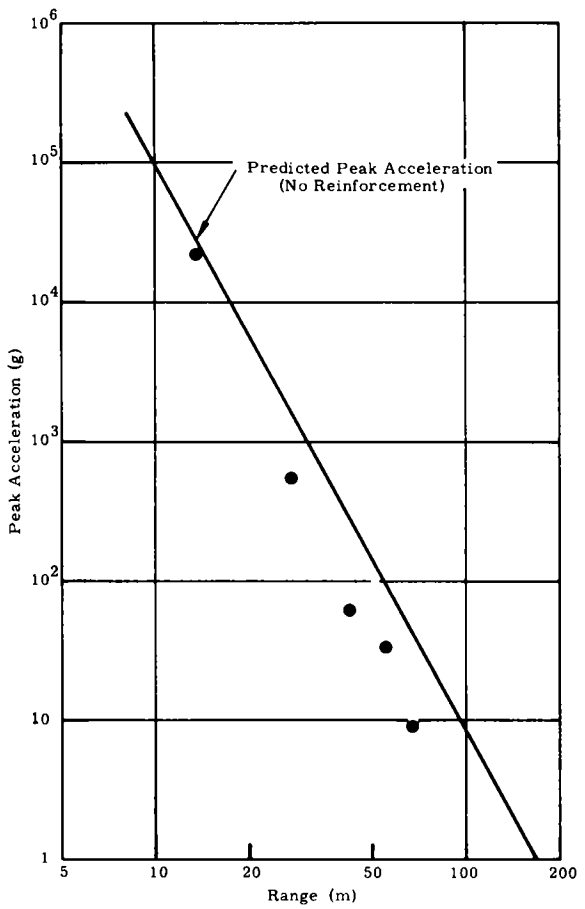

Fig. 4.3 Peak acceleration vs range.

(c) Particle Velocity. Although there appeared to be a temporary malfunction of the close-in velocity gauge, both gauges gave good records. The preliminary values are higher than had been predicted. Accelerograms from the three most distant holes were integrated to obtain peak velocities. All the peak velocity data points are shown in Fig. 4.4 together with the predictions from Table 4.3.

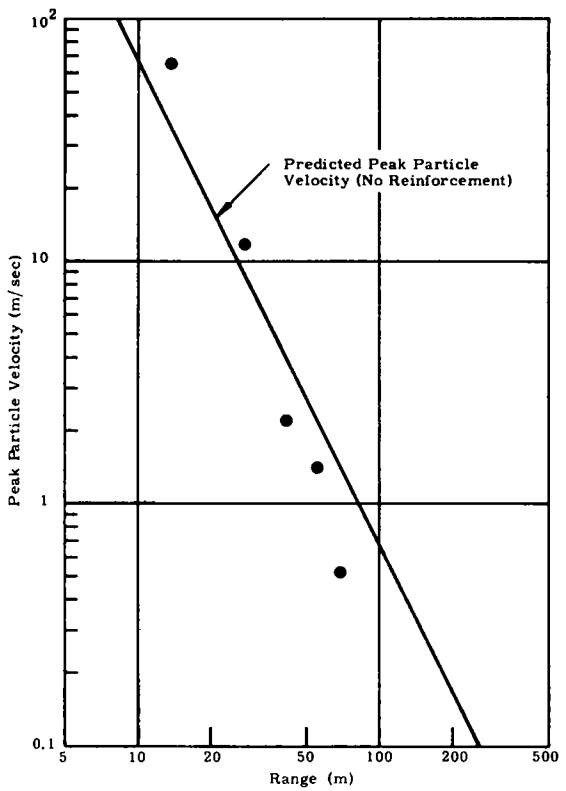

Fig. 4.4 Peak particle velocity vs range.

(d) Hole Diameter Measurements. Postshot measurements will be made after the sand back fill is removed from the five holes. These measurements will be presented in the WES final report.

4.4.2 Strong Motion Seismic Results. Table 4.5 lists the peak transitory earth particle motions in terms of displacement and acceleration as read from the USC and GS records by R. F. Beers, Inc. These data are plotted in Figs. 4.5 and 4. 6 along with predictions based on contained explosions in alluvium and tuff.

Maximum particle motions indicated asymmetrical seismic wave propagation only at small source-to-detector distances. The stations at 173 and 222 m recorded accelerations in line with the row which were about one-half those recorded at the same

TABLE 4.5 PEAK SURFACE MOTION FROM THE DUGOUT EVENT

Station	Distance (m)	Component	Acceleration (g)	Acceleration Period (sec)	Displacement (cm)	Displacement Period (sec)
S-1	200	Z	1.02×10^{0}	0.10		
		R	1.72×10^{0}	0.10		
		T	1.81×10^{0}	0.22		
S-2	250	Z	6.06×10^{-1}	0.09		
		R	4.64×10^{-1}	0.10		
		T	4.83×10^{-1}	0.03?		
S-3	630	Z	1.54×10^{-1}	0.08		--
		R	1.98×10^{-1}	0.13	2.26×10^{-1}	0.57
		T	1.34×10^{-1}	0.08	4.79×10^{-1}	0.53
4	1580	Z	3.37×10^{-2}	0.26	2.08×10^{-1}?	0.35
		R	2.88×10^{-2}	0.19	1.34×10^{-1}	0.60
		T	3.68×10^{-2}	0.29	1.81×10^{-1}	0.73
W-1	173	Z	6.98×10^{-1}?	?		
		R	6.00×10^{-1}?	?		
		T	4.21×10^{-1}?	?		
W-2	222	Z	2.91×10^{-1}?	0.03?		
		R	1.18×10^{0}	0.065		
		T	3.85×10^{-1}	0.045		
W-3	603	Z	1.81×10^{-1}	0.08	4.97×10^{-1}	0.47
		R	9.9×10^{-1}	0.21	3.69×10^{-1}	0.37
		T	1.45×10^{-1}	0.14	2.28×10^{-1}	0.24
W-4	1435	Z	3.51×10^{-2}	0.30	2.91×10^{-1}	0.42
		R	4.12×10^{-2}	0.33	1.60×10^{-1}	0.70
		T	4.74×10^{-2}	0.33	1.48×10^{-1}	0.40

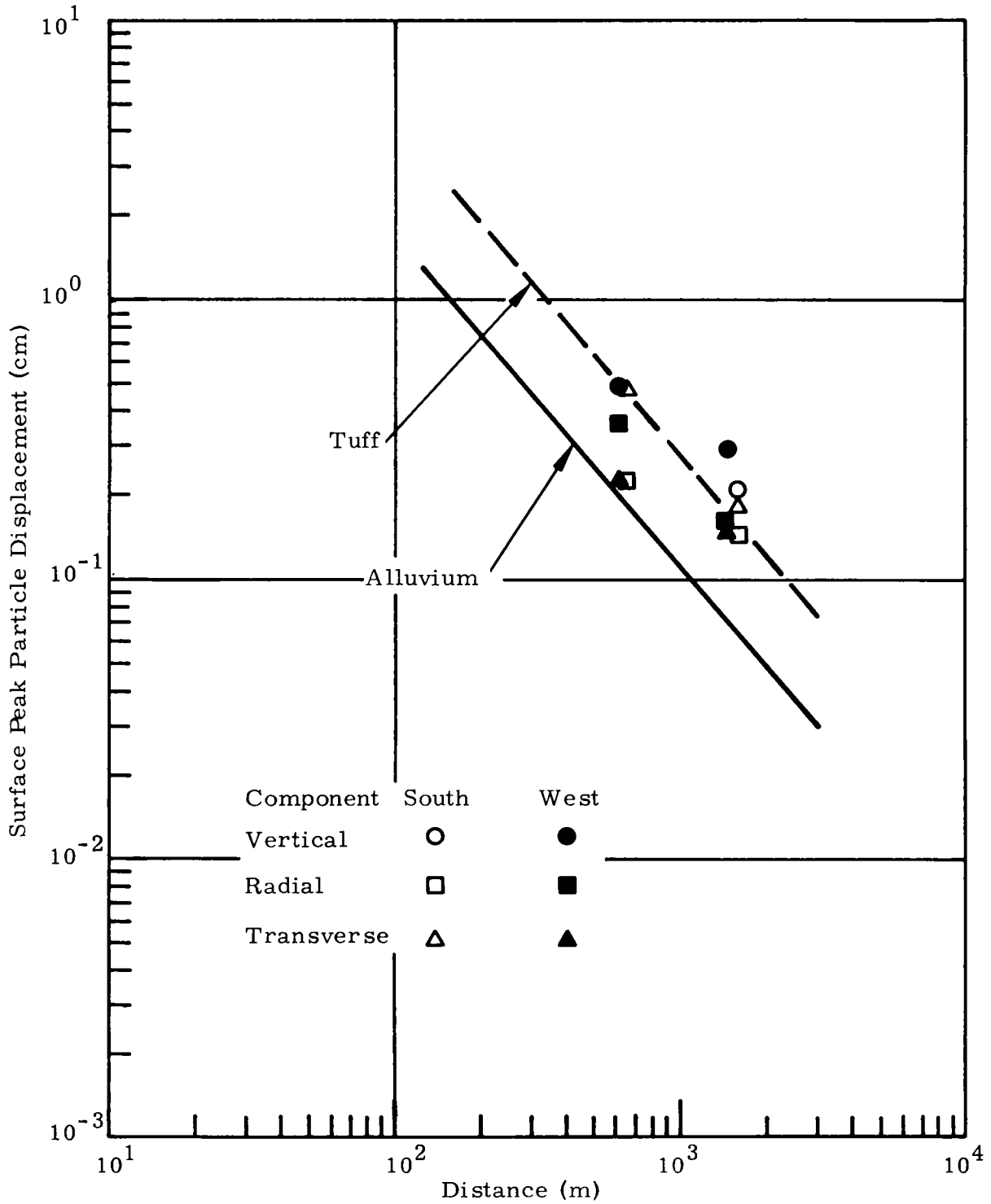

Fig. 4.5 Peak surface particle acceleration vs distance.

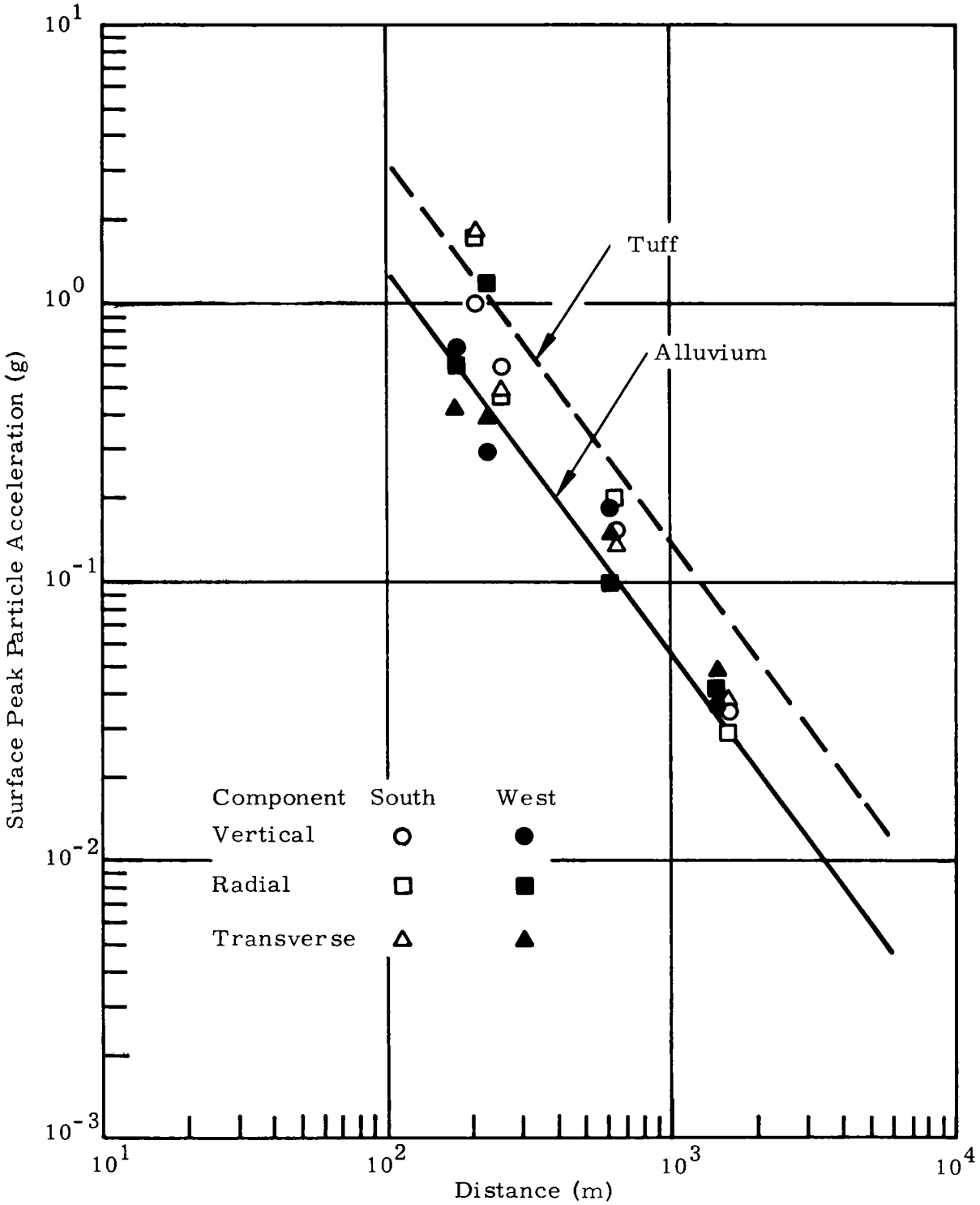

Fig. 4.6 Peak surface particle displacement vs distance.

ranges perpendicular to the row. Displacement measurements were not made at these ranges. At 600 and 1580 m maximum motions were nearly the same along the two recording azimuths, indicating that at ranges which were large relative to the total length of the row charge, the seismic signal appeared to originate from a point source.

(a) Comparison with Danny Boy. The maximum ground motions from Projects Dugout and Danny Boy can be compared, assuming equivalent seismic energies from high explosive and nuclear detonations of the same yield. Maximum displacements and accelerations from Danny Boy (Ref. 4) were scaled to the Dugout results, assuming superposition of the signals at the source so that it looks like a 100-ton explosion, and using the yield exponents of 0.38 for displacement and 0.27 for acceleration derived from the Sedan and other alluvium cratering detonations. Superposition at the gauge would lead to predictions from Danny Boy that will be larger by a factor of about 3. The vertical, radial and tangential components were averaged for each station. Figure 4.7 is a graphical presentation of the results and shows that the assumed yield exponents and source superposition fitted the data quite well. If in fact a high explosive shot produces more seismic energy than a nuclear detonation of the same yield, then Fig. 4.6 would indicate the necessity of larger yield exponents than those used here.

4.5 CONCLUSIONS

4.5.1 WES Project. Although analysis of the data has not been completed, the preliminary results appear to agree fairly well with predictions. Dugout results will be compared with Danny Boy earth motions and analyzed in an attempt to determine stress and strain levels, contributions from the individual charges, and the relationships between stress levels and emplacement hole failure probability.

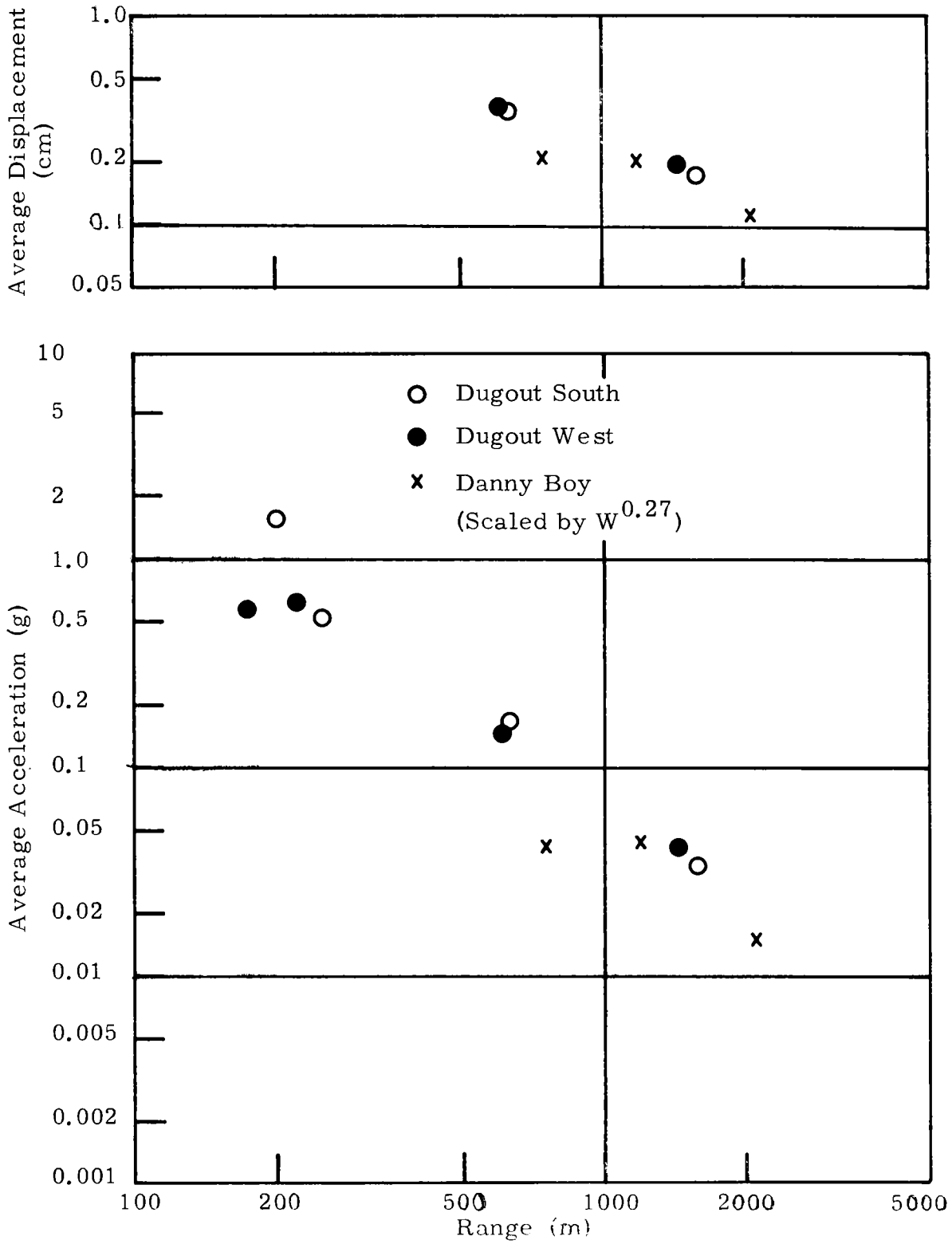

Fig. 4.7 Average peak displacements and accelerations for Dugout and Danny Boy.

4.5.2 Strong Motion Seismic Program. Asymmetrical seismic propagation was observed only at the two closest stations at ranges of 0.172 km west and 0.200 km south. Using the total yield of 100 tons, these ranges correspond to scaled distances of about 0.4 km/kt$^{1/3}$ (1300 ft/kt$^{1/3}$). At 600 and 1600 m, maximum motions were nearly identical on the two perpendicular lines. Thus for cratering detonations the scale of Dugout it appears there is no detectable deviations from an isotropic distribution of the seismic energy at ranges of concern for damage.

Prediction functions for displacement and acceleration from a nuclear detonation in tuff are satisfied very well by the Dugout measurements. Previous empirically determined yield exponents of 0.38 for displacement and 0.27 for acceleration work very well at the ranges of concern for ground shock damage for scaling the Danny Boy results to Dugout when the assumption of source superposition is used. Insufficient data are available at present to determine the adequacy of this assumption or scaling procedure at the closer ranges where asymmetrical seismic propagation was observed.

REFERENCES

1. L. J. Cauthen, Jr., "Survey of Shock Damage to Surface Facilities and Drilled Holes Resulting from Underground Nuclear Detonations," Lawrence Radiation Laboratory, UCRL-7964, 1964.

2. T. H. Pearce and W. V. Mickey, "Operation Nougat, Strong Motion Measurements, Project 1.4," DASA, VUP-2301, October 1962.

3. "Underground Test Program, Vol. II, Rock," Engineering Research Associates.

4. T. H. Pearce and W. V. Mickey, "Project Danny Boy Seismic Effects from a Nuclear Cratering Experiment in Basalt, POIR-1813 (IRT-1812), September 1962.

5. W. V. Mickey, "Project Dugout, Strong Motion Measurements," PNE-605 U. S. Coast and Geodetic Survey, to be published.

6. L. F. Ingram, "Project Dugout, Deep Underground Shock Measurements," PNE-609, Waterways Experiment Station, to be published.

CHAPTER 5

AIR BLAST

5.1 INTRODUCTION

Air blast represents one of the areas of major concern for nuclear excavation. Damaging air blast signals from megaton-sized cratering detonations can occur off site in two ways (Ref. 1). The first is from so-called close-in air blast transmitted more or less isotropically through the atmosphere; the second is from long-range air blast signals refracted back to earth at ranges of 100 to 300 miles by high-velocity winds in the troposphere and ozonosphere. An extensive amount of data on these two air blast phenomena have been collected on past cratering explosions with both chemical and nuclear explosives and in alluvial and hard rock materials (Refs. 2-7). This experience has been, in its entirety, with single detonations. Only very preliminary experiments had been conducted on air blast waves from row charges (Ref. 8).

Dugout thus represented the first opportunity to obtain data on the character of the air blast signals generated by a row-charge cratering detonation. Past experience with air-blast signals from single chemical explosive cratering detonations in the Buckboard Mesa basalt (Ref. 3) formed the basis for interpretation of the results from Dugout in terms of the relationship between single and row charges. The data from the nuclear cratering detonation Danny Boy then allowed the basis for extending these data to nuclear row charges in hard rock. Complete discussions of the air blast programs will be found in References 10 and 11.

5.2 EXPERIMENTAL PROCEDURE

5.2.1 Close-In Air Blast. Close-in air blast from Dugout was measured along two lines, one parallel to the row to the west and one perpendicular to the row to the south opposite the center

charge. Measurements were made at five stations along the south line and at seven stations along the west line. Two gauges were placed at each station. Table 5.1 gives the ranges used and Fig. 5.1 shows a plan view of the array. Note that ranges to the west line are given both from the westernmost charge of the Dugout array (charge K) and from the center charge (charge I).

5.2.2 Long-Range Air Blast. Thirteen microbarograph stations at distances ranging from 2 miles (3.2 km) to 120 miles (190 km) were operated on Dugout. The azimuth and range of these stations are listed in Table 5.2. Figure 5.2 shows a plan view of the microbarograph layout. Because of the prevailing easterly direction of the ozonospheric winds at this time of the year, the long-range stations were all located west of the Dugout site. In an effort to detect nonisotropy of the long-range air blast signal, microbarograph stations were located both north and south of the Dugout array in addition to the usual stations to the west.

Three 1.2-ton H. E. bursts on 15-ft platforms were scheduled to fire at H - 2 minutes, H + 3 minutes, and H + 5 minutes. Recordings of waves from these calibration shots were to be scaled to 20-ton H. E. free-air bursts for comparison with Dugout recordings and calculation of transmissivity values. In addition, another 1.2-ton H. E. surface burst was scheduled at H + 8 minutes to compare with blast waves from platform bursts and verify the height-of-burst parameter used in scaling calculations.

Upper air rocket soundings were also taken at two times on shot day by Sandia Corporation at the Tonopah Test Range to determine wind conditions in the ozonosphere between 100,000 and 200,000 feet.

5.3 PREDICTED RESULTS

5.3.1 Close-In Air Blast. Predictions for air blast results on Dugout were based on the measurements made on Shot 13 of Project Buckboard (Ref. 3). This shot was a 20-ton TNT charge

TABLE 5.1 CLOSE-IN AIR BLAST RESULTS, PROJECT DUGOUT

Range (nominal) (m)	(ft)	First peak (mbar)	(psi)	Second peak (mbar)	(psi)
South (perpendicular)					
52	170	19	0.28	30	0.44
		17	0.25	26	0.375
107	350	1.6	0.023	8.3	0.12
		2.6	0.037	11.5	0.167
259	850	0.26	0.0038	5.7	0.083
		0.30	0.0044	5.8	0.084
702	2300	0.38[b]	0.0055[b]	6.9[b]	0.1000[b]
		0.97	0.0014	1.4	0.0205
1523	4994			0.60	0.0086
				0.45	0.0065
West (parallel)[a]					
52	170	7.0	0.102	12.0	0.174
(79)	(260)	6.5	0.094	10.8	0.156
107	350	0.48	0.007	5.2	0.076
(134)	(440)	0.65	0.0094	4.6	0.067
259	850	0.083	0.0012	1.9	0.028
(287)	(940)	0.172	0.0025	1.5	0.022
458	1500	0.079	0.00114	1.5	0.0223
(485)	(1590)				
704	2307	0.12	0.0017	1.04	0.015
(731)	(2397)	0.11	0.0016	0.83	0.012
1040	3410	0.031	0.00045	0.40	0.0058
(1068)	(3500)				
1430	4690		--	0.52[b]	0.0076[b]
(1458)	(4780)		--	0.12[b]	0.0017[b]

[a]Range as measured from westernmost charge (K). Numbers in parentheses are range as measured from center charge (I).

[b]Dubious value. Will probably change after system check and gauge recalibration.

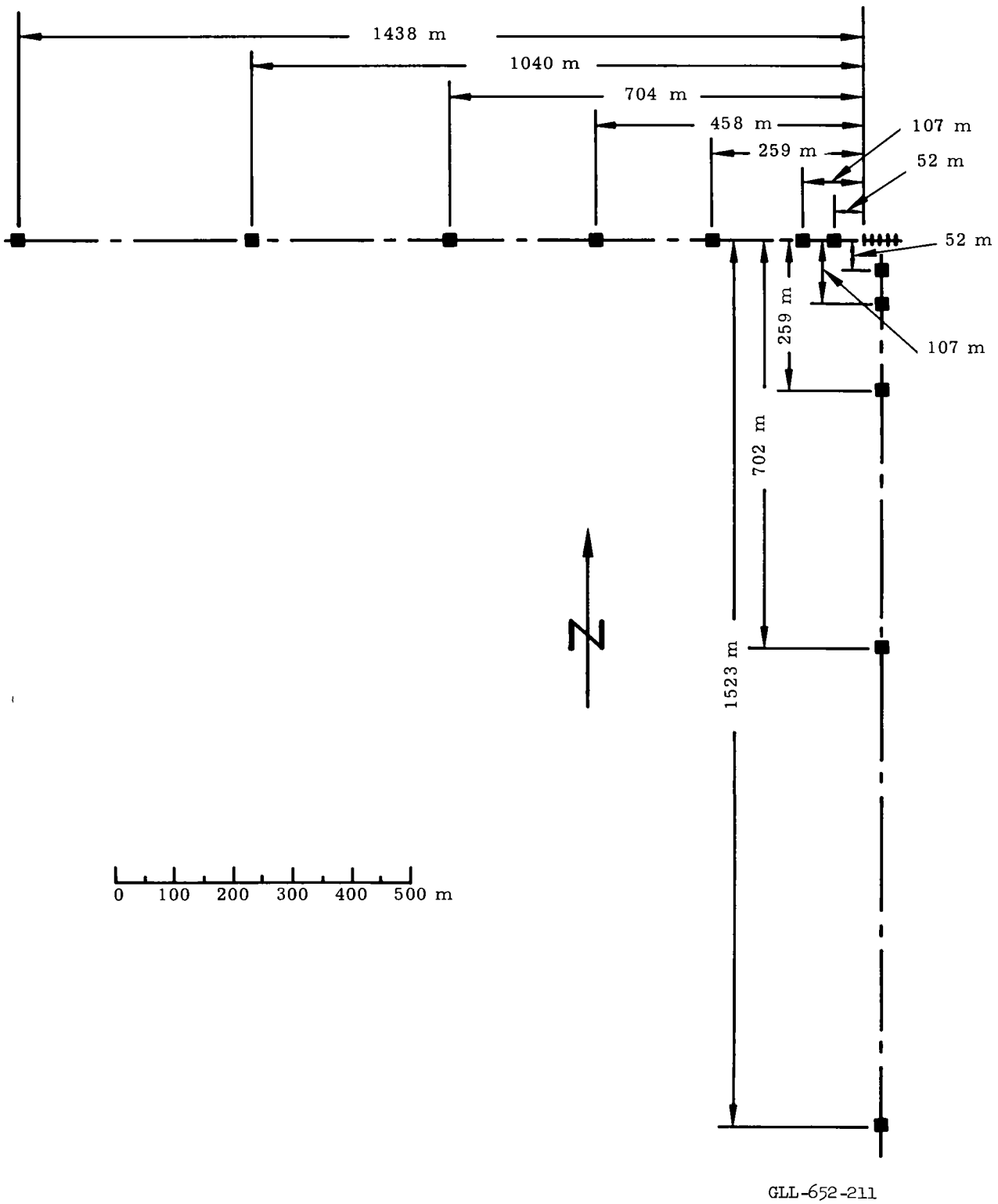

Fig. 5.1 Close-in air blast gauge layout, plan view.

TABLE 5.2 DUGOUT MICROBAROGRAPH DATA SUMMARY

Station	Dugout bearing (deg)	Dugout range (ft)	(km)	Signal type	Av. vel. (ft/sec)	Peak-to-peak pressures (μb) Dugout (0 sec)	H.E. #1 (+4 sec)	H.E. #2 (+120 sec)	H.E. #3 (+300 sec)	H.E. #4 (+480 sec)
2-mile	170	13,075	4.0	T	1140	324	5936	4587	5067	7122
5-mile	175	30,943	9.4			Not operated				
10-mile	186	54,341	16.6	T	1146	23.6	23.6	37.8	26.0	33.0
CP-1	124	102,222	31.2	T	~1140	No signal > 7-15 μb wind noise level				
Baker	173	672,345	205.1			No correlated signals, large electric pulse noises				
China Lake	217	644,079	196.4	Z	951	9.9	40.3	31.1	37.2	21.7
Lone Pine	249	531,903	162.2	Z	924	No[a]	18.3	Recorder quit		
Deep Springs	282	490,984	149.7	Z	917	6.1	17.0	12.6	10.7	9.5
Bishop	279	603,795	184.2	T	1171	2.2	7.4	1.8	No[a]	1.6
				Z	955	5.4	41.4	35.8	38.6	22.2
Tom's Place	283	698,382	213.0	Z	975	20.8	55.9	72.5	104.2	79.5
Tonopah T. R.	335	279,947	85.4	T	1136	3.6	8.2	8.6	8.0	5.8
Coaldale	307	560,081	170.8	Z	940	6.3	12.2	13.8	2.13	20.9
Clear Creek	357	632,203	192.8	Z	970	<1.2	2.1	2.3	2.8	0.5

[a]Overlapping signals could not be separated.

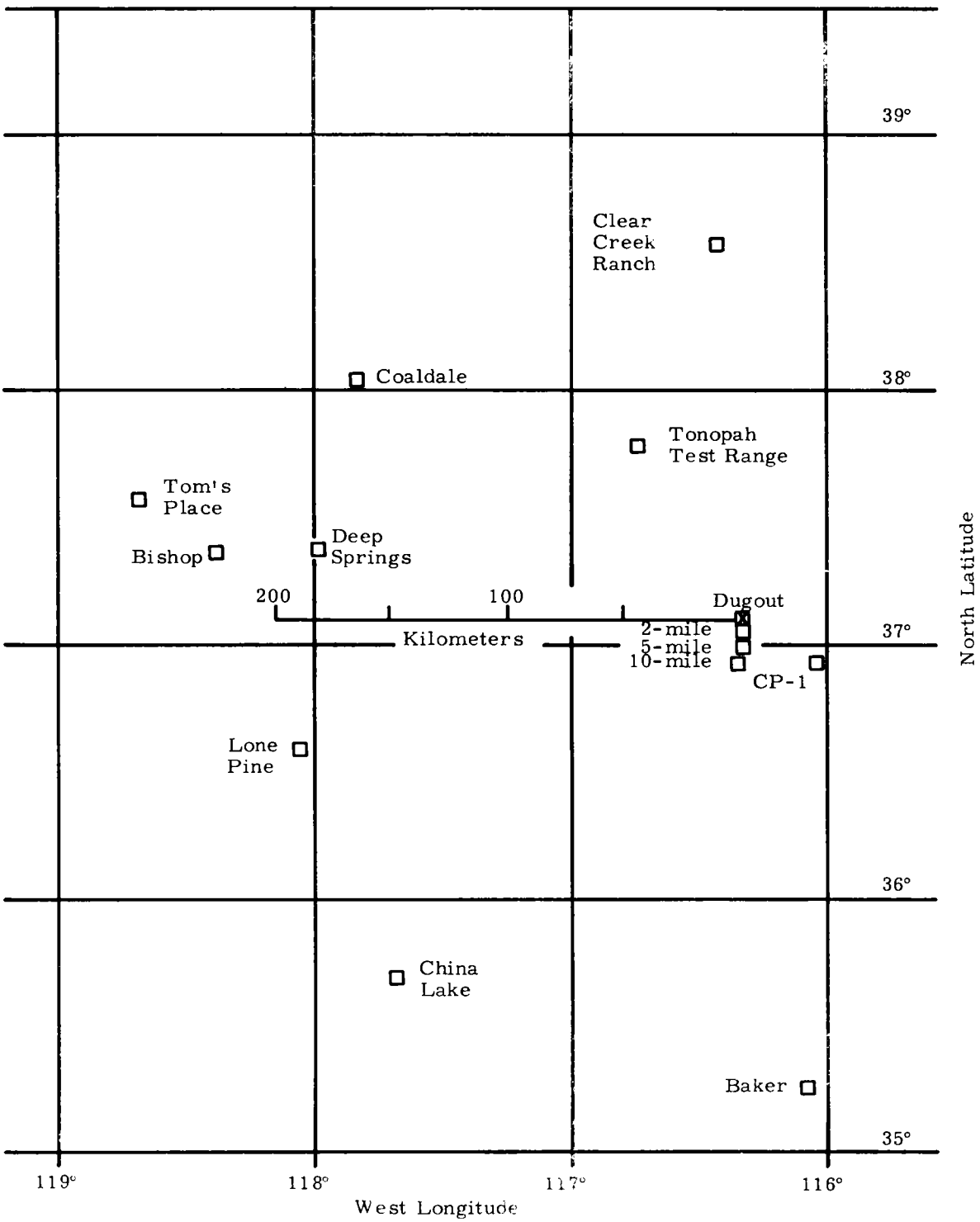

Fig. 5.2 Layout of microbarograph stations.

detonated at a depth of 58.8 ft (17.9 m) in the same basalt medium as Dugout. As is characteristic of chemical explosions, the close-in air blast signal was composed of two distinct signals. The first signal results from a ground-shock-induced wave which travels initially at the sonic velocity of the shot medium. At greater distances this wave tends to travel at sonic velocity in air. This pulse is followed by a second pulse, related to the venting of the gas generated by the explosion. For the Dugout scaled depths of burst, this second signal is generally much larger than the first signal.

The data from Shot 13 of Project Buckboard indicates a relationship of peak overpressure vs range and yield for a single shot in accordance with the equations

$$P_1 = 3.4 \times 10^7 \left[\frac{R}{\left(5W_{0.02}\right)^{1/3}} \right]^{-3} = 3.4 \times 10^6 \, R^{-3}$$

$$P_2 = 10^4 \left[\frac{R}{\left(5W_{0.02}\right)^{1/3}} \right]^{-1.36} = 3.5 \times 10^3 \, R^{-1.36}$$

If it is assumed that superposition occurs at the gauge, we would have prediction functions of

$$P_1 = 5 \times 3.4 \times 10^7 \left(R/W_{0.02}^{1/3} \right)^{-3} = 3.4 \times 10^6 \, R^{-3}$$

$$P_2 = 5 \times 10^4 \left(R/W_{0.02}^{1/3} \right)^{-1.36} = 3.5 \times 10^3 \, R^{-1.36}$$

Note that the two superposition assumptions lead to the same function for the first peak. These prediction functions are plotted in Figs. 5.3 and 5.4.

5.3.2 Long-Range Air Blast. Predictions for long-range air blast signals could be made on the basis of microbarograph measurements made on Shot 13 of Project Buckboard using the

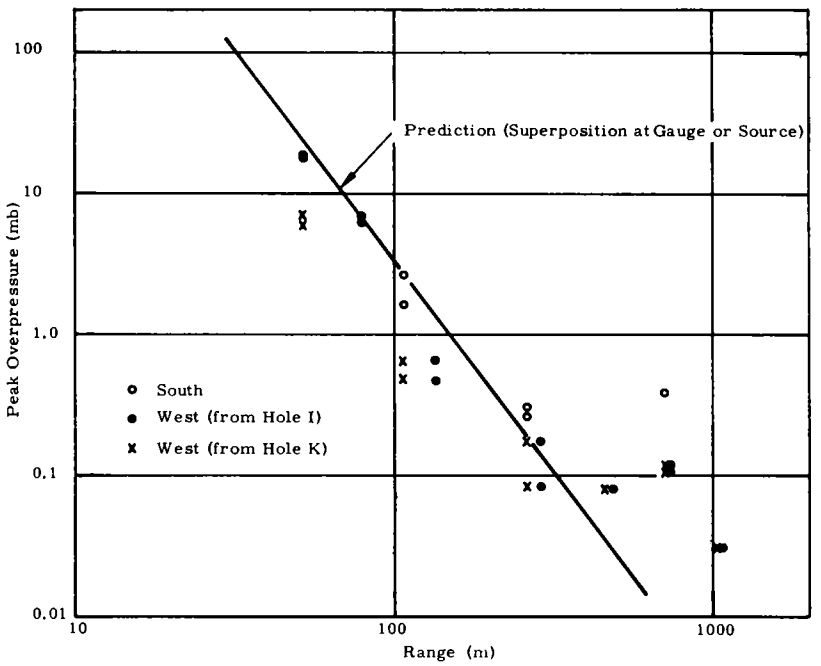

Fig. 5.3 Close-in air blast peak overpressure vs range, first peak.

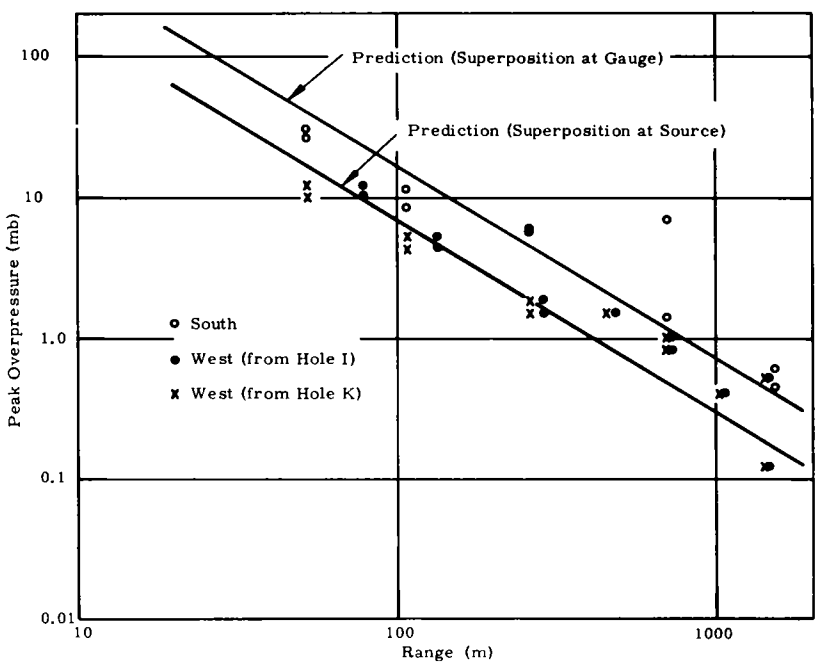

Fig. 5.4 Close-in air blast peak overpressure vs range, second peak.

same assumptions as above regarding superposition. Since long-range air blast at the caustic range has been shown to scale approximately as $W^{0.4}$, superposition at the gauge would lead to signals five times Buckboard 13, whereas superposition of the source would give signals $5^{0.4} = 1.91$ times Buckboard 13. Figure 5.5 shows the Buckboard long range microbarograph data scaled by these two methods.

5.4 RESULTS AND DISCUSSION

5.4.1 Close-In Air Blast. Table 5.1 gives the peak overpressures recorded for the first and second peaks on Dugout. All channels operated satisfactorily. Two gauges gave results that appeared doubtful. In general, the signals from the two gauges at each station compared very favorably. Although the first and second peak behavior noted for single high-explosive charges was present for the Dugout row charges, the behavior following the second charge was significantly different and is not fully understood at the present time.

(a) First Peak Data. The peak overpressures corresponding to the smaller first peak associated with the ground-shock-induced wave are plotted in Fig. 5.3. Signals in the direction perpendicular to the array at ranges from 50 to 300 m agree quite well with the prediction function. Signals in the direction parallel with the array also agree with the prediction function if their ranges are measured from the center charge. Beyond that range they deviate quite markedly with the slope changing to approximately R^{-1} between 300 and 1000 m. The signals propagated parallel to the array were generally lower than those in the perpendicular direction by a factor of 1.5 to 2 depending on whether the parallel direction is measured from the center charge or the end charge, respectively.

(b) Second Peak Data. The peak overpressures corresponding to the second, or gas-venting peak, are plotted in Fig. 5.4. The

data from both lines agree quite well with the predictions made on the basis of Buckboard 13. The signal transmitted perpendicular to the array was generally greater than the signal transmitted parallel by a factor of about 1.5, measuring the parallel line from the center charge. Measuring the distance from the end charge yield an isotropy factor of only about 2.0.

The data appears to have a slope somewhat less than the predictions, being about $R^{-1.2}$. It should be noted that the Buckboard data spanned only the range from 18 m to 130 m and further, that the farthest-out data points were at a flatter slope than the average $R^{-1.36}$ slope. Thus, the portion of the predicted curves between 100 and 1000 m is probably somewhat lower than is proper and the agreement between prediction and experiment is better than indicated.

The scatter is such as to make it difficult to say which superposition assumption is correct, although a reasonable estimate of the close-in air blast signal resulting from the venting gases can be made by assuming that source superposition applies to the signal propagated parallel to the array and gauge superposition applies for signals propagated perpendicular to the array.

5.4.2 Long-Range Air Blast. As a result of a faulty relay, the H - 2 minute calibration shot did not close until it was hit by the shock wave from Dugout at H + 4 seconds. The other calibration shot fired approximately as planned at H + 120 seconds, H + 300 seconds, and H + 480 seconds.

Preliminary results from these shots as well as Dugout are summarized in Table 5.2. Excellent recordings were obtained at eight stations: 2-mile, 10-mile, China Lake, Deep Springs, Bishop, Tom's Place, Tonopah Test Range, and Coaldale. Stations at Baker and Clear Creek were manned on an outside chance that ozonosphere winds would deviate from normal summer easterly flow. This would have carried waves to one or the other

station in a north or south direction. It was hoped to record relatively strong waves emitted perpendicular to the charge row which was oriented east-west. Minimum wave strengths from the charge row end were expected to be sent out in the west direction of strongest atmospheric propagation.

At Clear Creek, possible weak ozonosphere waves may have been recorded; there appears to be some appropriately correlated noise and it has been reported. However, propagation was too weak to show a Dugout oscillation in excess of about 1-μb ambient noise amplitude. At Baker, there also may have been signals of 5-10 μb amplitudes but some local electrical equipment was pulsing one recorder so it is impossible to ascertain necessary signal correlation.

Two wind chaff rocket firings were made at Sandia Corporation's Tonopah Test Range. Generally strong easterlies prevailed to give strong ozonospheric blast propagation toward the westerly direction.

As can be seen in Fig. 5.5, the results from Dugout compare very well with the predictions. The signals propagated in the north-south direction generally fell somewhat below the predicted levels, while the signals propagated to the west, southwest, and northwest fell between the limits determined by the two superposition assumptions.

The above agreement between predictions based on Buckboard 13 and Dugout may only be fortuitous since the location and degree of focusing is strongly dependent on meteorological conditions. Comparison of the calibration signals from Buckboard 13 and Dugout show that the Dugout calibration signals were a factor of 3 to 4 higher than Buckboard 13, indicating significantly greater focusing conditions for Dugout. When this factor is taken into consideration almost all of the data fall below the lower limit, and it appears that the source superposition assumption leads to

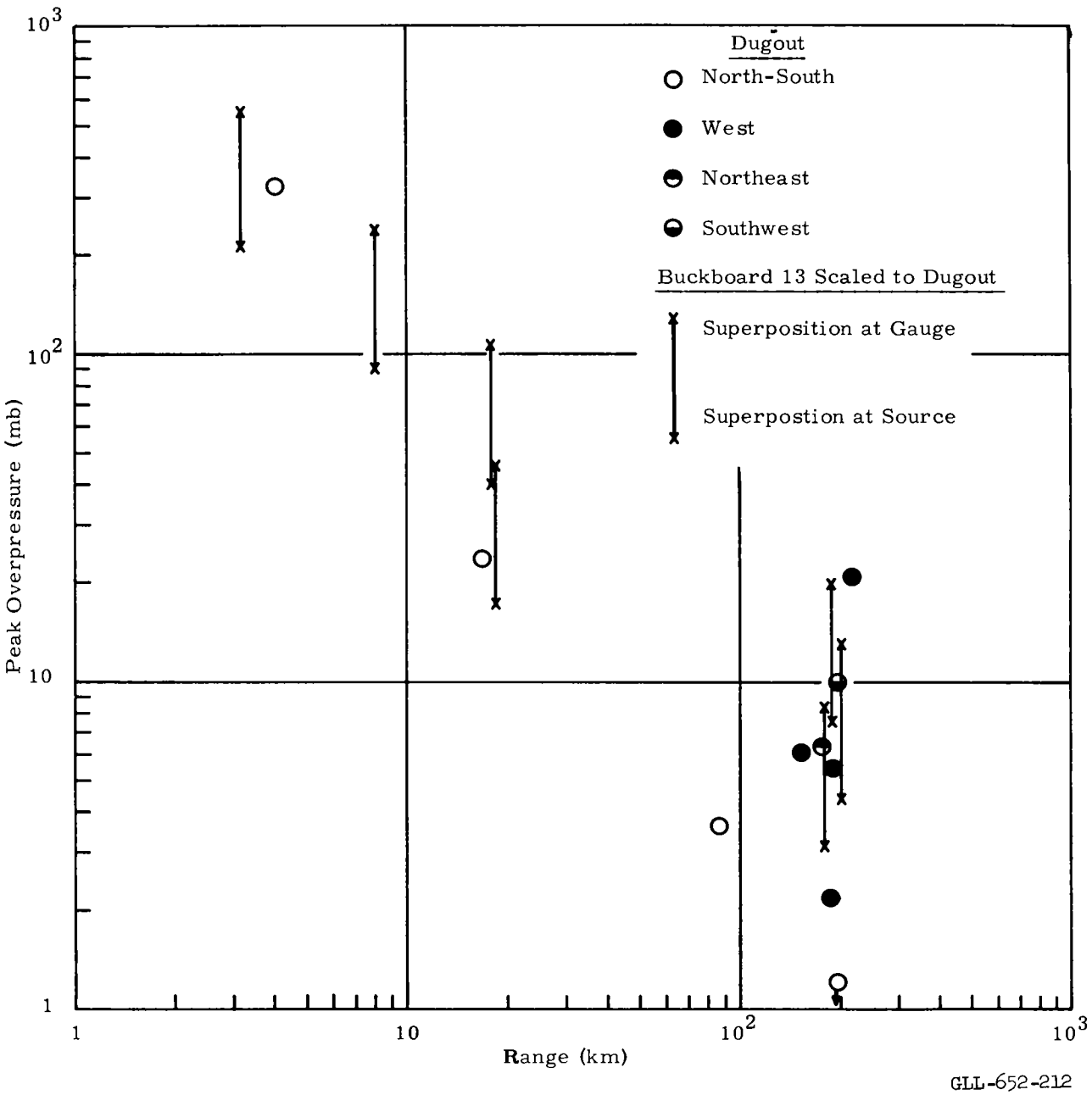

Fig. 5.5 Microbarograph results.

better upper limits for the long-range microbarograph signal than does gauge superposition.

Because of the above problem of variation in atmospheric conditions, it is perhaps more valid to look at the transmissivity factor calculated by comparing the Dugout signal and the calibration signals. This factor relates to how well a cratering signal is transmitted relative to the signal from the yield on the surface. Table 5.3 shows a tabulation of transmissivity factors calculated from the first three calibration shots. The factors f_{20}^{1}, f_{20}^{2}, f_{20}^{3} and the average $\overline{f}_{20}$ were calculated assuming that Dugout was a 20-ton shot. The factors $\overline{f}_{gs}$ and $\overline{f}_{ss}$ correspond to (1) assuming superposition of the five blast waves at the gauge, which reduces the factor $\overline{f}_{20}$ by 5, or (2) superposition at the source, which reduces the factor $\overline{f}_{20}$ by $5^{0.4} = 1.9$.

Source superposition leads to an average transmission factor of 0.11 ± 0.04, in excellent agreement with the factor from Buckboard 13 of 0.127. Gauge superposition gives an average of 0.044 ± 0.013, significantly lower than Buckboard 13. Averaging the north-south stations and the west stations separately leads to transmission factors of 0.15 ± 0.03 and 0.069 ± 0.025 respectively, showing approximately a factor of two stronger propagation in the direction perpendicular to the array. These results are in agreement with the close-in air blast results for isotropic air blast propagation.

5.5 CONCLUSIONS

5.5.1 Close-In Air Blast. Results from Dugout indicate that the close-in air blast signal from a row of five chemical charges in basalt can be predicted on the basis of air-blast data from single cratering events, within a factor of two, by assuming that

(a) The signal propagated in a direction parallel to the array results from superposition of the signals at the source,

TABLE 5.3 LONG-RANGE AIR BLAST TRANSMISSIVITY FACTORS

Station	Direction	Transmissivity factors f_{20}^1	f_{20}^2	f_{20}^3	$\bar{f}_{20}$	$\bar{f}_{gs}$	$\bar{f}_{ss}$
2-Mile	South	0.026	0.034	0.030	0.30	0.06	0.16
10-Mile	South	0.48	0.30	0.43	0.40	0.08	0.21
China Lake	Southwest	0.12	0.15	0.13	0.13	0.026	0.068
Deep Springs	West	0.17	0.23	0.27	0.22	0.044	0.12
Bishop	West	0.14	0.058	--	0.10	0.02	0.052
		0.062	0.071	0.066	0.066	0.013	0.035
Tom's Place	West	0.18	0.14	0.095	0.14	0.028	0.073
Tonopah Test Range	North	0.21	0.20	0.21	0.21	0.082	0.11
Coaldale	Northwest	0.24	0.22	0.14	0.19	0.038	0.10
Clear Creek	North	<0.27	<0.25	<0.20	<0.20	<0.048	<0.13
		Over-all average				0.044 ± 0.02	0.11 ± 0.04
		Average north-south				0.068 ± 0.013	0.15 ± 0.03
		Average west				0.026 ± 0.010	0.069 ± 0.025
		Average northwest-southwest				0.032 ± 0.006	0.084 ± 0.016

and

(b) The signal propagated in a direction perpendicular to the array results from superposition of the signals at the gauge.

The above conclusions mean about a factor of 1.5 to 2.0 between the two directions for five charges and apply approximately to both the first and second peak.

5.5.2 Long-Range Air Blast. The microbarograph signals at long ranges from the Dugout event compared very favorably with predictions made on the basis of Buckboard 13 results. Further, they indicated that

(1) Assuming a source superposition for the long-range air blast signals leads to an average transmissivity factor of 0.11 ± 0.04, which is in excellent agreement with that derived on Buckboard 13, and

(2) The signal propagated in the direction perpendicular to the array is about 35% greater than the average and the signal propagated parallel to the array was about 35% less than the average for total isotropy factor for the long range air blast of about 2.

REFERENCES

1. J. W. Reed, "Air Blast from Cratering Explosions," Proceedings of the Third Plowshare Symposium, TID-7695, pp. 169-180, April 1964.

2. L. J. Vortman et al., "Project Stagecoach: 20-Ton H.E. Cratering Experiment in Desert Alluvium," Chapter 9, Final Report SC-4596(RR) Sandia Corporation, May 1962.

3. L. J. Vortman et al., "Project Buckboard: 2-Ton and 1/2-Ton High Explosive Cratering Experiments in Basalt Rock," Chapter 9, Final Report SC-4675(RR), Sandia Corporation, August 1962.

4. W. R. Perret et al., "Project Scooter," Chapter 6, Final Report SC-4602(RR), Sandia Corporation, October 1963.

5. J. W. Reed and H. W. Church, "Sedan Long-Range Blast Propagation," Final Report PNE-202F, Sandia Corporation, June 1963.

6. J. W. Reed, "Long-Range Air Blast Measurements and Interpretations," PNE-1809, Sandia Corporation.

7. J. W. Reed, "Close-In Air Blast from a Nuclear Detonation in Basalt," PNE-1810, Sandia Corporation.

8. Private communication, J. W. Reed, Sandia Corporation.

9. Private communication, L. J. Vortman, Sandia Corporation.

10. L. J. Vortman, "Project Dugout, Air Blast from a Row Charge in Basalt," PNE-608, Sandia Corporation, to be published.

11. J. W. Reed, "Project Dugout, Row Charge Blast Wave Observation at Long Range," PNE-607, Sandia Corporation, to be published.

CHAPTER 6

CLOUD PHENOMENA

6.1 INTRODUCTION

Base surge cloud and main cloud phenomena associated with a cratering detonation are of great importance for nuclear excavation. This is because these clouds determine the initial configuration of the radioactivity vented from such an excavation. Therefore understanding of the mechanics of cloud formation and development must be increased so that accurate predictions for future excavation experiments and applications can be made.

Specifically, the effect on cloud dimensions and development of single- and multiple-charge arrays, yield, depth of burst, medium, and meteorological conditions must be determined.

Previous experience with cloud studies have been confined primarily to single charges in alluvium and basalt. Data from a few row charges in alluvium have been presented in a previous report (Ref. 1). The Dugout event presented the first opportunity to study the base surge and main cloud formation from a row charge cratering experiment in hard rock.

In particular, Project Dugout permitted the study of the relationship between the maximum base surge radius formed by a row charge and that formed by a single charge in the same medium and at the same scaled depth of burst. Data presented cover the base surge height and radius and main cloud height as a function of time for this row-charge cratering experiment in hard rock.

6.2 EXPERIMENTAL PROCEDURE

6.2.1 Base Surge Photo Stations. The data-acquisition system for the Dugout event was designed to yield base surge cloud height and radius history as a function of time. To

accomplish this, motion pictures were taken from three vantage points. The first was a helicopter flying a circular orbit above ground zero at a height of about 1220 m (4000 ft) above the top of the mesa. The other vantage points were two ground camera stations located 914 m (3000 ft) north and 503 m (1650 ft) west of ground zero. The helicopter motion pictures were used to study surge cloud radius growth. The ground photographic stations were used to study cloud height histories.

6.2.2 Main Cloud Stations. In addition to the above photographic coverage provided by LRL-N, the Weather Bureau sponsored a study of main cloud height on Dugout. For this program, Edgerton, Germeshausen, and Grier, Inc. (EGG) photographed the main cloud at long range from two camera stations. One station was 6800 m (22,302 ft) to the north of the Dugout and the other was 9170 m (30,121 ft) to the northeast. The location of all the above stations are indicated in Fig. 6.1.

6.2.3 Target Array. To provide points of reference, an array of bright orange colored targets were placed on the surface at intervals of 92 m (300 ft) in two orthogonal rows. Each target location consisted of two separate targets, one mounted vertically and the second placed horizontally on the ground. This target array is shown in Fig. 6.1.

In order to determine the elapsed time, a flash bulb ignited at detonation time recorded the relevant time origin on the film.

From the position of the base surge radius and height with respect to the targets, the framing speed (48 frames per second), and number of elapsed frames, the position of the base surge radius and height vs time was determined.

6.3 PREDICTED RESULTS

Estimates were made for the Dugout base surge height and radius on the basis of data obtained on Project Danny Boy, Pre-Buggy, and Pre-Schooner. A previous study had indicated that

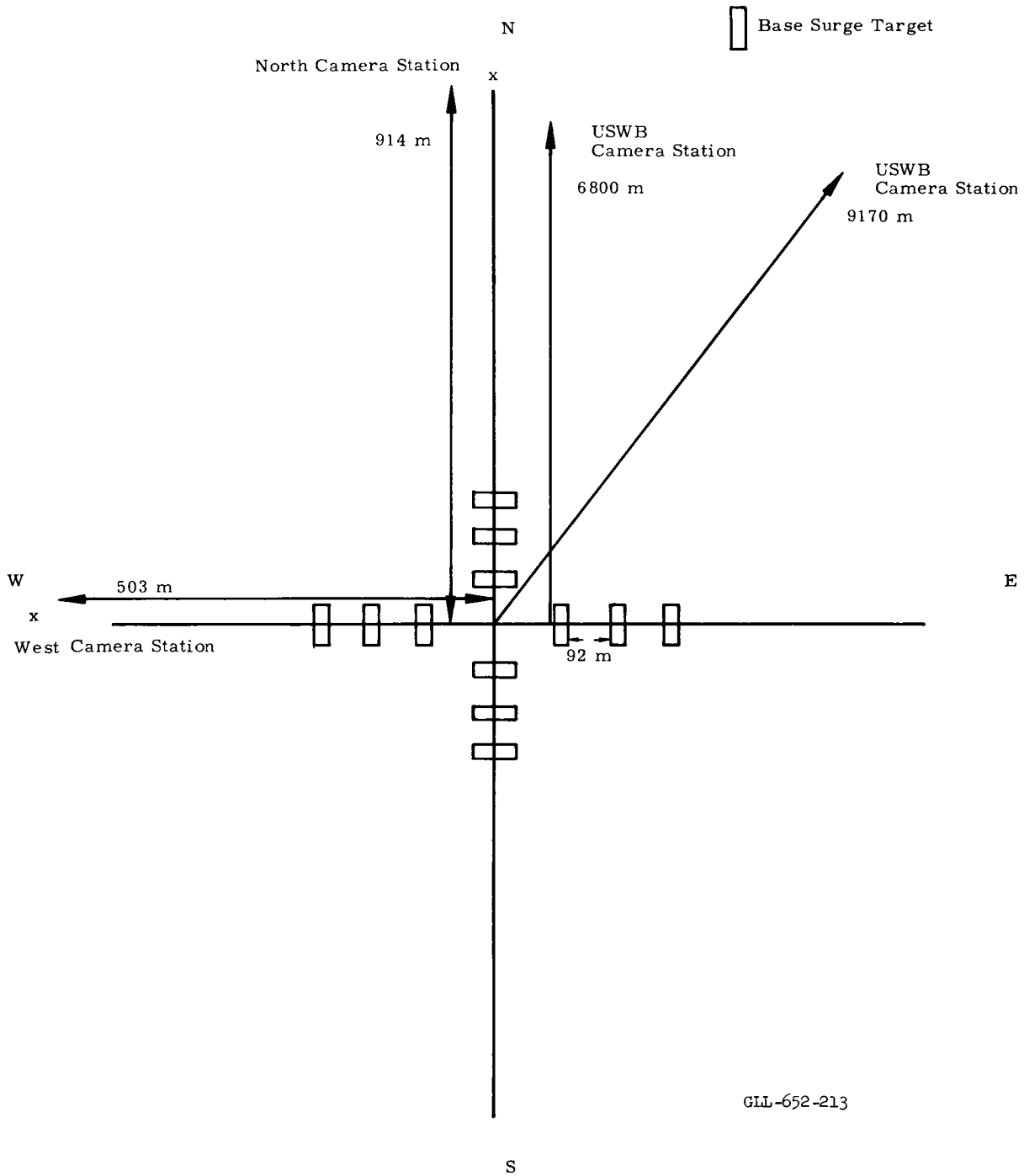

Fig. 6.1 Target and camera array.

the neutral atmosphere base surge radius in a given medium for a constant scaled depth of burst scaled as the 0.3 power of the yield and the base surge height as the 0.2 power of the yield. Data from the Pre-Schooner series of 20-ton cratering detonations were used to develop a curve of scaled neutral atmosphere base surge radius vs scaled depth of burst for basalt shown in Fig. 6.5. The scaled depth of burst for Dugout was determined by dividing the depth of burst by the cube root of a single Dugout charge, 0.020 kt. Using the curve, a maximum base surge radius was then determined for 1 kt. The predicted Dugout base surge radius was then obtained by scaling this radius for 1 kt to the total Dugout yield of 0.10 kt using the 0.3 power of the yield. The above procedure resulted in a neutral atmosphere prediction of base surge radius for Dugout of 395 m (1300 ft). For comparison of the actual Dugout base surge cloud radius with this prediction, the Dugout result must be corrected to a neutral atmosphere using the empirical relationship developed in Reference 1. This provides that the maximum base surge radius be increased in a linear proportion with the environmental lapse rate in the layer containing the base surge, $-\partial T/\partial Z$, where T is temperature in °C and Z is the height in meters.

The base surge height was scaled from the Danny Boy height. This introduces some error because the Danny Boy scaled depth was 45 $m/kt^{1/3}$ and Dugout was 66 $m/kt^{1/3}$. Since there are no reliable data relating base surge height to scaled depth of burst, the predicted base surge height for Dugout was scaled directly from the Danny Boy base surge height of ~435 m using the 0.2 power of the yield. This then gave a predicted base surge height of ~326 m for Dugout.

Little reliable data are available on main cloud heights from cratering events; therefore a prediction for Dugout was made from the Sedan event, which had a scaled depth of burst of 137 $ft/kt^{1/3}$.

Scaling from Sedan using the 0.2 power of the yield gave a predicted main cloud height for Dugout of ~925 m (3000 ft).

6.4 RESULTS

6.4.1 Base Surge Dimensions. The maximum cross wind base surge radius as measured from the helicopter reached ~320 m (1050 ft) in about 43 seconds. A time history curve of base surge radius is shown in Fig. 6.2. A maximum base surge height of 350 m (1160 ft) was reached in about 8 minutes, and the main cloud reached an altitude of ~1220 m (4000 ft) in about 8 minutes. The time history for these heights, as obtained from the EG and G long-range photography, are shown in Figs. 6.3 and 6.4.

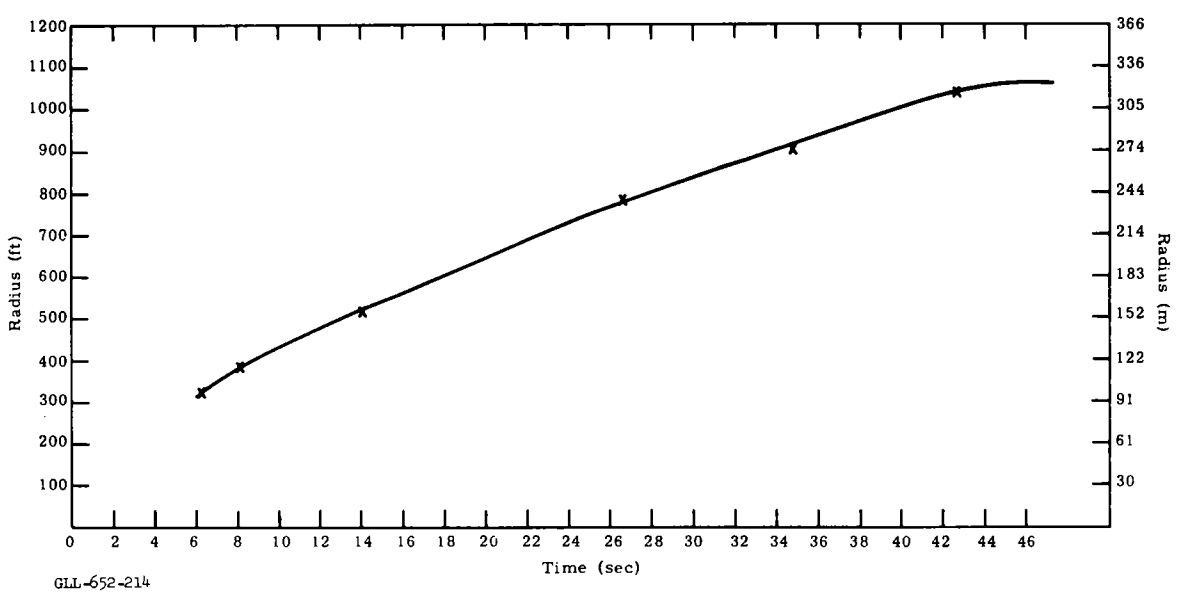

Fig. 6.2 Dugout base surge radius vs time.

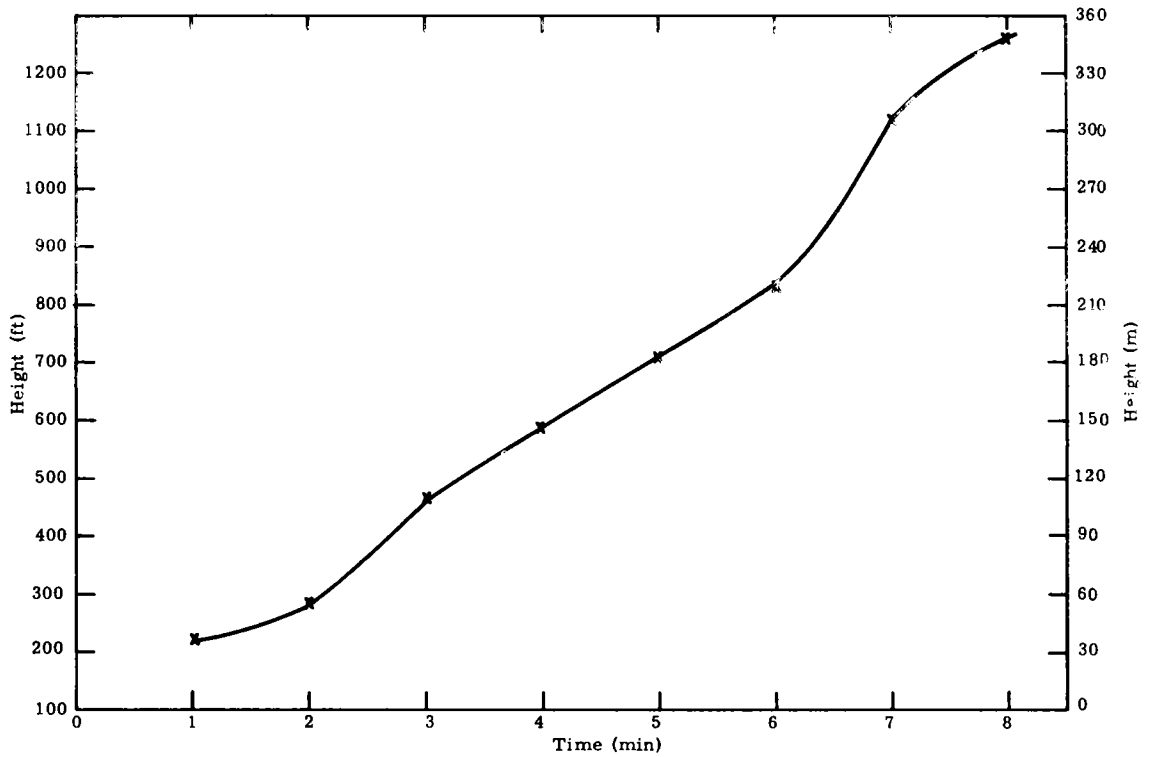

Fig. 6.3 Dugout base surge height vs time.

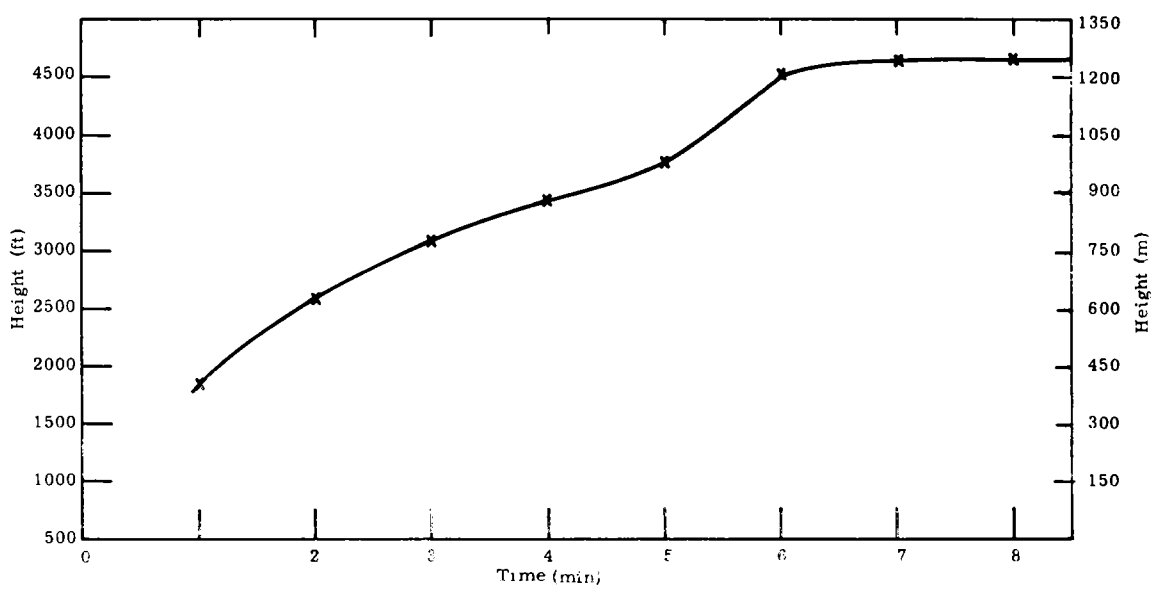

Fig. 6.4 Dugout main cloud height vs time.

6.5 DISCUSSION AND CONCLUSION

Correction of the above observed maximum cross-wind base surge radius for the observed atmospheric stability gives a neutral atmosphere base surge radius for Dugout of 403 m (1320 ft), which compares very favorably with the prediction of 395 m (1300 ft). The predicted base-surge height was ~326 m (1070 ft) and that observed was ~354 m (1160 ft). The predicted main cloud height was ~925 m (3000 ft) and that observed was ~1220 m (4000 ft).

The observed maximum base surge radii from various cratering detonations in alluvium and basalt were corrected to a neutral atmosphere and scaled to a 1-kt yield and plotted as a function of the scaled depth of burst. These curves for alluvium and basalt are shown in Fig. 6.5.

It is evident from this curve that the scaled maximum base surge radius for Dugout is about twice that for the single charge Pre-Schooner Alfa event where Alfa is one-fifth the yield and at the same depth of burial.

The maximum base surge radius for the events in basalt appears to be significantly less than those for comparable events in alluvium. This may be due to one of these factors:

1. Since basalt is a dry medium, a relatively smaller amount of noncondensible gas will be produced and vented than occurs in alluvium;
2. Significant amounts of gas may leak from the cavity into the fractured basalt during the gas acceleration phase, leading to a much smaller amount of gas being vented; or
3. A larger particle size in the aerosol for basalt than for alluvium, which would lead to a shorter airborne period.

After the first few seconds the Dugout base surge takes on the characteristics and appearance of a surge cloud generated by

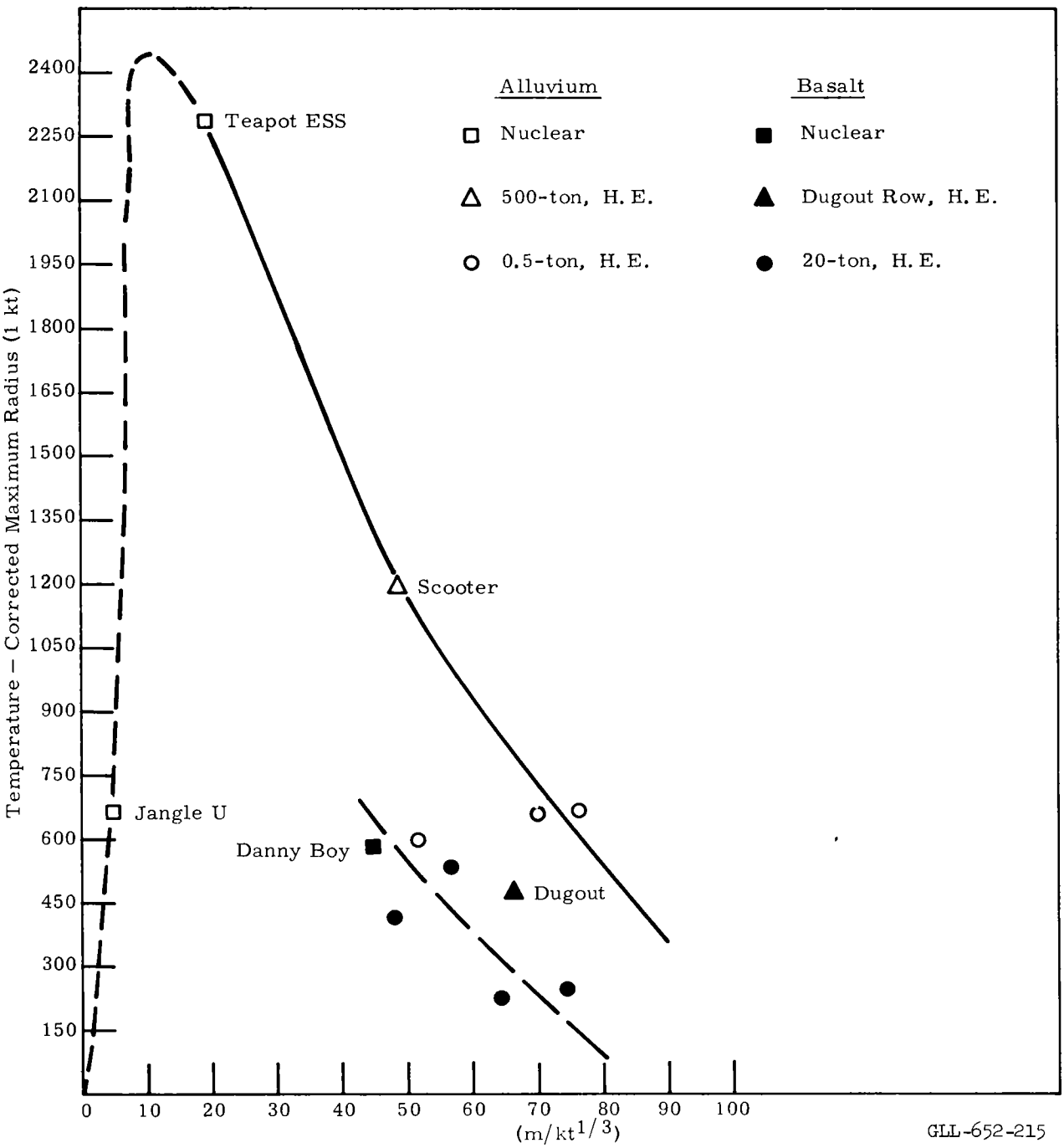

Fig. 6.5 Scaled maximum base surge radii vs scaled depth of burst, alluvium and basalt.

a single charge located beneath the central ground zero, although about twice as large as one would expect on the basis of single-charge scaling.

REFERENCES

1. J. B. Knox and R. Rohrer, "Base Surge Analysis," Lawrence Radiation Laboratory, Livermore, Final Report for Project Pre-Buggy, PNE-304, 1963.

2. J. B. Knox, "Cloud Rise Prediction for Uncontained Nuclear Explosions," Lawrence Radiation Laboratory Internal Memorandum, 1961.

3. R. Rohrer, "Project Pre-Schooner Base Surge and Cloud Formation," Lawrence Radiation Laboratory, PNE-503.

4. R. Rohrer, "Project Dugout, Cloud Development States," Lawrence Radiation Laboratory, PNE-604, to be published.

DUGOUT TECHNICAL REPORTS

Report No.	Agency	Author	Title
PNE-600F	LRL	Nordyke, et al.	Technical Director's Summary Report – Project Dugout
PNE-601F	NCG	Spruill	Crater Measurements
PNE-602F	WES	Strohm	Crater Explorations
PNE-603F*	LRL	Terhune	Surface Motion Measurements
PNE-604F	LRL	Rohrer	Cloud Development
PNE-605F	CGS	Mickey	Strong Motion Measurements
PNE-607F	SC	Reed	Multiple Row Charge Blast Wave Observations at Long Range
PNE-608F	SC	Vortman	Air Blast From a Row Charge in Basalt
PNE-609F	WES	Ingram	Deep Underground Shock Measurements

*PNE-603F and PNE-606F incorporated under one document number per request of Milo Nordyke.